University of Alberta

Electric Breakdown of Thin Liquid Films

By

Farshid Karimi Mostowfi

A thesis submitted to the Faculty of Graduate Studies and Research in partial fulfillment of the requirements for the degree of **Doctor of Philosophy**.

Department of Mechanical Engineering

Edmonton, Alberta
Fall 2007

Your file Votre référence
ISBN: 978-0-494-32991-7
Our file Notre référence
ISBN: 978-0-494-32991-7

Abstract

An experimental technique is developed for assessing stability of thin liquid films by application of electrical forces and simultaneous measurement of the electric conductivity of the system. The concept involves creating a thin film at the intersection of two micro-channels etched onto a glass substrate. Once a thin film is created, a ramped DC potential difference can be applied across it. The electrical stresses developed at the film interfaces lead to its rupture above a threshold potential. The potential at which the film ruptures is used to assess the stability of the film. Small channel dimensions in this microfluidic platform allow characterization of thin films formed between micron-sized droplets at high capillary pressures, which is difficult to attain using conventional thin film characterization techniques. The results of DC potential breakdown of films show that critical potential can be considered as a measure of thin film stability. Stability measurements using this technique were in accord with Langmuir adsorption model.

Furthermore, impedance spectroscopy is used to measure capacitance of the films formed using the developed microfluidic device. The capacitance measurements led to the estimation of the film area which is unknown in the microfluidic device to the vantage point along the surface of the film. The effect of drainage

time and adsorption time of films is studied using impedance spectroscopy. Similar to DC measurements, capacitance measurements of the film also suggested a Langmuir adsorption trend. Moreover, capacitance measurement of films under the effect of DC potential was conducted. The results showed a dependence of capacitance to square of applied DC potential.

To my beloved wife, Neda

and

To my source of inspiration, my mother

Acknowledgements

I would like to take this opportunity to express my gratitude to my supervisors Drs. Bhattacharjee, Czarnecki and Masliyah for their constant support. I wish to thank Dr. Bhattacharjee for indulging me in my studies so that I could develop my skills as an independent researcher. I am greatly indebted to Dr. Czarnecki, without whom this work would have been nearly impossible. His constant support and in depth knowledge was essential to this work. I wish to thank Dr. Masliyah for being the constant source of encouragement during my research.

I would like to thank Syncrude Research Center for providing such a wonderful and friendly research environment without which this research was impossible. I would like to thank Tom Tran, Dr. Kevin Moran, and Dr. Michael Lipsett for their great support throughout this work.

I am indebted to my great friends Nikolay Panchev, Dr. Khristo Khristov, and Dr. Elek Musial for sharing their vast knowledge of thin films with me. I would like to acknowledge Stephanie Bozic and Dr. Ken Westra at Nanofab , University of Alberta for providing a unique microfabrication facility.

In addition, I wish to thank all of my colleagues in CCFLab including Neda, Tania, Jeff, Shahnawaz, Yibing, and Erika for creating such a friendly working environment.

Edmonton, Alberta — Farshid Mostowfi

August , 2007

Table of Contents

List of Tables

List of Figures

List of Symbols

Π	disjoining pressure [Pa]
Π_{EL}	electrostatic disjoining pressure [Pa]
Π_{VW}	va der Waals disjoining pressure [Pa]
Π_{ST}	steric disjoining pressure [Pa]
P_{in}	hydrostatic pressure inside a droplet [Pa]
P_l	hydrostatic pressure of surrounding oil [Pa]
P_c	capillary pressure [Pa]
h	distance [m]
V	electric potential [V]
I	electric current [A]
ω	frequency [Hz]
ϕ	phase [rad]
ϕ_v	phase of potential [rad]
ϕ_i	phase of current [rad]
Δ	thickness change of a film [m]
L	thickness of a film [m]
ϵ	dielectric constant [F/m]
E_Y	modulus of elasticity [Pa]
ΔP	pressure drop across an interface [Pa]
P_w	pressure in the water phase [Pa]
P_o	pressure in the oil phase [Pa]
γ_{ow}	interfacial tension of oil/water interface [N/m]
R_1	radius of curvature [m]
R_2	radius of curvature [m]
F	Maxwell stress on an interface [Pa]
E	electric field [V/m]

ΔV	potential drop across a film [V]
δ	thickness of a film [m]
I_0	amplitude of current [A]
t	time [s]
R	resistance [ohm]
C	capacitance [F]
V_0	amplitude of potential [V]
Z	impedance [ohm]
G	conductance [mho]

Chapter 1

Introduction

1.1 Introduction

Emulsions are ubiquitous in nature, industry, and household. Milk, butter, mayonnaise, and cosmetics are examples of emulsions used in daily life. Emulsions are inherently unstable, meaning that they have a limited lifetime, after which phase separation takes place. Maintaining a precise control over stability of an emulsion plays a major role in industry. Therefore, emulsion science plays an important role in industry where most of such products are made. For instance, in production of many cosmetic or food products, the goal is to increase the lifetime of the emulsion, which, in turn, results in increased shelf-life of the product. On the other hand, in many industries, formation of unwanted emulsions is a recurring challenge that costs significant amounts of time and resources.

In petroleum industry, mixing of water with crude oil results in formation of highly stable emulsions. Entrainment of water droplets into the oil phase poses a significant challenge in petroleum industry. The presence of water not only reduces the oil quality, but also its associated salts may form corrosive or even explosive substances in the refining processes. Therefore, separation of water from crude oil is a major issue of concern.

In the case of conventional oil, the source of water is existence of table waters close to oil reservoirs. The water is usually produced along with the oil and

forms an emulsion. Major offshore oil spills are another host for entrainment of water droplets into oil and formation of emulsions. In the non-conventional production of heavy oil (bitumen) from oilsands, water is deliberately added to the oilsand to recover the bitumen from sand grains. The added water readily forms a water-in-oil emulsion, which must be separated from the bitumen later in the extraction process.

Different techniques are employed to separate the water from oil. Gravitational settling or centrifugation are common techniques incorporated for separation of water from oil. However, these techniques are capable of separation up to 98% water. The remaining water droplets are so small ($< 10\mu m$) that density difference methods such as sedimentation or centrifuging are not capable of separating the water droplets. Therefore, in petroleum industry, de-emulsifiers are added to the emulsion to reduce the stability of the emulsion. De-emulsifiers promote breakdown of the emulsion by changing the interfacial characteristics of the emulsion system.

The above examples elucidate the need for control or alteration of stability of an emulsion. Increase or decrease of emulsion stability is achieved by introducing new chemicals to the system. However, a reliable control of emulsion stability can not be achieved without measurement. In other words, to manipulate a parameter effectively, one needs to measure it first, leading to the need of development of stability measurement techniques for emulsions.

Despite the vast application of emulsion systems in most major industries, the measurement techniques developed for emulsion stability are extremely limited. The common industrial practice for emulsion stability measurement is the so called "Bottle Test", which is described in detail in the next chapter. Unfortunately, the bottle test does not provide a sound quantitative information regarding stability of an emulsion. Even qualitative comparison is somewhat difficult.

As will be discussed in Chapter 2, stability of an emulsion can be studied from a different perspective, which is stability of thin liquid films formed be-

tween dispersed droplets. Although stability of a thin film may not provide all the required information about stability of an emulsion, it has commonly been observed that emulsion stability largely depends on stability of thin liquid films formed in the emulsion. To study thin liquid films, thin liquid film apparatus (TLF apparatus) has been developed and is widely used for thin film studies [Derjaguin *et al.*, 1954; Exerowa and Scheludko, 1971*a*]. The TLF apparatus has proven to be very successful for foam film (gas bubbles in liquid such as soap bubbles) experiments where diameter of the film is in the order of millimeters. However, the TLF apparatus is incapable of forming small films ($< 100\mu m$). Therefore, our knowledge of micron sized and high pressure films formed in many emulsions is limited. Furthermore, all thin film theories predicting film's behaviors, such as drainage and breakup, are based upon such large films. This leads to the question as to whether such theories are accurate enough for small scale films. For instance, lens formation [Ivanov, 1988] is a phenomena widely observed and studied in large scale films. In small scale films, however, formation of lenses due to high capillary pressure and rigidity of the interface may not be observed [Velev *et al.*, 1995].

The primary goal of this study is to move the boundaries of thin liquid film experiments to micron sized emulsion films using microfluidic and microfabrication techniques. Such experiments would improve our knowledge of thin films and consequently, emulsion stability by directly exploring the film formation and rupturing phenomena at a length scale that represents the emulsion droplet diameters encountered in reality.

1.2 Objectives

The first objective of this study is to develop an experimental setup, using which micron sized emulsion films can be formed. To form such films, one needs to consider the physical conditions pertaining to the actual emulsions and to recreate those conditions in a laboratory environment. Consequently, droplet size, film area, capillary pressure, and chemical composition have to

be replicated accordingly. The focus of this work is on water-in-oil emulsion films encountered in the petroleum production industry such as presence of water droplets in reservoir fluids, or de-emulsification of water from extracted bitumen in oilsands processing.

The second objective of this research is to incorporate the lab-on-a-chip concept to develop a microfluidic setup that can form stable thin films of microscopic dimensions, destabilize such films by application of an external force in a controlled manner, and measure the characteristics of the thinning film, particularly, the applied force corresponding to which it ruptures. Due to high capillary forces in small channels, creating a hydrostatic condition in which a stationary interface can be formed is an intricate task. Moreover, thermal and pressure fluctuations would affect the balance of pressure in the channels. Therefore, maintaining a hydrostatic condition during the measurement is critical.

The third objective is to explore the concept of electric breakdown and its applicability in characterization of thin films. Application of a DC electric field across thin films results in electrical forces that can be manipulated quite efficiently by adjusting electric potentials. The goal of this research was to explore whether electrically induced destabilization of thin films could provide meaningful information regarding film stability. Furthermore, electrochemical detection is used to assess rupture of a film. Rupture of a film can be detected by monitoring its conductance. Before breakup, the non-conducting film imposes a substantial resistance on the circuit. Once the film breaks, the conductance of the film increases significantly which can be detected using a sensitive ammeter.

The fourth objective of this study is to investigate drainage behavior of micron sized and high pressure emulsion films, since there is no experimental data available in literature. This study was conducted by means of impedance measurement of the film during drainage and adsorption time. Furthermore, the effects of DC electric field on the capacitance of films is studied. A ramp DC potential destabilizes the film while an AC signal measures the impedance changes in the film.

The fifth objective of this study is to evaluate functionality of the developed experimental setup in an industrial emulsion system. The common practice in industry for emulsion stability measurement is the "bottle test", which does not provide insight or quantitative information about emulsion stability.

The objectives of this research are summarized as follows:

1. Develop an experimental setup to study thin liquid films at micron scale.
2. Incorporate microfluidic techniques to create stable hydrostatic conditions to form thin films.
3. Employ electrochemical destabilization/detection of the film and study applicability of electric breakdown as a stability criterion.
4. Study drainage behavior of micron size emulsion films and the effect of DC field on the capacitance of the film.
5. Explore applicability of the developed technique for an industrial emulsion system.

1.3 Thesis Outline

Chapter 2 of the thesis provides an introduction to thin liquid films and emulsions. Furthermore, two standard experimental systems currently used for research and industrial practice are described. In that chapter, an overview of the major research and technical elements of the thesis are presented, including a brief and critical literature review of each element. Following an introduction to thin films and related experimental techniques, electric breakdown of thin films are reviewed. Then, microfluidics and its developments are described including some recent developments on application of microfluidics in emulsion studies. The last section reviews impedance spectroscopy and its applications in membrane studies followed by concluding remarks.

Chapter 3 provides details of fabrication of the chip and the specific steps taken to develop the device. This chapter fulfils the first two objectives presented in the previous section. First, the design concept is described followed by illustration of the final working prototype. Development of the final prototype was achieved through fabrication of eight versions (generations) of the device. Each version was a modification of the previous versions based on the challenges faced during the experiments. Therefore, the challenges and consequent modifications of the microfluidic device and the setup are described. The experimental setup is comprised of three sub-systems, namely fluid, electrical, and visualization, which are described in Chapter 3 in detail. Several emulsion systems studied in this work are described, including preparation, stabilization, and characterization. Finally, experimental procedures including chip preparation and film formation are presented. Details of fabrication and developed procedure for the microfluidic device are presented in appendix A.

Chapter 4 describes the studies pertaining to objectives three, four, and six of this research, namely, applicability of DC potential as a measure of stability, application of electrochemical detection for assessing film rupture, and possible application of the developed system for industrial systems. In this chapter the results of DC breakdown of the films are presented starting with a concise theoretical background of the electric breakdown of thin liquid films. Then the results of the electric breakdown of lecithin and TEGOPREN films are compared. Comparison of the lecithin results with Langmuir adsorption kinetics and isotherms are presented in this chapter followed by results of bitumen films as a typical industrial surfactant.

Chapter 5 presents the results of AC measurements, fulfilling the fifth objective of the thesis. This chapter covers the theoretical foundation of impedance spectroscopy as well as a brief description of the principal concepts such as equivalent circuit and Nyquist plot. Then the development of the equivalent circuit for the chip is described. Impedance spectroscopy was employed to estimate the film area, to study the effect of surfactant adsorption time, and the

effect of DC polarization on the capacitance of the film.

The last chapter of this thesis is focused on the conclusion and suggestions for future works.

Chapter 2

Thin Liquid Films and Water in Oil Emulsions

2.1 Background and Overview

A brief overview of the main subjects incorporated in this thesis are presented in this chapter. First, emulsions and thin films are described followed by common experimental tools available to study their behavior. Then, literature is reviewed. In the next sections impedance spectroscopy, electric breakdown of thin films, and the latest developments are discussed in more details. Finally, development of microfluidics and their applications in emulsions and electric break down of emulsion films are reviewed.

2.1.1 Emulsions and Thin Liquid Films

An emulsion is defined as "a fluid colloidal system in which liquid droplets and/or liquid crystals are dispersed in a liquid" [IUPAC, 1979]. In other words, in an emulsion, one liquid (dispersed phase) forms suspended droplets in the other one (continuous phase). An emulsion is not a stable state of matter (it is a meta-stable system) [Sjoblom, 1996]. Therefore, given sufficient time, dispersed droplets in the emulsion coalesce, eventually, forming a single continuous phase separated from the dispersing medium by a single interface.

The longevity of the meta-stable emulsion state depends on the rate of coa-

lescence of the dispersed droplets; the higher the rate of coalescence, the shorter the life time of the emulsion. The rate of coalescence can be altered by addition of surfactant molecules to the system. Presence of an emulsifier surfactant can impede coalescence by forming a repulsive interfacial barrier between the droplets. A de-emulsifier surfactant, on the other hand, promotes separation of the phases by increasing the rate of coalescence. Figure 2.1 is a micrograph of water in diluted bitumen emulsion. In the figure, micron-size water droplets are dispersed in the oil phase. Adsorption of surface active molecules in bitumen onto the water/oil interface stabilizes the emulsion.

Stability of an emulsion depends largely on formation and stability of thin liquid films. When two droplets approach each other, the continuous phase may form a liquid film, preventing them from coalescence. The overall stability of the emulsion is directly related to the stability of the liquid film. Therefore, stability of thin liquid films is considered as the cornerstone of emulsion stability [Stubenrauch and von Klitzing, 2003]. In industrial practices, however, stability of an emulsion against coalescence is often understood as stability against flocculation which is not the subject of this study.

In general, when two interfaces approach each other (*e.g.* two droplets, two solid particles, or one droplet and a flat solid wall as depicted in Fig.2.2), at small separations, the intermolecular forces, such as van der Waals and electrostatic interactions come into the picture [Kralchevsky and Nagayama, 2001]. Figure 2.2 depicts typical scenarios in which thin films are formed. In Fig. 2.2a, two solid walls are separated by a fluid forming a film. In Fig. 2.2b, two droplets (or gas bubbles) are floating in a second continuous fluid. The interaction of the two interfaces causes the two droplets to flatten, forming a circular film. Figure 2.2c shows film formation between a liquid droplet and a flat surface. A film is called "thin" if its thickness is small enough so that the surface forces of the two adjacent surface become evident.

Figure 2.3a schematically, depicts two water droplets in an oil medium attached to each other (flocculated). The thin layer of oil separating the two

droplets is the thin liquid film [Ivanov, 1988]. The film resembles an interfacial energy barrier which must be overcome by the droplets in order to coalesce. The reason for stability of the film is the repulsive disjoining pressure (Π) [Kralchevsky and Nagayama, 2001; Stubenrauch and von Klitzing, 2003; Sheludko, 1967; Exerowa and Kruglyakov, 1998], which is due to the surface forces. Disjoining pressure can be defined as the sum of the surface forces per unit area. Disjoining pressure is a function of the film thickness, h

$$\Pi = \Pi(h) \tag{2.1}$$

and it can be repulsive ($\Pi > 0$) or attractive ($\Pi < 0$) depending on the forces involved. Assuming that the individual interacting forces are independent of each other, the net disjoining pressure can be defined as a sum of the individual disjoining pressures:

$$\Pi = \Pi_{EL} + \Pi_{VW} + \Pi_{ST} \tag{2.2}$$

where Π_{EL}, Π_{VW} and Π_{ST} are disjoining pressure contributions due to electrostatic, van der Waals and, steric interactions, respectively. Depending on the type of the film, other sources of disjoining pressure such as structural forces may be added to the right hand side of the equation.

Figure 2.3b shows the force balance on one of the droplets. In equilibrium condition, the disjoining pressure balances the capillary pressure (the pressure difference between inside and outside of the water droplet).

$$P_{in} = \Pi + P_l \tag{2.3}$$

where P_{in}, Π, and P_l represent hydrostatic pressure inside the droplet, disjoining pressure, and the pressure of the oil phase, respectively. Equation 2.3 can be written as

$$\Pi = P_{in} - P_l = P_c \tag{2.4}$$

where P_c is the capillary pressure of the droplet. Therefore, one may conclude that a thin film is stable if the condition of Eq. 2.4 is satisfied ($\Pi = P_c$).

Figure 2.4 depicts a typical disjoining pressure isotherm (disjoining pressure, Π, vs. thickness, h) for a general case where both van der Waals attraction and electrostatic repulsion exist. The dashed line $\Pi = P_c$ represents capillary pressure of the droplets or the equilibrium disjoining pressure. In Fig. 2.4, there are three solutions of Eq. 2.4 as the line $\Pi = P_c$ intersects the disjoining pressure isotherm at three points. The first point (point 1) corresponds to an equilibrium state called "Common Black Film" where the thickness of the film is h_1. Common black films are stabilized by double layer repulsion. Point (2) is an unstable equilibrium state which experimentally is not observable since $\partial\Pi/\partial h > 0$ [Kralchevsky and Nagayama, 2001]. The last intersection (point 3) corresponds to a Newton black film, which is a very thin film stabilized by short range steric interactions [Ivanov, 1988]. Figure 2.5 depicts a schematic diagram of these films. The top diagram schematically shows a Newton black film. All the films studied in this research are sterically stabilized. Since the main focus of this study is oil films formed between water droplets, electric double layer interactions can be considered negligible. Double layer repulsions usually happen in water films where free ions exist as depicted in Fig. 2.5b.

To break a stable thin liquid film, one needs to apply an external force to the film. The applied excess force will be counteracted by the disjoining pressure to maintain integrity of the film. Once the external force exceeds the disjoining pressure, the film will drain and eventually rupture. The excess force can be a mechanical pressure (which is commonly used in the TLF apparatus) or an electrical force due to an electric field applied across the film. In this study, electrical destabilization mechanism is utilized. The nature of this force will be discussed in Chapter 4.

2.1.2 Available Experimental Techniques

In this section two experimental techniques commonly used in thin film/emulsion studies are described. The first one, the thin liquid films (TLF) apparatus, is intended for film studies whereas the second experimental method, the bottle

test, is intended for bulk emulsion studies. The latter is primarily employed in industrial settings.

Thin Liquid Film Apparatus

Conventional experimental studies on thin film stability are generally performed on films of a liquid formed in a drilled cavity of a porous or solid substrate [Derjaguin *et al.*, 1954; Exerowa and Scheludko, 1971*a*], which is suspended in a second liquid. The thin liquid film apparatus (henceforth called TLF apparatus) depicted in figure 2.6 is a well-known and widely used system to create and study thin films. It employs a porous glass in which a millimeter size hole is drilled. The porous glass is soaked with oil and immersed in the second fluid (generally an aqueous solution). The film is formed in the hole by increasing the aqueous phase pressure. The two oil/water interfaces are pushed against each other and form the film. Using interferometry techniques, the thickness of the film can be measured accurately. In this technique, it is also possible to measure the film area, which is important in calculation of specific capacitance (capacitance per unit area F/cm^2). Panchev *et al.* [2006] added a pair of electrodes to the thin liquid film apparatus. Therefore, they conducted both electric breakdown and capacitance measurements of thin films of diluted bitumen in toluene.

The most important limitation of porous plate techniques is the limitation of minimum film area. The film cross-sectional area in these techniques is limited by the size of the cavity that can be formed in the substrate. Typically, the minimum size of the cavity is no less than a few hundred microns, which corresponds to a minimum film diameter of $250\mu m$. Such film diameters are observed in millimeter size droplets that are considerably larger than many emulsions observed in nature or industry. Miniaturization of these techniques have been attempted [Velev *et al.*, 1995; Pereira *et al.*, 2001], however, film diameters smaller than $100\mu m$ have not been achieved. Furthermore, the capillary pressure, and consequently, the equilibrium film thickness may be different than those observed in reality. This gives rise to the question as to whether models developed and

tested based on these techniques predicting phenomena such as film formation, thinning and breakup are applicable to microscale emulsion droplets.

Bottle Test

The common practice in industry to measure stability of emulsions is the "Bottle test" [Goldszal and Bourrel, 2000]. In this technique, the emulsion is formed by shaking a bottle filled with the two immiscible liquids and the surfactant. Once the emulsion is formed, its stability can be studied by monitoring droplet size distribution changes over time or by tracking the phase separation process.

In the petroleum industry, in particular, the bottle test technique is used to find the best de-emulsifier for water in petroleum emulsions. De-emulsifiers in oil industry are mainly polymer surfactants that change the interfacial properties of the oil/water interface so that the chance of coalescence increases. Following the formation of an emulsion, the bottle is left for a certain period of time, during which de-emulsification happens. This leads to liberation of water from the oil, the amount of which is the measure of the efficiency of the de-emulsifier. This test has to be repeated many times due to the different available de-emulsifiers and their wide spectrum of concentration. Furthermore, the type of crude oil varies from one reservoir to another, so finding the best match for every specific oil is a very time consuming task. Unfortunately, bottle test does not provide any quantitative insight regarding microscopics of the film or that of the emulsion. Figure 2.7 shows a photograph of a typical bottle test experiment. In the photograph, the bottles are filled with an emulsion of water in bitumen with different de-emulsifying agents. The black portion of each bottle on the top is the bitumen and the middle portion (white) is the liberated water. The test is based on qualitative measures such as clearness of the water phase or the height of each phase. Such vague and rough measures commonly used in industry necessitate development of new stability measures and measurement techniques.

2.2 Impedance Spectroscopy

Impedance spectroscopy may be defined as a technique for electrochemical characterization of interfacial processes. The basic concept of impedance measurement is described in Fig 2.8. In the figure, a simple R-C circuit is connected to an AC power supply. While the potential source dictates a potential difference (V) with defined frequency (ω), amplitude ($|V|$), and phase angle (ϕ_V) regardless of the driven circuit (assuming the power source is powerful enough), the current passing through the whole circuit is a function of both power source and the driven circuit. The current can be characterized by the amplitude ($|I|$), frequency (ω), and phase (ϕ_I). These parameters reveal a wealth of knowledge about the electrochemical characteristics of the system under investigation such as ability of the system to store or transfer charge. The frequencies of the current and potential are the same (ω), but amplitude and phase difference between potential and current constitutes the basis for calculation of impedance for a given frequency. The values measured for impedance, Z are in the form of complex numbers, containing real and imaginary parts.

$$Z = R + jX \tag{2.5}$$

The real part represents the resistance and the imaginary part is called reactance.

The history of impedance measurements goes back to the early days when electrical engineering was emerging. However, Cole and Cole [1941] were among the first who presented impedance data in real/imaginary plots which has become the modern way of impedance presentation ever since. Nowadays such plots are called Nyquist plot in which real and imaginary parts of impedance data are plotted as horizontal and vertical axes respectively.

Randles and Somerton [1952] used impedance spectroscopy to measure the reaction rate at the electrode/electrolyte interface. They developed a simple equivalent circuit for the double layer formed at the electrode/electrolyte interface. Sluyters and Oomen [1960] were among the first researchers who used

impedance plane plots for electrolytes.

By developing new tools and accurate electronics, impedance spectroscopy has become the method of choice in measurements. Many researchers used impedance spectroscopy for bilayer lipid membranes (BLM) which are reviewed in the next section. The theory of impedance spectroscopy is also addressed in chapter 5.

2.3 Electric Field and Thin Liquid Films

Electric breakdown of biological membranes has been widely studied during the last century, however, the prime focus of such efforts has been on reversible breakdown of membranes. The reversible breakdown (electroporation) is a phenomenon in which small holes are formed in a membrane temporarily. This happens due to a short pulse of electric field across the membrane, which lasts for few microseconds without damaging the integrity of the membrane. Electroporation is of considerable interest in molecular biology as a means of injecting molecules into viable cells without damaging them. However, if such potential is applied for a long period of time ($\sim$ 1 s) the membrane or the film ruptures permanently. Similarly, a thin film or a membrane undergoes a permanent breakdown, if a ramped DC potential is applied. The latter method (ramped potential) is the primary technique for rupturing films in this study. If a membrane ruptures permanently, the cell dies. Therefore, in studies related to electroporation of biological membranes, the focus has generally been on short potential pulses. This is why permanent breakdown of films or membranes using electric field has received little attention in literature. Therefore, studies on DC breakdown, particularly on thin films (not membranes) are extremely rare.

The first application of electrical measurements for thin films was conducted by Fricke [1925]. He investigated blood cell membranes using impedance measurements. Fricke roughly estimated the dielectric constant of the membrane, using which he calculated the thickness of the cell membrane ($3.3nm$). The only uncertainty in his measurements was the dielectric constant of the membrane,

however, his measurements had resolution of $1\mathring{A}$. Since Fricke was interested in thickness measurement of the membrane, he did not use DC electric field.

One of the first comprehensive investigations on the effect of electric fields on thin films and membranes was the work of Hanai *et al.* [1964, 1965]. They studied the effect of electric field on thin liquid films and conducted electric breakdown of thin films mediated by DC field. Hanai *et al.* also studied the capacitance of lecithin films using impedance measurements. They measured the specific capacitance (capacitance per unit area) and thickness of the film as $\sim 0.4\mu F/cm^2$ and $\sim 5nm$, respectively. They reported that the results of DC breakup suffered from poor reproducibility.

Babakov *et al.* [1966] studied influence of electric field on capacitance of phospholipid membranes. They concluded that the change in capacitance of the film is not due to compression, rather, change in area of the film causes increase in capacitance. Rosen and Sutton [1968] also studied capacitance and resistance of lecithin in n-heptane in presence of DC polarization but, unlike Babakov *et al.*, they correlated the change of capacitance due to the electric field to the compressive force of the field rather than change of area of the film. They also noticed that the capacitance of the membrane changes with electrolyte concentration for a given potential.

White [1970] conducted extensive measurements of capacitance of bimolecular membranes. He measured the capacitance of the film under DC polarization and confirmed Rosen and Sutton's finding regarding correlation of capacitance with square of the potential. He also investigated the torus or annulus of the film and took into account the film area expansion due to applied electric field [White, 1972; White and Chang, 1981].

Crowley [1973] developed one of the first theories explaining the behavior of bilayer lipid membranes under the effect of electric field. He modeled the membrane as a bulk elastic layer under the electric force. In other words, he assumed that the membrane is an elastic material such as a spring with a spring constant. Using Rosen and Sutton's measurements, he combined the Hooke's

law with the electric compressive force:

$$\Delta/L \simeq \frac{1}{2}\frac{\epsilon V^2}{E_Y L^2} \tag{2.6}$$

where L and Δ are thickness and change in thickness of the film. Potential, dielectric constant, and modulus of elasticity are represented by V, ϵ, and E_Y, respectively. This simple model confirmed Rosen and Sutton's observations which correlated change in capacitance to the square of the potential. Evans and Simon [1975] extended Crowley's simple modulus of elasticity idea to a full 3-D picture considering three elastic constants.

Zimmermann *et al.* [1974] studied electric break down of human and bovine red blood cells as well as *E. coli B.* They found the electric field at which break down occurs to be of the order of $4 \times 10^6 V/cm$. Coster *et al.* [1976] studied the effect of turgor pressure (osmotic pressure inside a cell) on the critical potential required for cell breakup. They found a linear decrease in potential with the increase of pressure. Zimmermann *et al.* [1980] extended Crowley's model and added the term for mechanical compressive pressure to account for cell internal pressure.

Following Hanai *et al.*, Kruglyakov and Rovin [1978, 1993] studied the effect of electric field on the film stability. They showed that application of potential difference across a thin liquid film reduces its life time. Furthermore, they showed that the film interfacial tension depends linearly on the square of the applied potential, confirming the results reported by Crowley [1973] and Requena *et al.* [1975].

Benz *et al.* [1979] were among the first groups to study reversible breakdown of bimolecular membranes systematically. They reported that if a high potential (well above critical potential) is applied across a film for a very short duration ($\sim 1\ ns$) the rupture of the film is reversible. Pethica and Hall [1982] analyzed the effect of DC polarization on membrane by means of thermodynamics. They clearly pointed out the lack of disjoining pressure measurement in experimental data and emphasized on necessity of its measurement for a comprehensive modeling. Chernomordik *et al.* [1983] studied reversible breakdown of membranes.

They studied the effect of a pulse potential on a membrane which results in a gradual increase in conductance. They reported a decrease of up to 7 orders of magnitude in resistance while the membrane is macroscopically intact.

Dimitrov and Jain [1984] categorized the basic characteristics of dielectric breakdown of films. They showed that the break down potential depends upon composition and structure of the membrane. They also reported that break down potential does not depend significantly on the pH of the aqueous phase. Finally, Dimitrov and Jain concluded that the critical potential depends on the exposure time or pulse duration as well.

Recently, Anklam *et al.* [1999] studied thin liquid films formed in water in oil emulsions stabilized by comb-graft copolymers. They conducted both DC breakdown and AC impedance spectroscopy in their experiments. They estimated the critical electric field at which the film breaks $\sim 10^7 V/m$. In their measurements, Anklam *et al.* noticed the leaky behavior of the film. In other words, although the film was seemingly intact, it showed substantial current leakage. Assuming formation of pores in the film, they estimated the number of holes to be one having a diameter equal to the film thickness.

The above review was aimed at describing the current understanding of electric breakdown of thin films. However, electric field has been used for breakup of polydispersed emulsions in petroleum industry. Cottrell and Speed [1911] filed the first patent on the application of electric field for coalescence of water in oil emulsions. Bailes and Laraki [1981 and 1987] also used the technique for separation of an aqueous phase from an organic phase. Recently, Midttun *et al.* [2000] studied the effect of crude oil resins on the stability of water in oil emulsions using time-domain spectroscopy in high external electric field.

2.4 Microfluidics

The concept of micro-total analysis systems (μ-TAS) was introduced in 1989 to integrate several steps of analytical processes into a micro fabricated fluid device [Manz and Becker, 1998; Bruin, 2000]. One of the first practical implementa-

tion of such devices was developed by Harrison *et al.* [1993]. Using chemical etching of glass, they formed microchannels on the glass substrates. Then, they utilized electroosmotic pumping to drive the flow and electrophoresis technique to separate sample components.

One of the earliest designs of microfluidic devices is comprised of a cross geometry channel as shown in Fig. 2.9. Two intersecting microchannels are etched on the glass substrate. Each channel has two reservoirs at the two ends, four in total. Two of the reservoirs are commonly used for the input liquids (such as sample and buffer) and two for wastes. Although this simple geometry is widely used, new generations are geared towards more complicated designs, incorporating electrodes, multi layers of substrates and more channels.

Recently, Chabert *et al.* [2005] studied electro-coalescence of two water droplets in a non-conducting surfactant free liquid. They incorporated a $560\mu m$ ID Teflon capillary tube as the experimental cell filled with the non-conducting fluid. Two water droplets ($\sim 560\mu m$ diameter) were injected in the tube. Electrodes were placed outside of the tube at 2 mm distance. They applied 2000V AC potential with the frequency up to 1 kHz.

Ahn *et al.* [2006] studied electro-coalescence of emulsion droplets in a microfluidic device. They developed a micro chip to coalesce two emulsion droplets in a microchannel. Figure 2.10 shows the schematic configuration of their design. The design consisted of two T-junctions to form two streams of water droplets dispersed in oil phase. Then the two streams unite into one stream to form doublets. Once the stream of doublets pass over the electrodes, an AC potential breaks the film and the two droplets coalesce. A similar experiment was conducted by Priest *et al.* [2006] where a series of water droplets in a microchannel were passed over a pair of electrodes (Fig. 2.11). The electrodes could fire and coalesce every pair of droplets selectively. Although the microfluidic devices developed by Ahn *et al.* and Priest *et al.* employ the principle of electric breakdown of emulsion films, they are however, rather focused on mixing applications. Their works do not include any measurements with regards to

thin films such as impedance measurements, thinning behavior or film stability.

2.5 Conclusion

In this chapter the background of thin liquid films and the basic concepts were described. The common experimental techniques along with their pros and cons were discussed. Conventional emulsion assessment techniques such as bottle test lack solid quantitative measure of stability while advanced thin film experiments such as TLF apparatus are not suitable for micron size film areas. Recent microfabrication developments have paved the road for small scale experiments, however, these experiments are generally intended for mixing applications and stability of the film has not been the focus of these studies.

In addition to thin liquid films, three other vital topics pertinent to the main subjects of the thesis, namely impedance spectroscopy, electric breakdown of films, and microfluidics were presented. However, more detailed theoretical background of DC breakdown and AC impedance spectroscopy will be presented in Chapters 4 and 5.

The review of existing literature showed the lack of research performed on micron-sized thin films. Furthermore, electric breakdown of the thin films are poorly studied and to our knowledge there is no similar work done in which electric breakdown is used as a measure of film stability.

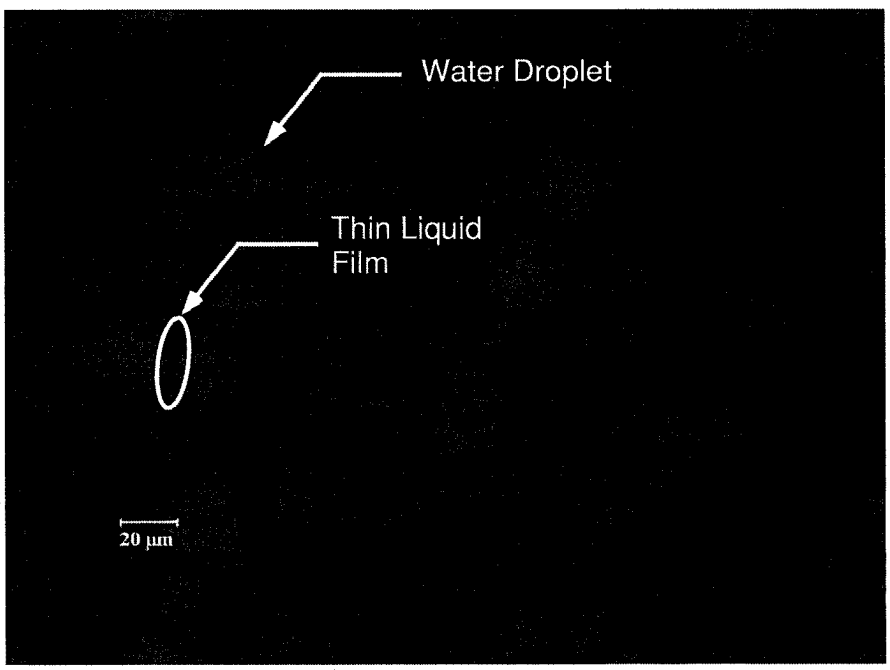

Figure 2.1: An oil/water emulsion system. A thin liquid film formed between two water droplets is circled. The oil phase is diluted bitumen in toluene.

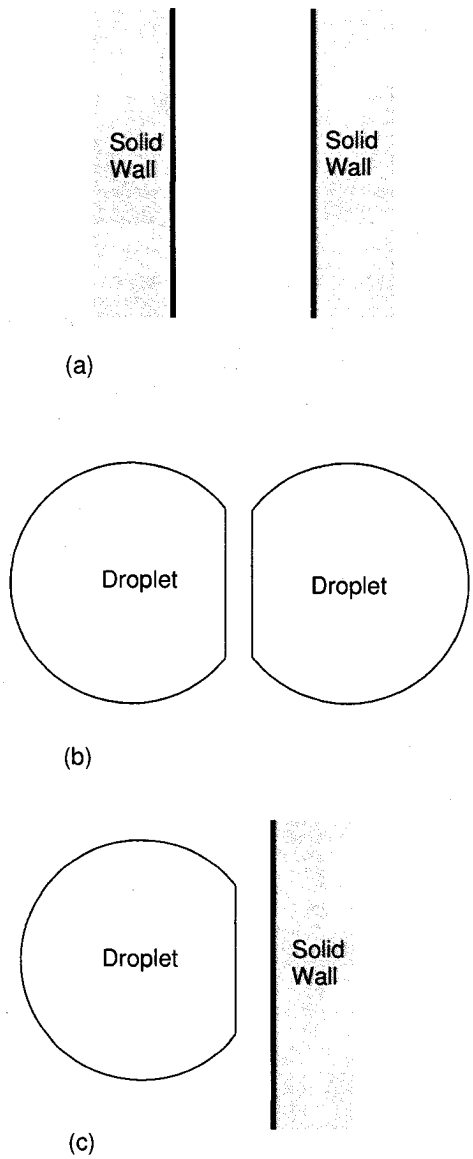

Figure 2.2: Three different scenarios in which films are formed. (a) A thin film formed between two flat surface. (b) Two droplets (or bubbles) separated by a thin film. (c) A film formed between a flat surface and a bubble/droplet.

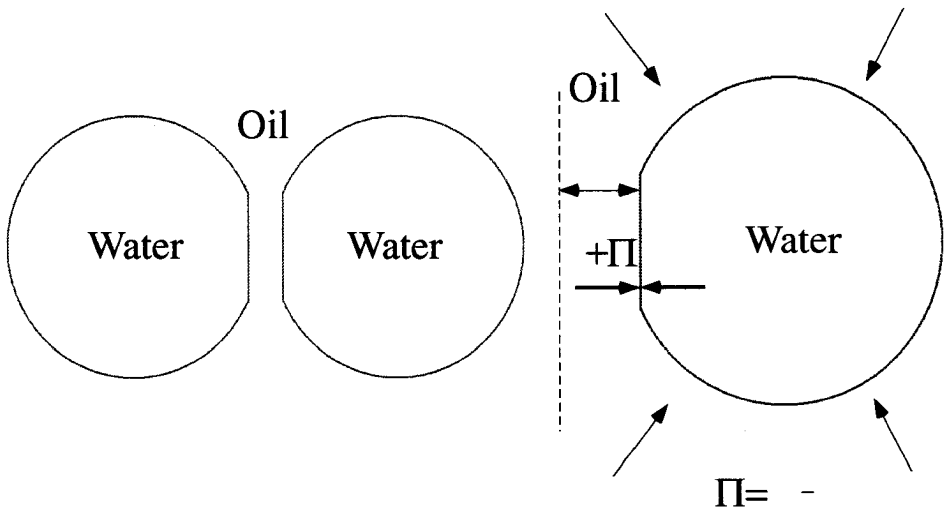

Figure 2.3: a) Two water droplets dispersed in an oil phase which forms a thin liquid film. b)The force balance on one of the droplets. The sum of the disjoining pressure Π and liquid pressure P_l balance the internal droplet pressure P_{in}.

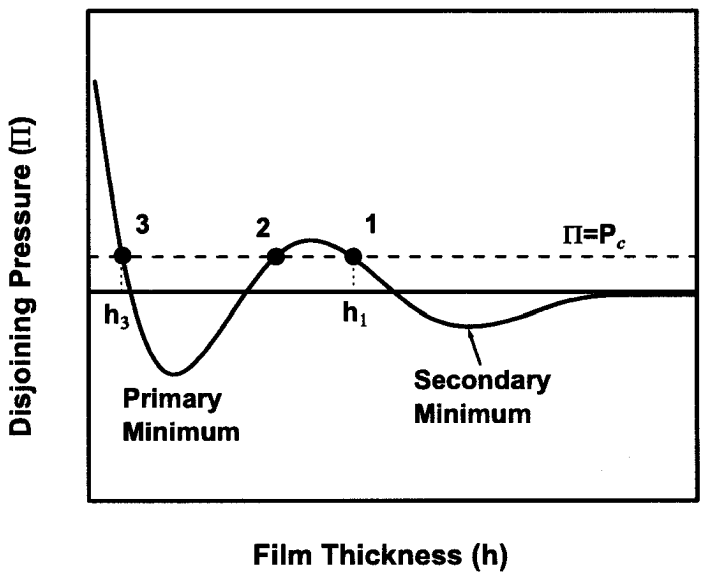

Figure 2.4: A typical disjoining pressure isotherm. The intersection of the line $\Pi = P_c$ with the isotherm determines the equilibrium conditions.

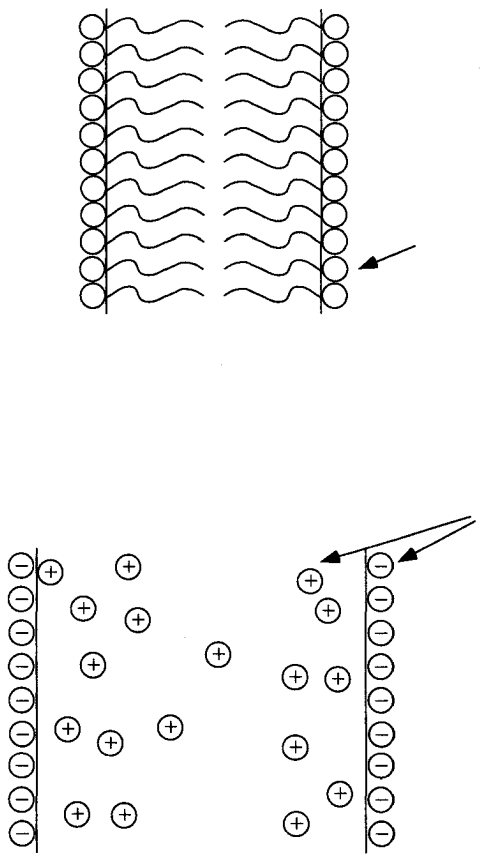

Figure 2.5: Schematic diagram two commonly observed films. (a) A Newton Black Film (NBF) which is stabilized by short range steric repulsion. (b) a Common Black Film (CBF) which is stabilized by double layer repulsive interactions.

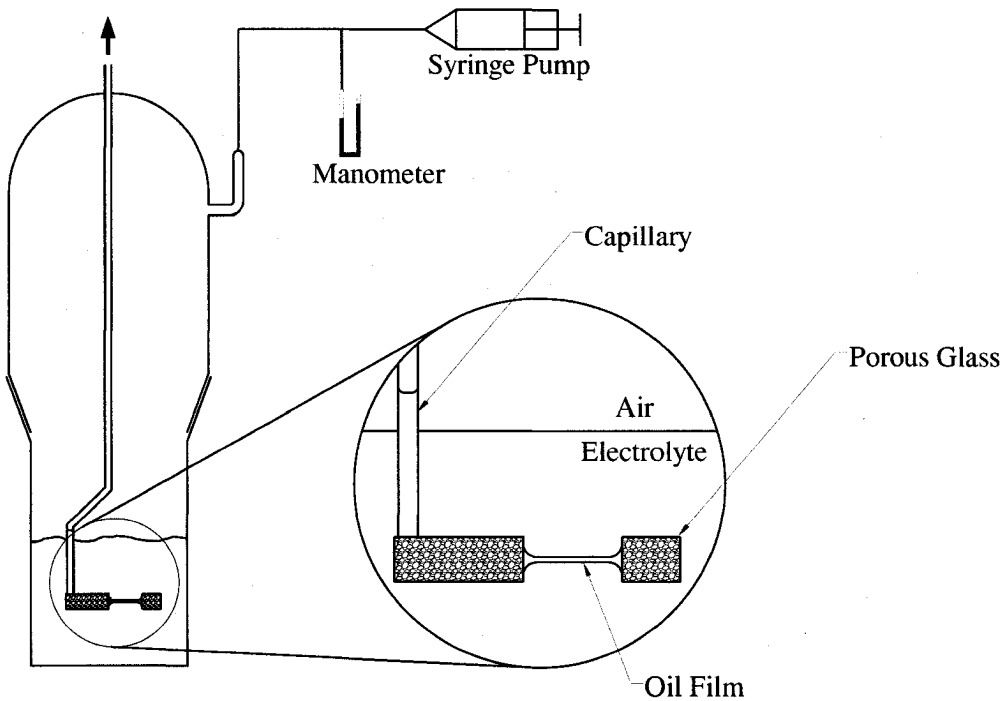

Figure 2.6: A schematic diagram of the "thin liquid film" (TLF) apparatus. The porous glass is soaked with oil and the film is created in the hole. By increasing the pressure of the water phase, the thinning process starts and the oil drains out to the capillary.

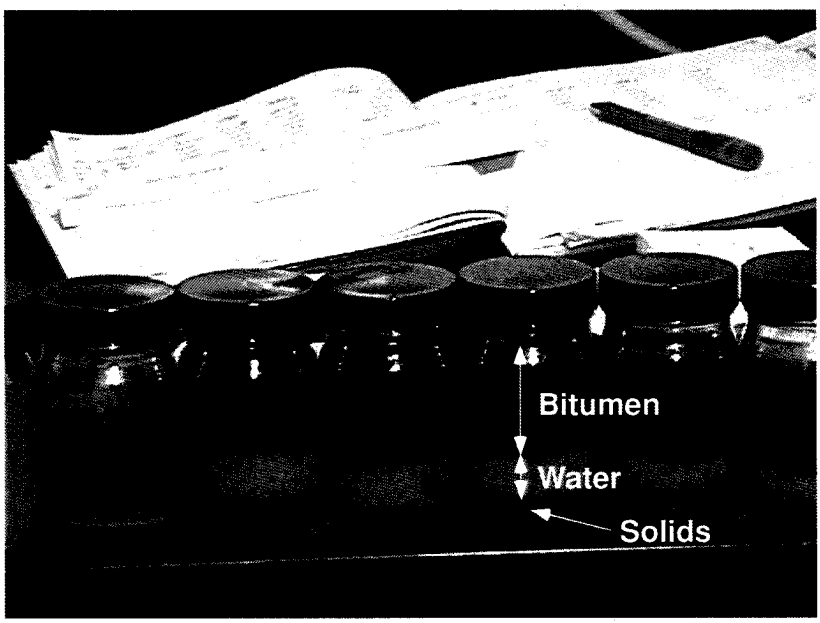

Figure 2.7: The bottle test. Bottles filled with emulsion are left for segregation. Courtesy of Tom Tran from Syncrude Ltd., Edmonton, Canada.

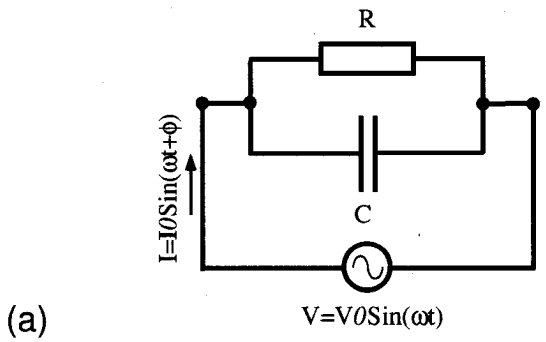

(a)

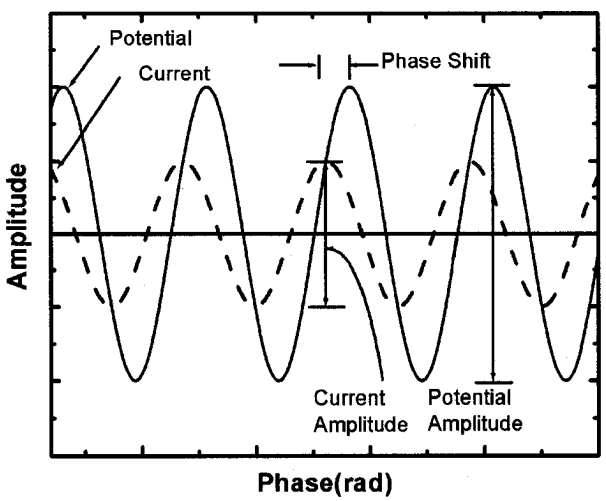

(b)

Figure 2.8: (a) A typical R-C circuit. The phase shift between current and potential is shown in (b). The solid line shows an AC potential with a known frequency and amplitude. The dashed line depicts the current. The difference between the phases and amplitudes of the two signal determines the impedance of the system for a given frequency.

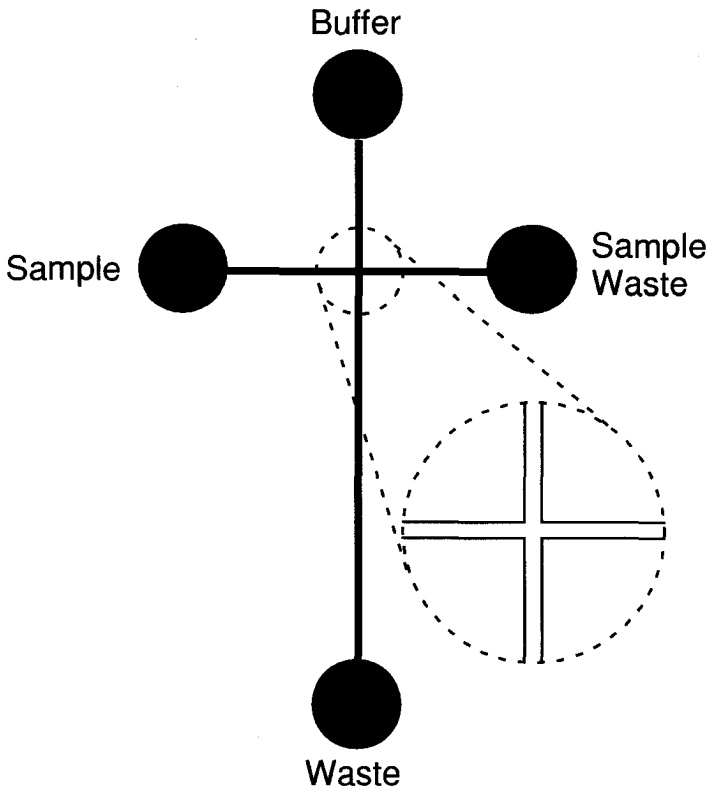

Figure 2.9: A typical cross geometry in microfluidic devices which was adopted in this research as the starting point.

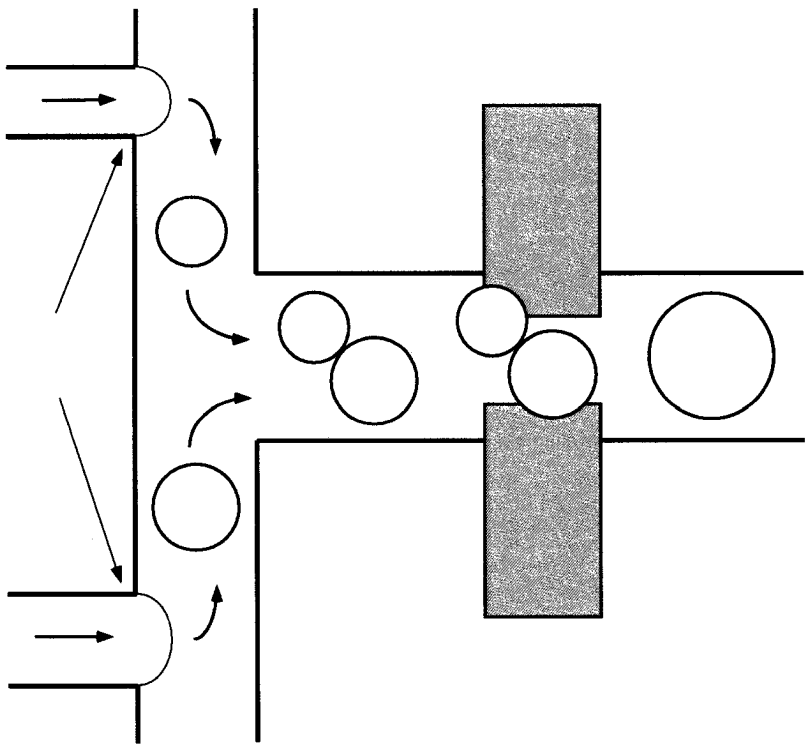

Figure 2.10: The design of the microfluidic system developed by Ahn *et al.* [2006]. The droplets are formed in the two T-junctions and fused on the electrodes.

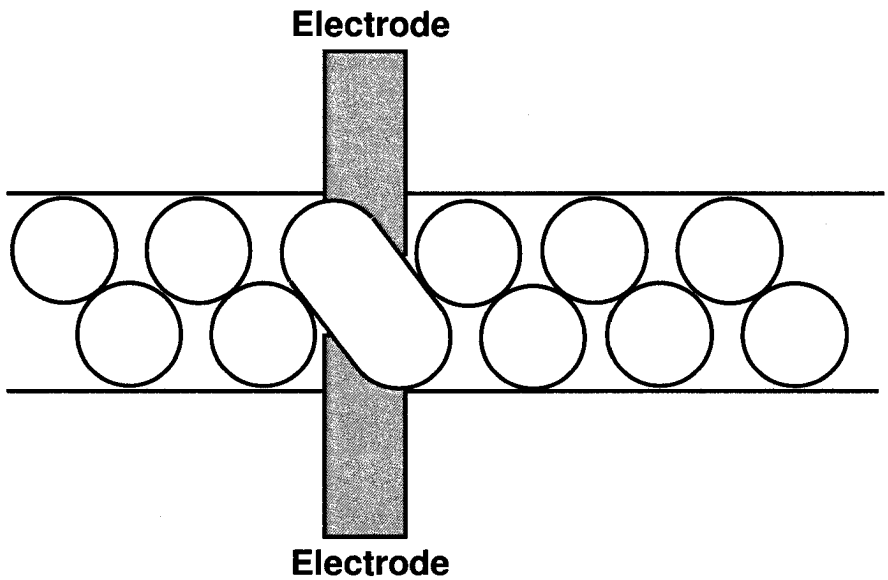

Figure 2.11: Schematic diagram of the microfluidic device developed by Priest *et al.*[2006]. An array of emulsion droplets are formed and electrodes perform targeted breakup.

Chapter 3

Microfluidic Chip Fabrication and Experimental Setup

3.1 Introduction

In this chapter, development of the microfluidic device and the experimental setup are discussed. First, the main objectives of development of the microfluidic device are introduced. Then the concept of the microfluidic device is discussed. It is important to note that, to the knowledge of the author, there is no similar microfluidic device or experiment reported in literature which is capable of forming micron-sized films. The final design is then detailed in the section entitled "Final Design". To achieve the desired stability and accuracy criteria in the device, a series of modifications both in the chip and the experimental setup were incorporated. These modifications resulted in substantial improvement in the stability of the formed interfaces.

The experimental setup is discussed in detail, followed by a brief description of the materials used in the experiments. In the last section, the experimental procedure for preparing the chip and forming thin liquid films of microscopic dimensions is described.

3.2 Microfluidic Chip Design Objectives

The primary objectives of the microfluidic device are to (i) replicate the conditions in which emulsion films (primarily water-in-oil) are formed between micron-sized water droplets and (ii) to measure stability of these films employing electrochemical destabilization and detection.

To achieve the above mentioned goals, extremely small oil/water interfaces have to be formed with a radius of curvature less $10\mu m$. Furthermore, these small interfaces with high pressure drops across them need to be moved back and forth in the microchannel in a controlled manner with a resolution of less than $5\mu m$. A conventional microfabrication technique [Gad-el Hak, 2002; Cheng and Kricka, 2001] is used to enable characterization of small droplets and films. Since high capillary pressure systems such as microchannels are more susceptible to pressure driven or electrokinetic flow, the design of the setup has to be in a way to keep a stable interface at the junction where two interfaces are close to each other.

Once the film was formed, a DC polarization voltage was applied across the electrodes placed in the water channels, which in turn de-stabilizes the film. Once the polarization potential exceeds a certain threshold, the film breaks. The breakup of the film is similar to discharge of a capacitor, which can be detected using an abrupt change in the current passing through the system. To apply the potential and monitor the current, a potentiostat can be used (see Fig. 3.1).

3.2.1 Design Concept

Figure 3.1 depicts the schematics of a microfluidic chip. Two intersecting channels delivering water and oil are embedded into the substrate. In the figure, channels A and B deliver aqueous electrolyte solution and oil respectively. The two immiscible liquids form two curved interfaces at the intersection. Once the two interfaces are formed, they can be pushed against each other, resulting in the formation of a flat thin liquid film, as shown in the Fig. 3.1. It should be

noted that when only two liquids are involved in the process of film formation (*e.g.* water and oil), a surfactant must be used as a film stabilizer, otherwise the film will not be stable.

Two electrodes are placed inside the water channels, creating an electrical contact with the electrolyte solution. The electrodes are connected to an external power source using two attached wires. The external source can apply a DC or an AC potential, while an electrometer in series can measure the current passing through the system. The response of the system to the DC and AC signals are of interest in this work and will be discussed in Chapters 4 and 5, respectively.

Using microfabrication and microfluidics [Harrison *et al.*, 1993; Cheng and Kricka, 2001] techniques, one can achieve small channel size. Employing conventional photolithography methods, it is feasible to fabricate features as small as a few microns in a glass substrate.

3.2.2 Final Prototype

The final configuration of the chip evolved over eight generations of design, fabrication and testing. The evolution of the final design and major modifications are explained in Section 3.4. In this section, the design features of the last two generations (7 and 8) are described.

Figure 3.2 is an SEM image of the generation seven microchip. All channels start with a wider section ($125\mu m$), then the width is reduced to the required size close to the intersection of the channels. The depth of channels in the micrograph is $8.5\mu m$. At the intersection, the width of the water and oil channels are $30\mu m$ and $20\mu m$, respectively. The tapered shape of the channels (particularly in water channels) plays and important role in stabilizing the system against external fluctuations such as thermal and pressure fluctuations.

Figure 3.3 is an optical microscope image of the intersection of the final (8th generation) chip. The horizontal channel is the water channel which includes the electrodes. The only difference between the last two generations is the

straight section of the water channel in version 7, which was discarded in the final version. The oil/water interfaces are schematically shown in Fig. 3.3 with dashed lines.

The wide straight section of the channels (the $125\mu m$ section) is 7.5mm long, connecting the input ports to the intersection of the channels. The thickness of the gold electrodes is $1\mu m$ placed on top of a 30nm chromium layer used as the adhesion layer. The width of electrodes at the wider section is $50\mu m$.

To maintain a robust control over the interfaces and improve the working condition of the chip, the oil channels are made hydrophobic by silanizing the substrate (using Trichlorosilane, Aldrich, USA), while the water channels remain hydrophilic.

Figure 3.4 depicts an exploded diagram of the microfluidic device. The substrates are made of glass. The bottom substrate contains the channels and electrodes, while the top substrate seals the channels and provides access to the channels through four drilled wells. Two input holes direct the electrolyte phase to the channels while the oil is injected through the third input hole well. The last hole is the exit of the system where all liquids can be drained out. The input tubes are connected to the chip using Nanoports® connections. The ports are glued to the top substrate. These provide a solid support for the nuts that connect the tubing to the chip. The size of the bottom substrate is $30mm \times 25mm$ while the top substrate is made slightly smaller than the bottom substrate with dimensions $25mm \times 25mm$. A photograph of the chip is depicted in Fig. 3.5.

3.3 Microfabrication

To fabricate the microfluidic device developed in this study, conventional photolithography and etching [Cheng and Kricka, 2001] technique was utilized. Figure 3.6 shows the three main steps of the technique. A conventional microfabrication process starts with thin layer deposition of a metal such as gold, chromium, aluminium, or titanium on the substrate. Once the layer deposits,

another layer of photo-sensitive polymer is spin-coated on the metallic layer. This polymer (or photo-resist) is sensitive to UV light. The pattern of channels or electrodes can be transferred to the photoresist using a mask. The mask is made of plane and transparent glass, except for the areas that are covered with chromium (electrodes or channels). The opaque parts protect the polymer from the UV light. Therefore, if the photoresist, covered with the mask, is exposed to UV light, the patterns on the mask are transferred to the photoresist. The exposed areas of the photoresist can be dissolved in a proper developer solvent, while the unexposed areas remain intact. Two separate masks were developed to transfer the patterns of the channels and electrodes onto the substrates. The masks were designed using L-Edit® software and produced using a DWL-200 (Heidelberg, Germany) laser mask writer.

After transferring the pattern to the photoresist, the etching of the exposed metal takes place. The substrate is immersed in a metal etchant which dissolves the metal through the small openings in the photo-resist. Following the etching process, the photoresist can be removed. This three-step cycle can be repeated as many times as needed. In the microfluidic device developed here, two complete cycles were employed; one cycle to form the channels and the second one to form the electrodes. Every microfabrication process, such as the one developed in this study, includes numerous intermediate steps that need to be considered. Details of these steps are provided in the next section and Appendix 1.

3.3.1 Fabrication of Bottom Substrate

Since the bottom substrate contains both channels and electrodes, it goes through the fabrication cycle (Fig. 3.6) twice. The first cycle was designed to etch the microchannels and the second one to form the electrodes.

After cleaning the substrate with Piranha (a mixture of 3 to 1 sulfuric acid and hydrogen peroxide), a 30nm layer of chromium and a 180nm layer of gold was deposited on the substrate using sputtering technique (Lesker, Germany). Since gold does not form a strong bond with glass, the chromium was applied

first to act as an intermediate adhesion layer. Following sputtering the metal layers, the substrate was spin-coated with a thin layer of photoresist HPR 504 (Fuji Film, Japan) followed by 30 minutes curing at 115 $^{\circ}C$. To transfer the patterns, a contact mask aligner (AB-M, USA) was used. The substrates were exposed to UV light for 4 to 5 seconds. After exposure, the substrates were immersed in diluted solution of developer Microposit 354 (Rohm and Haas, USA) for about 20 seconds. This dissolved the exposed areas of the photoresist, leaving the unexposed areas intact.

After careful examination of the patterns and their quality, they are ready for metal etching. Gold etching followed by chromium etching was carried out to get to the bare surface of the glass substrate. These two steps have to be conducted with care because the final size of the channels depends upon the quality and finished size of the features formed with the metal etching. The best glass etchant available is HF (hydrofluoric acid). Once the substrate was immersed in the HF solution, the etch rate was calculated several times by taking the substrate out of the solution and measuring the depth of the channel using an Alphastep 200 profilometer (Tencor, USA). When the depth of the channels reached the desired value ($8.5\mu m$ or $15\mu m$), the etching process was stopped and all of the remaining layers such as photoresist, gold and chromium were removed by appropriate etching. The etched glass substrate was cleaned using Piranha solution. The substrate at the end of this cycle consisted of two intersecting channels.

A second cycle of fabrication was necessary for patterning the electrodes. Similar to the first cycle, the second cycle started with deposition of chromium and gold. However, the thickness of gold layer was increased to $1\mu m$ to ensure good conductivity. The patterning process was similar to the patterning step described above. However, since the electrodes are placed at the bottom of the channels, there is a distance equal to the channel depth between photoresist layer and the mask. Therefore, diffraction of light could cause some difficulties in the quality of the pattern.

Once the patterns were formed, the electrodes were etched following the process described above. By removing the remaining photoresist from the substrate and proper cleaning (sometimes using cold Piranha), the substrate was ready for dicing. Each $4in. \times 4in.$ substrate contained 9 chips which were separated by cutting, employing a dicing saw.

To make the oil channel hydrophobic, it had to be silanized while the rest of the channels needed to remain hydrophilic. Therefore, partial silanization of the substrate was necessary. In order to silanize the oil channel, the water channels and the top surface of the substrate were masked with cover tape. Then the substrate was placed in a vacuum desiccator. Along with the substrates, a small beaker of trichlorosilane (Aldrich, USA) was placed in the desiccator for 2 hours. A layer of trichlorosilane would deposit on the oil channels and make them hydrophobic. After silanization, the bottom substrates were ready for bonding with the top substrates.

3.3.2 Fabrication of Top Substrate

The top substrate covers the bottom substrate and seals the channels. It also provides access to the microchannels through four holes. Therefore, fabrication of the top substrate was much easier than the bottom substrate. It includes the following three steps: drilling, dicing and silanization.

To drill the top substrates, two different methods were used. First, abrasive drilling using diamond coated drill bits (UKAM, USA) was employed. The diameter of these holes were $1mm$. There were 36 holes on each $4in. \times 4in.$ substrate ($9\frac{chip}{subst.} \times 4\frac{hole}{chip}$). Unfortunately, there was no programmable drilling machine available that could hold such small drill bits. Consequently, abrasive drilling would consume substantial amount of time. Furthermore, the recommended spindle speed by the drill bit manufacturer was 60,000 rpm, which was impossible to achieve using available machines, resulting in low quality of the holes and a greater chance of breaking the substrates during drilling. The second method utilized for drilling was a water jet technique. Using a programmable

water jet machine, up to 8 substrates were drilled together. Although the quality of holes was not uniform (some holes were oval), the water jet technique was preferred over abrasive drilling due to substantial savings in time and cost.

Once all 36 holes were drilled, the substrate could be diced into small pieces, each making a top cover of one microchip with four holes. Silanization was also necessary on the area that would cover the oil channel. Therefore, the top substrate was silanized similar to the bottom substrate. All parts of the substrate except the oil channel area were masked with cover tape and placed in the desiccator for silanization.

3.3.3 Assembly

Assembly of the microchip starts with the bonding of the two substrates. The two substrates were bonded using conventional glass bonding method which is based on attractive intermolecular Van der Waals forces. Two extremely clean and hydrophilic glass substrates with no particles in between can be bonded together by applying pressure. To make the bonding permanent, annealing can be used, in which case, the substrates are heated up to 500 $^{\circ}C$. However, due to some complications posed by this process, such as oxidation of electrodes and damage of the silanized area, no heat treatment was used.

The microfluidic device developed here includes three input ports (two input for water and one for oil) and one output port. The input connections are Nanoport assemblies (Upchurch Scientific, USA). They were glued to the surface of the glass using epoxy glue (Devcon, 5 Minute Epoxy, USA). Each electrode was connected to a wire using conductive glue (Conductive Epoxy, Circuitworks, USA) at the electrode pads.

3.4 Evolution of a Working Chip

3.4.1 Proof of Concept Experiments

A series of proof of concept experiments were conducted to study feasibility of forming interfaces and films in a microchannel. The first question facing this research was whether it would be possible to create a thin film of oil between two water interfaces in a microfluidic chip. The second goal was to determine the required instruments needed to perform the tests, particularly manipulating the oil/water interfaces with an accuracy of few microns.

To test the concept, standard microfluidic chips were purchased (Micralyne Inc., Canada). These chips were made of Borofloat glass with 1.1mm thickness each. They comprised of two intersecting channels $50\mu m$ wide and $20\mu m$ deep. These chips did not include electrodes. Figure 3.7 shows these standard chips. It also shows a schematic diagram of the chip's cross section.

Figure 3.8 depicts the results of these experiments. In the figure, the vertical channels carry the aqueous phase while the horizontal channel contains pure octane (Aldrich, USA). Since there was no added surfactant in these experiments, the film was inherently unstable. Figure 3.8 (a) to (c) depict that although two interfaces can be brought in contact at the channel intersection, it is extremely difficult to align them to form a thin film. The droplets often slid past each other. The film was asymmetric and no control on its shape could be exercised. Figure 3.8d depicts the intersection after coalescence.

This set of experiments revealed the difficulty of creating two interfaces at the intersection and the control of the interfaces with pumping small amounts of liquids. Following these experiments, the design and fabrication of the main experimental setup was initiated.

3.4.2 First Generation of Fabricated Chips

The first generations of the microfluidic devices are shown in Fig. 3.9 and 3.10. In the first figure, multiple electrodes are placed on the bottom substrate,

whereas in the second figure, just one pair of electrodes was deposited. The substrate was 0211 glass (Schott, Germany) with a thickness of $500\mu m$. Figure 3.11 depicts an SEM image of one of the designs. At the intersection of the channels, where the tips of the electrodes are placed, water wets the electrodes. At this point the gold electrodes have a narrow width ($\sim 10\mu m$). To connect them to the external circuit, the electrodes are passed over the edge of the channels to the top surface of the substrate where the width of electrodes increases to $50\mu m$.

Figure 3.12 shows the chip during a test. It is evident from the figure that the attempt to form the interfaces failed. It was impossible to form the interfaces and control their movements. Furthermore, since the pathway of the electrodes was placed on the top face of the substrate (at the wide end of the electrodes), bonding of the two substrates (top and bottom) was only possible when the thickness of electrodes was below $100nm$.

The preliminary design and configuration described above evolved into the final design of the chip and setup of the experiment after 8 iterations. These modifications included change of the substrate material, channel geometry and design, electrode design and thickness, and hydrophobic/hydrophilic treatment of the channel surfaces.

The most challenging aspect of design and fabrication of the microfluidic device developed in this work is the accurate control of the interfaces. Due to the nature of the microchannels, establishing a controlled stationary condition is a complex task. Since the radius of curvature is extremely small ($\sim 10\mu m$), the capillary pressure across the interfaces is substantially high. Figure 3.13 is a schematic diagram of the interfaces before and after film formation. Before film formation, using Laplace equation, the pressure drop across each oil/water interface can be written as follows

$$\Delta P = P_w - P_o = \gamma_{ow}\left(\frac{1}{R_1} + \frac{1}{R_2}\right) \tag{3.1}$$

where ΔP is the pressure drop across the interface, γ_{ow} is the interfacial tension of the oil/water interface, and R_1 and R_2 are the radii of curvature of the

interface. In order to form a uniform and flat film as shown in Fig. 3.13b, the pressure inside both water phases must be equal. Furthermore, all pressures must be kept constant during the time frame of the experiment. Therefore, the success of the experiment depends upon maintaining static condition at the intersection of the channels. Assuming stationary condition, all of the pressures are static pressures.

Consider the intersection of channels in Fig. 3.13. If the cross section of water channel at the intersection is $35\mu m \times 8.5\mu m$, then to push the interface $5\mu m$ forward, the volume that has to be injected is 1.4875 pico liter ($10^{-12}l$). Therefore, to move the interface with a resolution of $5\mu m$, one must maintain a resolution of a pico-liter over the volume of liquid in the water channels. Such a resolution imposes substantial complications in the design of the experiment. There are several other factors that can potentially destabilize the interface and prevent film formation. These effects are discussed in the next section.

3.4.3 Destabilizing Effects

Thermal fluctuations: Due to the extremely small channel size, any thermal fluctuations can cause movement of the interfaces. The sources of fluctuations can be change in room temperature, microscope light or simply a difference in the temperature of liquids. Apart from the microchip, which is made of glass, there are polymeric components in the system, such as tubing, that are more susceptible to volume changes due to substantially higher thermal expansion coefficients. Therefore, the volume of the liquids frequently change causing spontaneous movement of the interfaces. These fluctuations have much smaller time scale than the experiment.

Pressure fluctuations: Since the fourth hole or the drain of the system is open to atmosphere, any changes in the ambient pressure can affect the pressure balance of the system. There is also evaporation of the oil phase from the drain hole, which for lighter organic fluids such as toluene and n-decane used in this

study, can be substantial. The evaporation poses considerable problems due to temperature and concentration gradients, which in turn, result in liquid flow.

Adsorption: The interfacial tension of two fluids changes by the adsorption of surfactant. Increase of surface coverage of the surfactant corresponds to reduction in interfacial tension. Thus, either radius of curvature or pressure drop across the interface has to change. Under such circumstances, the curved interface moves to find a new equilibrium condition.

Electrical polarization: Stray electromagnetic waves can result in polarization of electrodes, thus affecting the precision of a test. In fact, preliminary experiments showed that electromagnetic waves emitted from surrounding instruments such as power supplies and fluorescent lamps can easily induce sufficient charge to spontaneously break a film.

3.4.4 Modifications

As mentioned earlier, holding the interfaces at a fixed position in the channels is extremely difficult. Unlike common microfluidic applications, where electrokinetic or pressure driven flow is desired, maintaining a static condition is crucial here. To improve the static condition inside the chip, few geometrical, mechanical, and chemical revisions were incorporated in the design. These modifications include both changes in chip design and in experimental setup over the course of a few generations/versions of development.

Modifications on the Chip

Silanization of the oil channel: The first modification employed after the first generation of the microchips was silanization of the oil channel. Glass is a hydrophilic material, so water wets the surface of the glass easily and controlling the interfaces becomes very difficult. It was also observed that in the presence of surfactants in the oil phase glass changes its hydrophilicity and the surface becomes heterogeneous, forming hydrophobic spots. This could happen

in matter of minutes, in which case film formation becomes impossible. By making the oil channels hydrophobic and having the water channels hydrophilic, the two liquids preferably stay in their respective channels and the formation of films becomes much easier. The last benefit of silanization is to reduce current leakage across the oil channel. Since glass is hydrophilic without silanization, water would wet the surface of the glass; therefore, there could be a leakage of current between the two electrodes through a thin wetting film of water in the oil channel.

Tapered channels: The tapered shape of the water channel (the horizontal channels in Fig. 3.3) plays a significant role in stabilizing the system. Since the microfluidic chip is prone to thermal/pressure fluctuations or interfacial tension changes due to adsorption, keeping the oil/water interfaces or the film at the intersection is a challenging task. In the case of straight channels, any temperature or pressure fluctuations will translate into substantial interface movement to compensate for the pressure changes, which is undesirable.

Referring to Fig. 3.3 or 3.13, it is discernable that as the water/oil interfaces are pushed toward the channel intersection through the convergent channels, the droplet curvature increases. According to Eq. 3.1, this will increase ΔP. Therefore, any small pressure or thermal fluctuation translates into curvature change of the oil/water interface within the tapered section. Therefore, the two interface can be kept within the tapered sections. In the case of a straight channel on the other hand, any pressure or thermal fluctuations causes significant displacement of the oil water interface, since the interface moves to compensate for the fluctuation.

Oil/water channel aspect ratio: It is important to note that at the intersection of the channels, the oil channel is much narrower than the water channels. If the oil channel is wider than water channels at the intersection, the interface tends to escape to the oil channel where exist a lower pressure thus, it is important to make the oil channel narrower than the water channel. In this

work, the minimum width of the oil channel is limited by microfabrication.

Evaporation: To reduce evaporation of the solvent from the drain, a custom-made reservoir was connected to the drain hole (Fig. 3.14). The reservoir has a large cross section ($\sim 50mm^2$) in comparison to that of the channel so that the static head of the liquid in the reservoir can be assumed constant. A very small hole is created on the top surface using a pin so that the pressure on the surface of the liquid in the reservoir is constant and evaporation is minimal. The reservoir is filled with the oil phase (containing a surfactant), therefore there is a substantial amount of the oil in the reservoir in comparison to the volume of evaporation.

Substrate material: In the first generation of the chips, 0211 glass was used as the substrate material. These glasses can be etched anisotropically, leading to the formation of trapezoidal a cross section with sharp corners, as depicted in Fig. 3.11. Those sharp corners are usually difficult to clean, therefore contaminated or hydrophobic spots may form. Borofloat glass on the other hand, delivers round corners since it can be etched isotropically, as depicted in Fig. 3.2. Hence, borofloat glass was used in the later chips.

Modifications of the Experimental Setup

Air cushion: To reduce pressure fluctuations inside the micro-channels, air reservoirs on the top of all working liquids were provided. Air, due to its compressibility, dampens pressure fluctuations and maintains a uniform pressure throughout the experiment. Figure 3.15 depicts the schematic diagram of the air cushions. A $2ml$ micrometer syringe, half of which is filled with the working liquid, was attached to the 3-way valves. The air pressure inside the micrometer syringe was also used for pressure measurements. Details are provided in Section 3.5.

Faraday cage: To reduce the effect of stray electromagnetic noise from the surrounding instruments, a Faraday cage was used. Without the cage, a persistent $60Hz$ noise was observed throughout the experiments. After adding the grounded Faraday cage, the disturbing effect of electromagnetic noise was reduced substantially.

Parallel resistor: As mentioned earlier, electromagnetic noise from surrounding environment can result in polarization of the electrodes and disruption of the film. Although a Faraday cage was provided to eliminate this effect, it proved to be insufficient. Therefore, a $5.6M\Omega$ resistor was placed in parallel with the chip to discharge the film. The resistor constantly discharges the capacitor from any instantaneous charge fluctuations except for the constant polarization provided by the potentiostat.

3.5 Experimental Setup

Figure 3.16 depicts flow chart of the experimental setup. The setup can be divided into three main sub-systems:

1. Fluid subsystem
2. Electrical subsystem
3. Visualization subsystem

Figure 3.17 shows a schematic diagram of the experimental setup. The fluid subsystem is designed to deliver the liquids to the chip. Furthermore, it allows for the measurement of the pressure inside each channel while maintaining a constant pressure on the liquids. It is comprised of the microfluidic device, manual microsyringe pumps, microsyringes, switching valves, micrometer syringes, pressure transducer and tubing. The electrical sub-system applies the polarization potential, measures of impedance and current, filters any electromagnetic noises, and acquires data. This sub-system includes the electrodes, Faraday cage, wires and connectors, parallel resistor, potentiostat/frequency response analyzer, and a computer. Lastly, the visualization subsystem provides optical feedback on breakup using an optical microscope. This subsystem is comprised of an inverted microscope, an anti-vibration table, CCD camera, video recorder and a monitor.

3.5.1 Fluid Subsystem

Three manual microsyringe pumps(World Precision Instrument, USA) were used, two for the electrolyte solution and one for the oil phase. Using a micrometer head, the manual microsyringe pumps are used to inject the fluids into the system. The fine resolution of the manual micrometer pumps (less than a micron) helps to maintain an accurate control over the fluid injected to the system. The success of measurements depends greatly upon the capability

of the system to maintain a very accurate control over the two oil/water interfaces. This has to be achieved despite the large capillary pressure due to very small droplet diameter.

The microsyringes used in the experiments are 10 and 50 μl glass syringes (Hamilton, USA). They are directly connected to the 3-way switching valves. Using 3-way switching valves, the microsyringes can be refilled.

Switching valves (Upchurch Scientific, USA) are used to direct the flow to or from the microsyringes. In normal condition, the 3-way valve connects all three elements (microsyringe, micrometer syringe and microchip) together, maintaining an equal pressure in the system. Since the microsyringes have very small volume ($\sim \mu l$), they have to be refilled once they run out of liquids. In that case, the valve closes the pathway between the microsyringe and the chip while the microsyringe and micrometer syringe are connected. Then the microsyringe can be filled from the micrometer syringe without altering the equilibrium condition inside the chip.

The micrometer syringes (Gilmont, USA) were used as reservoirs of liquids. The difference between "microsyringe" and "micrometer syringe" is that the former is a regular syringe with small volume (*e.g.* $10\mu l$), whereas the latter is similar to a micrometer in which the plunger moves back and forth by turning a thimble. Despite micrometer syringe's large volume (2.5 ml), a small amount of liquid can be injected to the system. Moreover, in the experimental setup developed here, micrometer syringes provide cushions of air on the liquids. The air cushions dampen any pressure fluctuation in the system due to thermal fluctuation. If there is any thermal expansion/contraction in the chip or tubing, the air cushion keeps the fluctuations to a minimum, due to air compressibility. Finally, the pressure inside the microchannel can be calculated using the pressure of the air cushion.

Since there is no flow during an experiment, the pressure is constant in every channel (taking into account the hydrostatic pressure due to the liquids inside the tubes and connectors). Therefore, one can measure the pressure in

the water and the oil channel separately. Care must be taken to keep the level of the liquid in the micrometer syringe equivalent to that of the microchannels so that the effect of liquid's hydrostatic pressure is canceled out (Fig. 3.15). The pressure difference between the oil and water phase is equivalent to the capillary pressure, as shown in Fig. 3.18. Since capillary pressure is equivalent to disjoining pressure when the system is in equilibrium, one can measure the disjoining pressure of the film in such high capillary pressure and small channel sizes by measuring pressure difference between the oil and water channels.

Because of the small cross section of channels at the intersection and the need for accurate control of the interface within a few micrometers, it is necessary to prevent any expansion or contraction of the system elements due to the applied pressure. Therefore, high strength components are used in all parts of the system. The tubing and connections used in the experiments are all manufactured from PEEK polymer (from Upchurch Scientific, USA) with 1/16" and 0.01" outside and inside diameters, respectively.

3.5.2 Electrical Subsystem

The electrical subsystem connects the gold electrodes to the electrical circuit and performs destabilization and frequency response measurements. Two wires are connected to the electrodes on the electrode pads. Since the polarization across the electrodes has to be kept constant during a test, a potentiostat was used. The electrochemical potentiostat used in this study was a Voltalab 80 (Radiometer Analytical, USA).

Impedance measurements were performed to estimate area of the film [Coster *et al.*, 1996; Hool *et al.*, 1998; Swayne *et al.*, 1998; Yaros *et al.*, 2003]. The impedance measurement instrument (or freqency response analyser) used in this study was primarily a Solartron 1260 (Solartron, USA) frequency analyzer. The Voltalab 80 was also used for some of the frequency response analysis. A frequency response analyzer applies an AC signal with known frequency and amplitude to the cell and measures the phase shift between current and volt-

age. Using this method, one can measure the impedance of the system over a frequency range. Further details of this technique are provided in Chapter 5. The Voltalab 80 can sweep frequencies from $1mHz$ up to $100kHz$, while the Solartron 1260 provides a wider frequency space from 1 μHz up to $32MHz$. A pentium II computer was used for data acquisition and to control the potentiostat and frequency response analyzer.

As described earlier, to discharge unwanted polarizations due to electromagnetic noise, a resistor ($5.6M\Omega$) was placed in parallel with the system. To reduce the effect of stray electromagnetic noise, a Faraday cage was mounted on the microscope. The cage consisted of a custom-made metal frame, wrapped in aluminum foil, which enclosed the chip. The microscope table was also covered with foil and connected to the cage, and the whole setup was grounded. Since the microscope lamp and lenses were outside of the cage, two small holes were pierced through the cage. A third opening on the foil was provided for the tubes and cables. Although these holes compromise the quality of the shield, the noise in measurement signals was reduced substantially.

3.5.3 Visualization Sub-System

An inverted microscope (Axiovert200, Zeiss, Germany) was used to acquire an optical feedback of the chip performance, film formation and breakup. Since the chip's fluid/electrical connections were all on the top, an inverted microscope provides a flexible platform for the chip. A CCD camera (KP-M22, Hitachi, Japan) was used to provide live video of the microscope image on a monitor. A VHS video recorder (Panasonic, Japan) was used to record the experiments. The microscope was placed on an anti-vibration table to reduce vibration, thereby increasing the stability of the system and avoiding unwanted film breakup.

3.6 Materials:

Four different systems were studied. The oil phase was toluene in all systems but the surfactant was different. A summary of the materials can be found in

Table 3.1.

3.6.1 Lecithin Experiment

This experiment was designed for complete DC and AC measurements. Lecithin was used for its wide applications in bioengineering and available studies in literature.

Water phase: The water used in this set of experiments was molecular biology grade distilled water (HyClone, USA) containing 1 wt. % ($0.1724M$) NaCl (Fisher Scientific, USA).

Oil phase: The oil was toluene (HPLC grade, Fisher Scientific, USA).

Surfactant: The surfactant used was soybean lecithin (L-α-Lecithin, Calbiochem, USA). The concentration was varied from 0.05 to 2 wt.% in toluene.

Preparation: It was recommended by the supplier to keep the lecithin in a closed bottle in a sub-zero refrigerator ($-20°C$). Fresh solution was made by dissolving the lecithin in toluene in desired ratio using a chemical balance. Care was taken to have all bottles cleaned so that no impurity could compromise the quality of the solutions. Preliminary experiments revealed that the age of the solution is a key factor, particularly in DC breakdown experiments. Therefore, every solution was prepared five days prior to experiment. Solutions were kept at room temperature during the aging period.

3.6.2 Bitumen Experiment (no de-emulsifier)

The bitumen experiment was intended to evaluate the capability of the experimental setup in measuring stability of an industrial emulsion.

Water phase: Deionized water with 1 wt. % NaCl (0.1724M).

Oil phase: Toluene (HPLC grade, Fisher Scientific, USA)

Surfactant: The surfactant was "Unitar" bitumen which is atmospheric topped bitumen that was produced with Syncrude's first generation cokers (Syncrude Canada Ltd., Canada).

Preparation: The bitumen solution was freshly made on the day of experiment. First, bitumen was diluted to the desired concentration in toluene. Then the solution was stirred for 30 minutes. Solids were separated using centrifugation. The solution was centrifuged at 13000 g for 30 minutes. After centrifugation the bottom part of the vial contained the solid contaminants. The samples were collected from the top half of the vial using a glass pipette.

3.6.3 Bitumen Experiment (with de-emulsifier)

Water phase: Deionized water with 1 wt. % NaCl (0.1724M).

Oil phase: Toluene (HPLC grade, Fisher Scientific, USA)

Surfactant: The bitumen was "Unitar" as in the previous section. A proprietary surfactant from Champion Technologies (Champion Technologies, USA) was used as a flocculating agent. Henceforth it will be called surfactant "A". This is the actual emulsion breaker currently being used at Syncrude's production facility at Fort McMurray. The de-emulsifier was a block copolymer.

Preparation: The supplied surfactant (chemical "A") was diluted in xylene to a concentration of 1,000 ppm as the first step. Desired concentrations were made by diluting the 1,000 ppm solution in toluene for each test. Centrifuged bitumen was freshly made using the procedure described in the Section 3.6.2. The surfactant (chemical "A") was mixed with the bitumen solution followed by 30 minutes of stirring.

3.6.4 TEGOPREN Experiment

The experiment with TEGOPREN was intended to compare the breakdown results with those of lecithin. Furthermore, TEGOPREN was used by Anklam *et al.* [1999, 2001] for similar experiments, therefore, the critical potential values could be compared with their results. Although, heterodispersity of TEGOPREN may pose difficulty in the interpretation of the experimental results, the comparison of its critical potential with those of lecithin films shows the wide spectrum of critical potentials and the versatility of the developed technique.

Water phase: The water phase consists of 1 M KCl (Fisher Scientific, USA) in molecular biology grade distilled water (HyClone, USA).

Oil phase: n-decane (HPLC grade, Fisher Scientific, USA)

Surfactant: TEGOPREN 7008 (polyether-alkyl-polmethyl-siloxane-copolymer, Degussa, Germany) is a water in oil emulsifier with substantial applications in food and cosmetic industries. It was diluted to 0.52 wt. % concentration in n-decane following the experimental procedure conducted by Anklam *et al.* [1999, 2001].

Preparation: TEGOPREN 7008, as received, was directly diluted in n-decane to 0.52 wt. %. No further purification or treatment was utilized.

3.7 Experimental Procedure

3.7.1 Preparing the Chip

The process of making a film in the chip started with filling up the chip with the liquids. The first liquid to be injected was the aqueous phase. In order to avoid any air bubble in the system, using a syringe (with needle), the holes and the Nanoports (Fig. 3.19) were filled with the aqueous solution. The filling procedure was intended to ensure that no bubbles would stay in the

system. Furthermore, water was sucked to the channel due to capillary action. The aqueous phase wetted the channel surface up to the point the surface was hydrophilic and water did not penetrate the oil channel. Subsequently, the oil phase was injected into the channels using the same approach. Since the oil channel was hydrophobic, the oil would wet the surface of the oil channel completely. The drain port also were filled with the oil.

Once all of the ports were filled, then the tubes were connected to the ports. One has to ensure that there were no air bubbles in the tubes by flushing the system before connecting to the ports. After connecting the tubes, the drain reservoir, which was filled with the oil phase, was placed on the drain port.

Following the connection of all ports, the microfluidic chip was placed on the microscope table. The electric wires were then connected to the resistor parallel to the potentiostat/frequency analyzer using crocodile connectors. Then the Faraday cage was placed to shield the assembled chip.

3.7.2 Film Formation

Before describing the process of forming the films, there are two important concepts that need to be clarified. These concepts are "Adsorption Time" and "Drainage Time" as discussed below:

Adsorption time [Ivanov, 1988; Exerowa and Scheludko, 1971*b*; Khristov *et al.*, 2000; Taylor, 2002; Anklam *et al.*, 1999*a*; Anklam *et al.*, 2001] is the time between formation of the oil/water interfaces and the film. This is the timeframe that most of the surfactant adsorption to the interface happens.

To maintain a uniform surface coverage of surfactant, the two oil/water interfaces were formed, as depicted in Fig. 3.13a. They were kept stationary at their position for a certain amount of time, which is called adsorption time. Keeping the surface coverage constant is an important parameter in thin film experiments as it affects equilibrium thickness, thinning speed and stability. The adsorption time can be controlled either using time measurements or by monitoring capillary pressure, since the adsorption correlates with interfacial

tension.

Drainage time[Ivanov, 1988; Exerowa and Scheludko, 1971*b*; Khristov *et al.*, 2000; Taylor, 2002; Anklam *et al.*, 1999*a*; Anklam *et al.*, 2001] is the time over which the thinning process takes place. In other words, this is the time after forming the film and before applying the electric potential. It is depicted in Fig. 3.13b. After formation, the film was kept stationary for drainage to take place. Within this time frame, the attractive interaction forces reduce the thickness of the film to an equilibrium value.

Once all connections were established, films were formed repetitively. The two water/oil interfaces were brought close together for adsorption to take place. It was important to keep the two interfaces as close as possible during the adsorption time (before forming the film) because a large deformation just before film formation would yield a substantial and nonuniform reduction in surface coverage. During the adsorption time, the interfaces were kept under constant observation due to movement of interfaces. The movement of the interfaces was due to slow adsorption process. The adsorption of surfactant to the interface corresponded to change of interfacial tension. Since the pressure in both water and oil channels were constant (due to connection to large reservoirs), the interface had to change its curvature or move to balance the pressure difference. Usually for such systems, the adsorption time until the equilibrium condition is reached can be in the order of hours. Parallel experiments with "Thin Liquid Film Apparatus" [Panchev *et al.*, 2006] on large area films ($\sim 500\mu m$) showed that, for lecithin and bitumen, this time is well over 10 minutes. For micron-sized interfaces, such as those studied in the microchip, the adsorption time can be as short as 2 minutes.

After the adsorption period, the two interfaces were brought together to form a film. One has to ensure that no flow condition exists in the oil channel. The film formation step needed to be carried out gently to avoid possible dimple formation [Ivanov, 1988]. Once the film was formed, its size was changed by adjusting pressures in the water channels. It was important to maintain a static

condition during the drainage time, since any changes during this period could affect the results of the test. Figure 3.20 depicts a typical film formed in a chip. Following a fixed drainage time, the film was ready for breakup due to the applied electrical potential. The results of DC breakup and AC impedance spectroscopy on these films are discussed in Chapters 4 and 5, respectively.

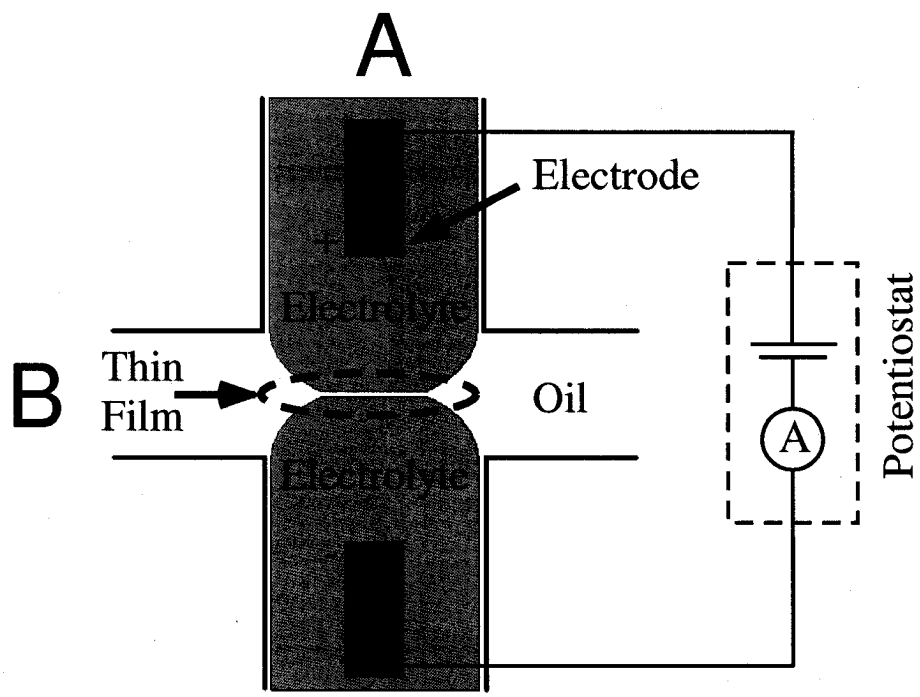

Figure 3.1: Schematic diagram of the microfluidic experimental setup. The microchip consists of two intersecting channels. Channel "A" delivers the aqueous electrolyte and Channel "B" delivers the oil phase. Electrodes are placed in the water channels. A potentiostat applies the programmed polarization across the electrodes and measures the current passing through the system.

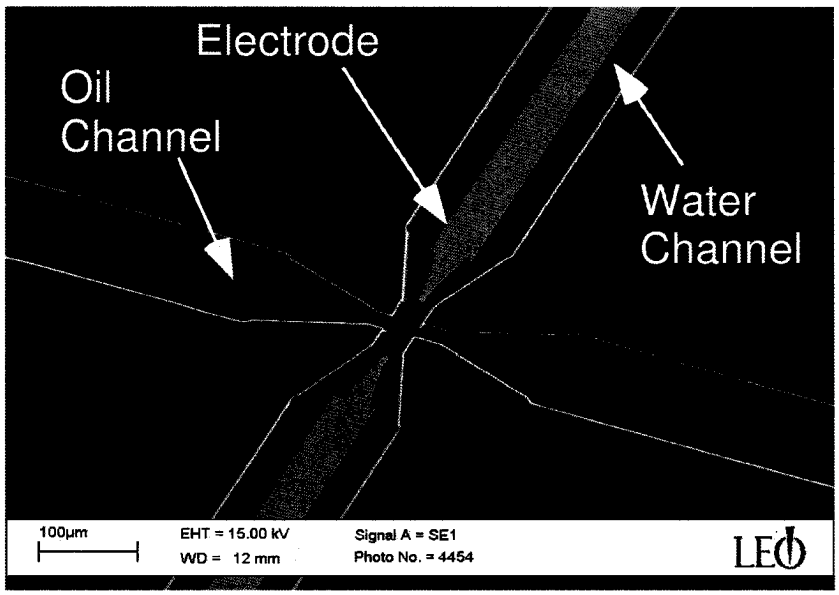

Figure 3.2: SEM image of the microfluidic chip. The electrodes are placed in the water channels. At the intersection, the size of oil and water channels are $20\mu m$ and $30\mu m$, respectively. The width of each channel increases to $125\mu m$ away from the intersection.

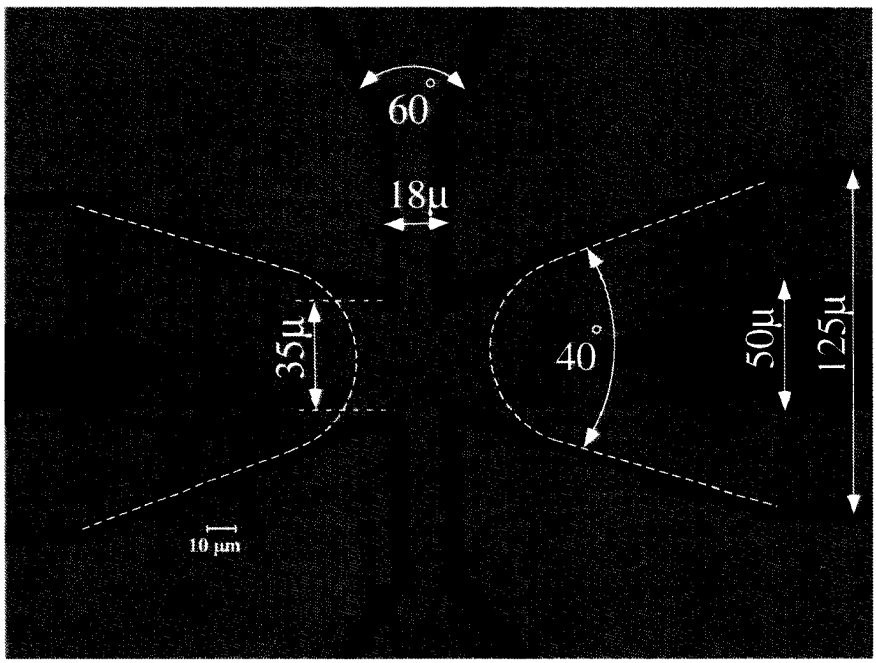

Figure 3.3: An optical microscope image of the chip. The depth of the channel is $8.5\mu m$ in this particular chip. The tapered shape of the water channels plays an important role in stabilizing the interfaces. The dashed line schematically shows the oil/water interfaces.

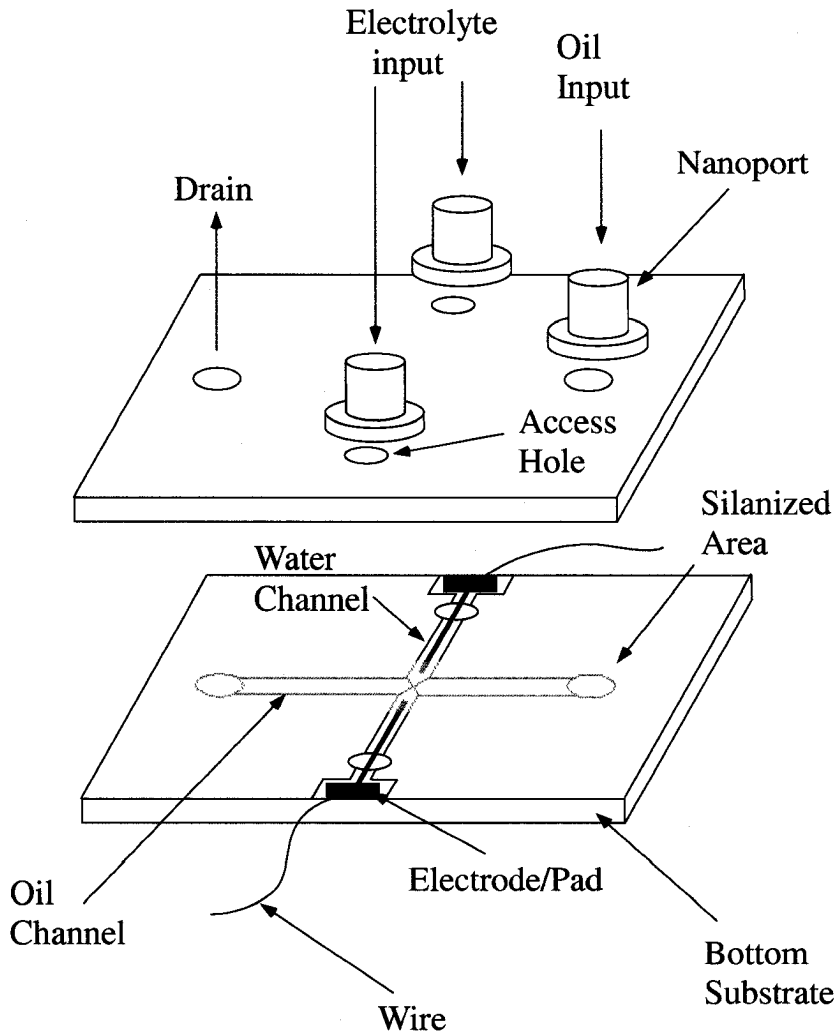

Figure 3.4: A schematic drawing showing an exploded view of the microfluidic device. The top substrate provides access to the channels through 4 drilled holes. The substrates are bonded together using conventional glass bonding technique. The Nanoport assemblies are glued to the top substrate. The hydrophobic region is shown in gray.

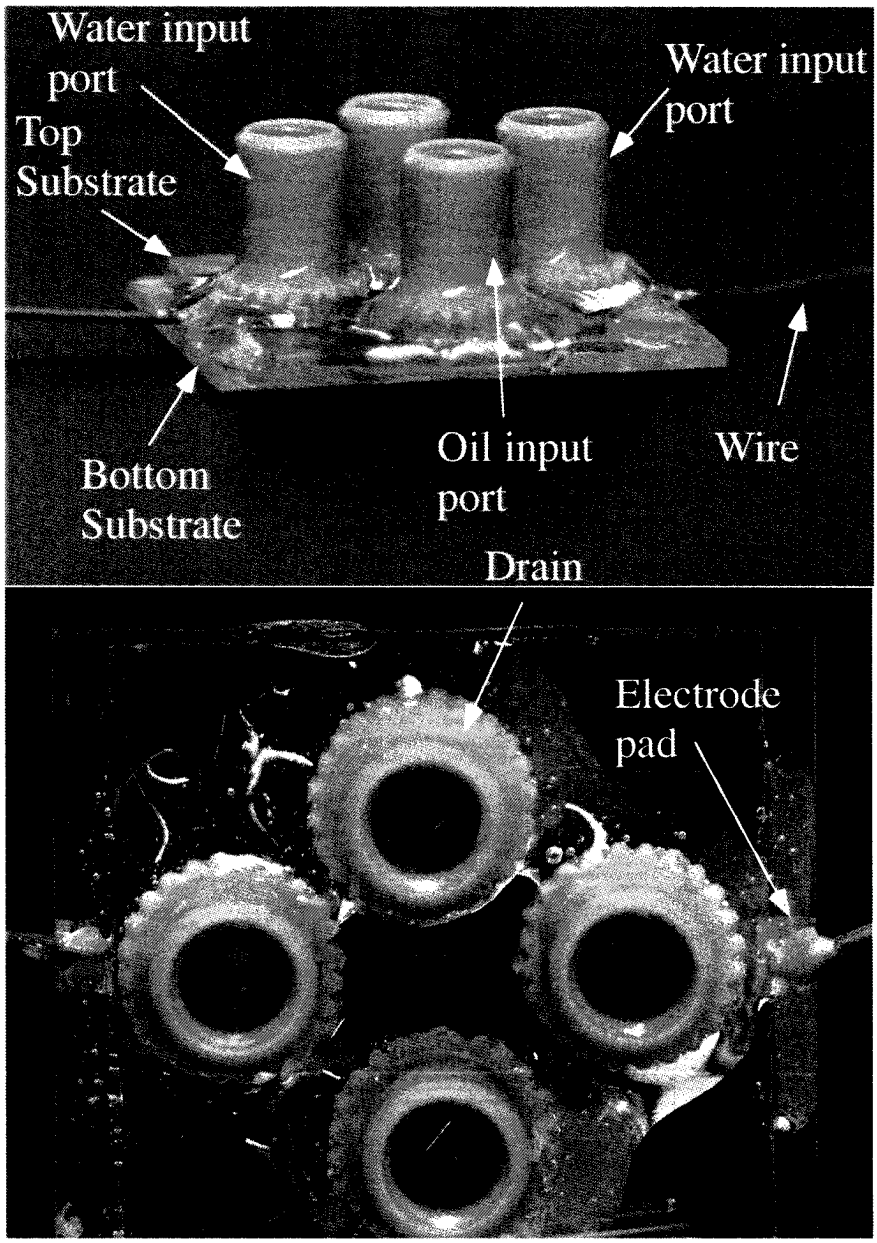

Figure 3.5: A photograph of the final prototype.

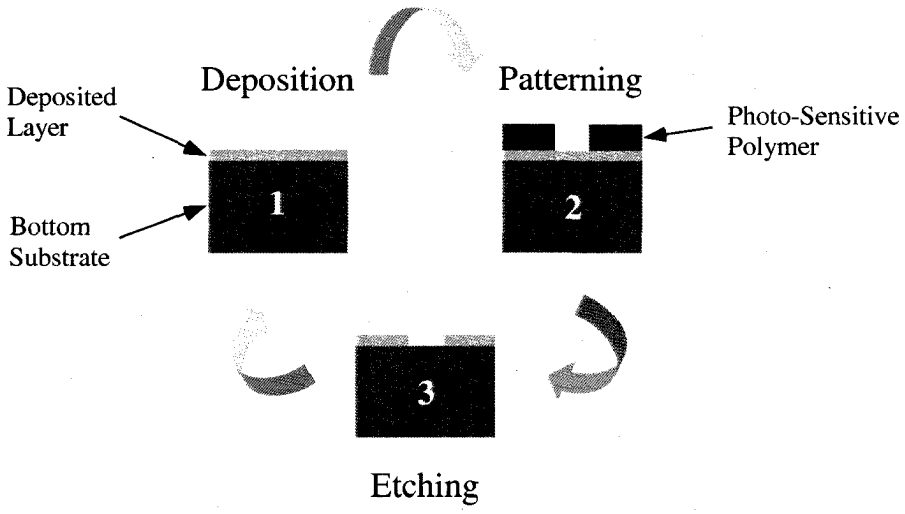

Figure 3.6: The three major steps in conventional photolithography microfabrication. These steps can be repeated as many times as required.

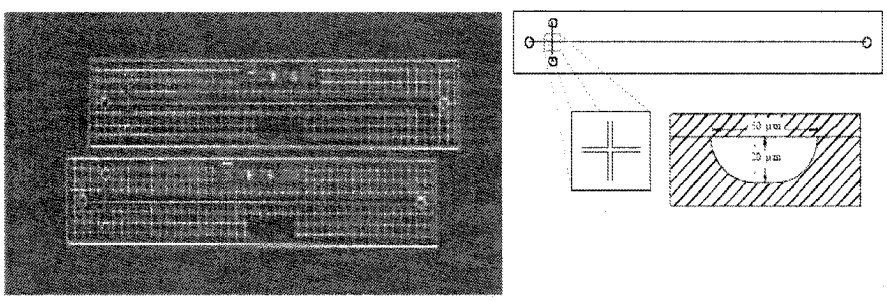

Figure 3.7: Standard microfluidic chips from Micralyne Inc. The crossing channels and the access holes are depicted in the schematic diagram. The cross section of the chip is also shown in the bottom right photograph.

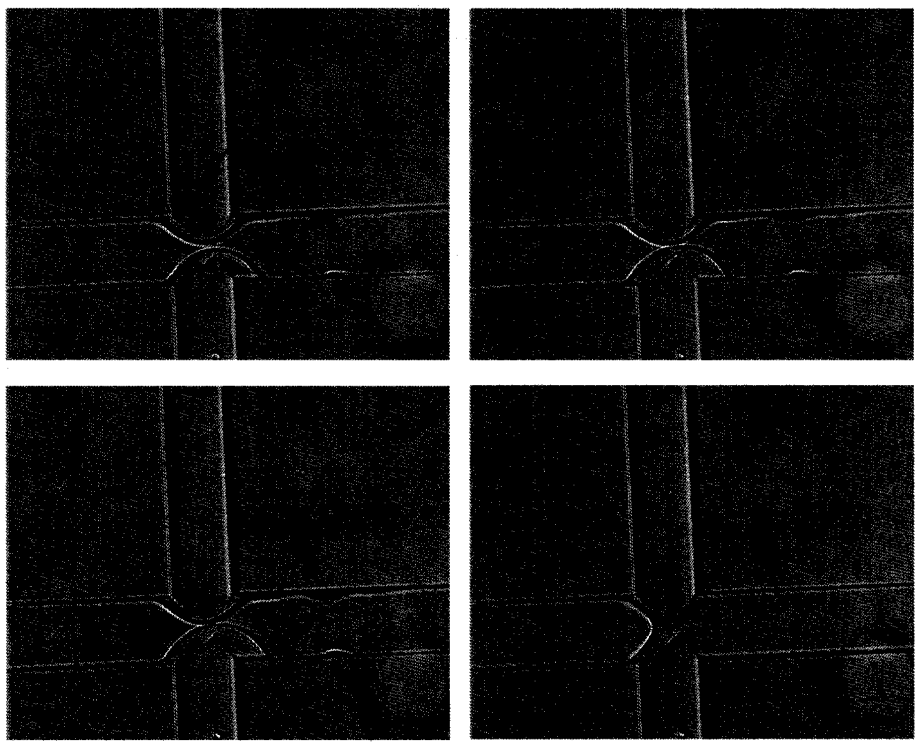

Figure 3.8: Two oil/water interfaces were created in a standard chip under the microscope. The aqueous phase is deionized water and the oil phase is octane. Figures a, b and c show the two oil/water interfaces brought together, whereas in Figure d the two interfaces have coalesced.

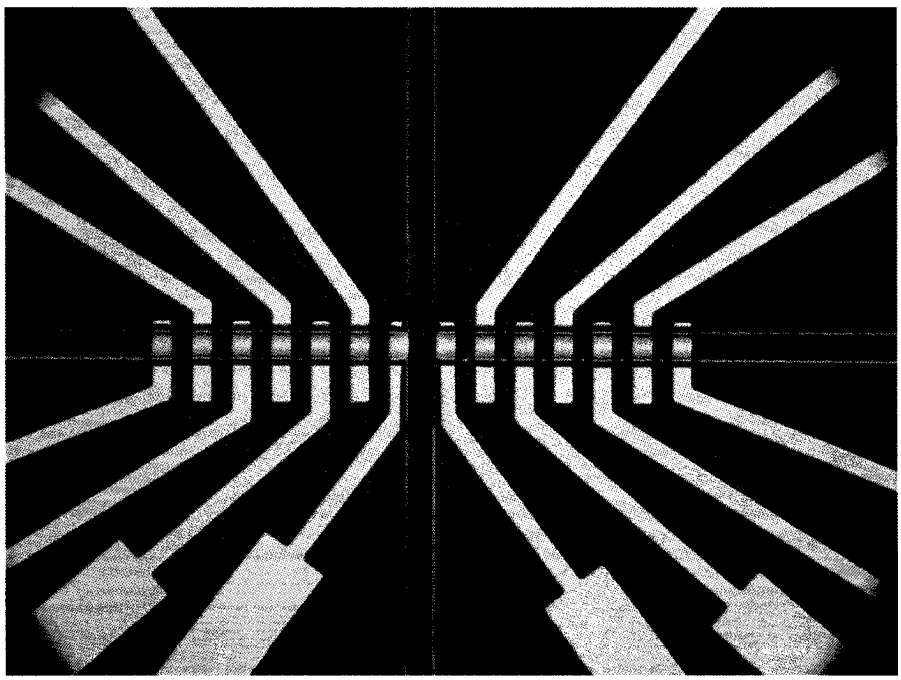

Figure 3.9: An optical microscope image of the first generation chip with multiple electrodes. The substrate material is 0211 glass ($500\mu m$ thick) and the thickness of electrodes is $80nm$.

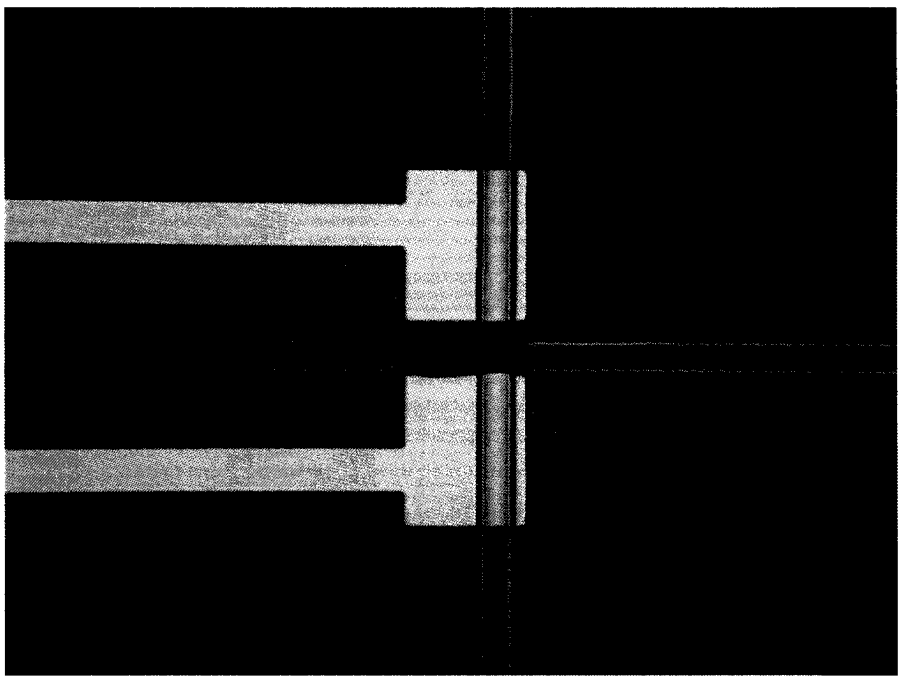

Figure 3.10: An optical microscope image of the second generation chip with single pair of electrodes. The substrate material is 0211 glass ($500\mu m$ thick) and the thickness of electrodes is $80nm$.

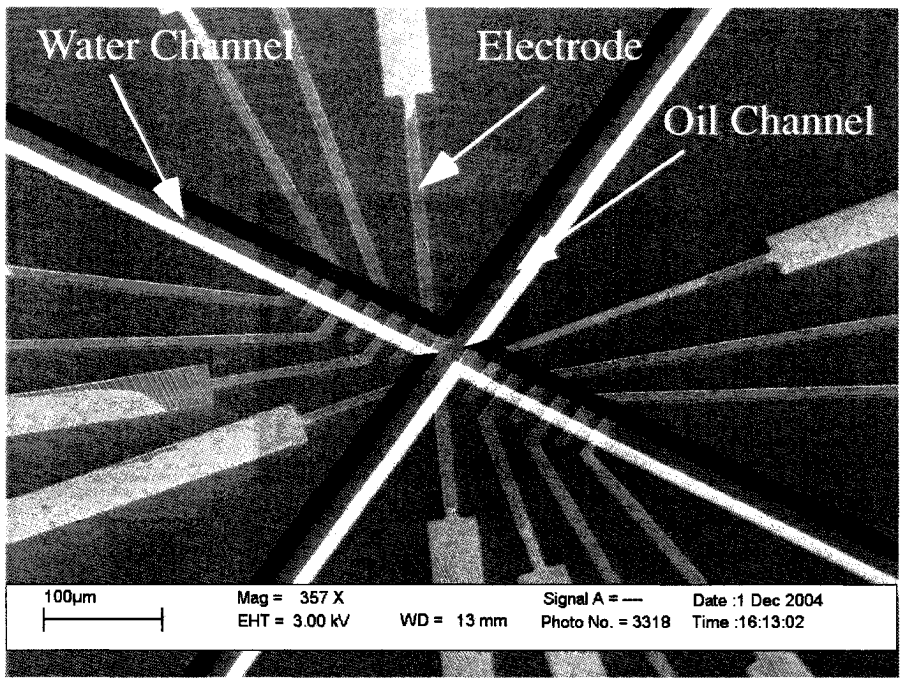

Figure 3.11: An SEM image of the first generation of the chip. The cross section of the chip is trapezoidal with sharp corner.

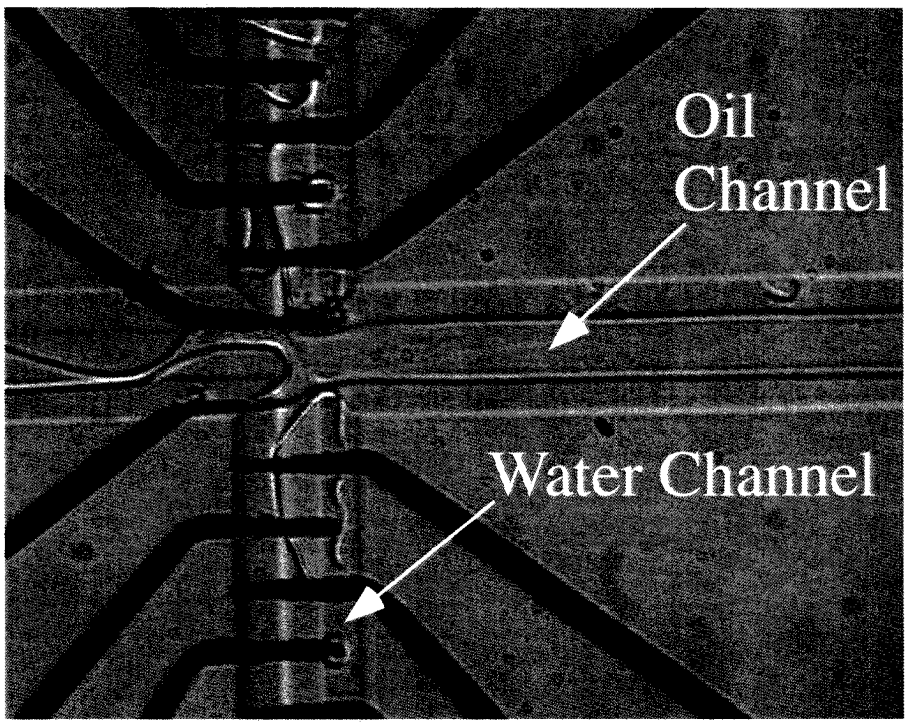

Figure 3.12: An optical microscope image of the experiment with the first generation of chips. It is evident from the image that attempts to form oil/water interfaces at the intersection failed. Furthermore, the image shows substantial heterogeneity of the channels surface. The aqueous phase is deionized water and the oil phase is decane.

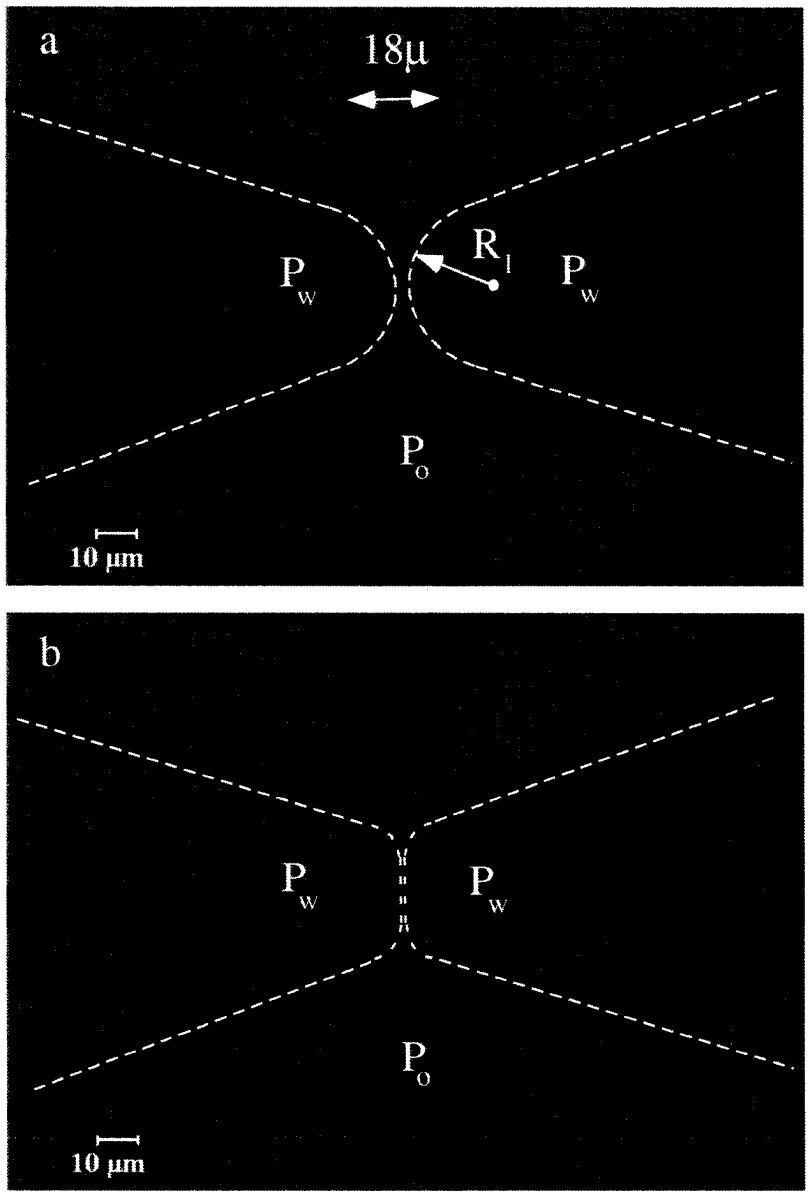

Figure 3.13: Intersection of channels in the final design. The dashed lines schematically show the oil/water interfaces before and after film formation. To maintain a stationary condition, all pressures (P_w and P_o) have to be constant during the experiment. One of the radii of curvature before film formation is shown as R_1. The second radius of curvature (R_2), which is in a plane normal to the plane of image, is not shown.

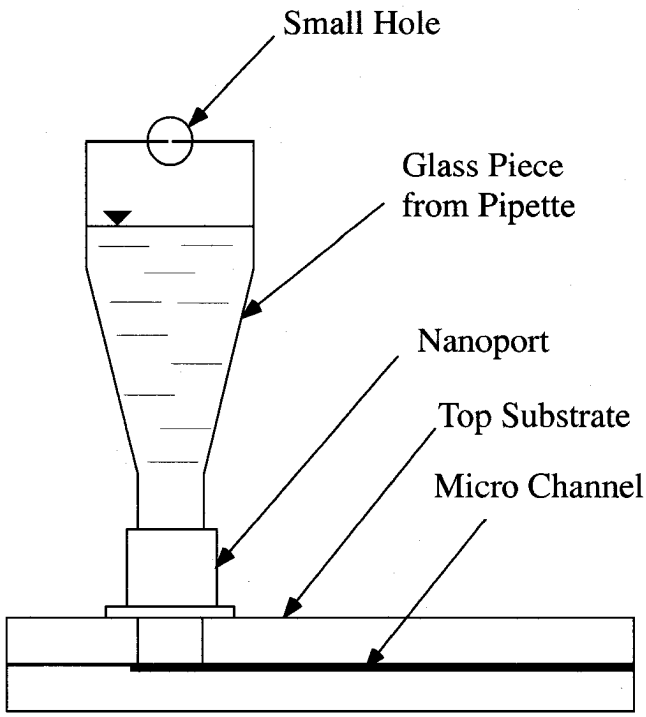

Figure 3.14: A schematic diagram of the drain hole. A glass piece that is made from a pipette is filled with the oil phase. The small hole on the top of the glass piece maintains an atmospheric pressure inside piece while minimizing evaporation of the solvent.

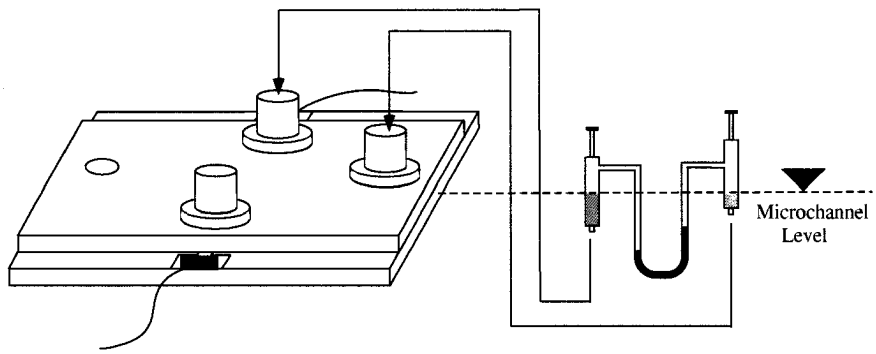

Figure 3.15: To cancel the effect of hydrostatic pressure in the connecting tubes, micrometer syringes are placed at an elevation such that the liquid inside the syringe is at the same level as that in the channels.

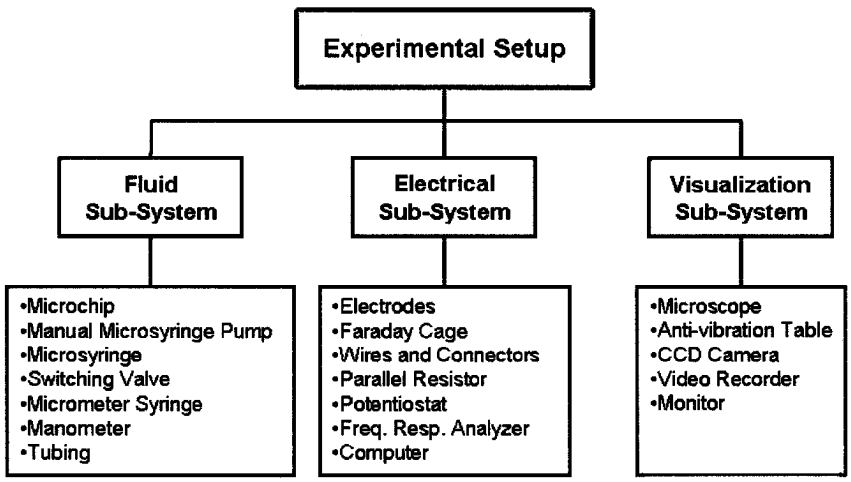

Figure 3.16: A block diagram of the experimental setup. The system is divided into three subsystems; fluid, electrical and visualization.

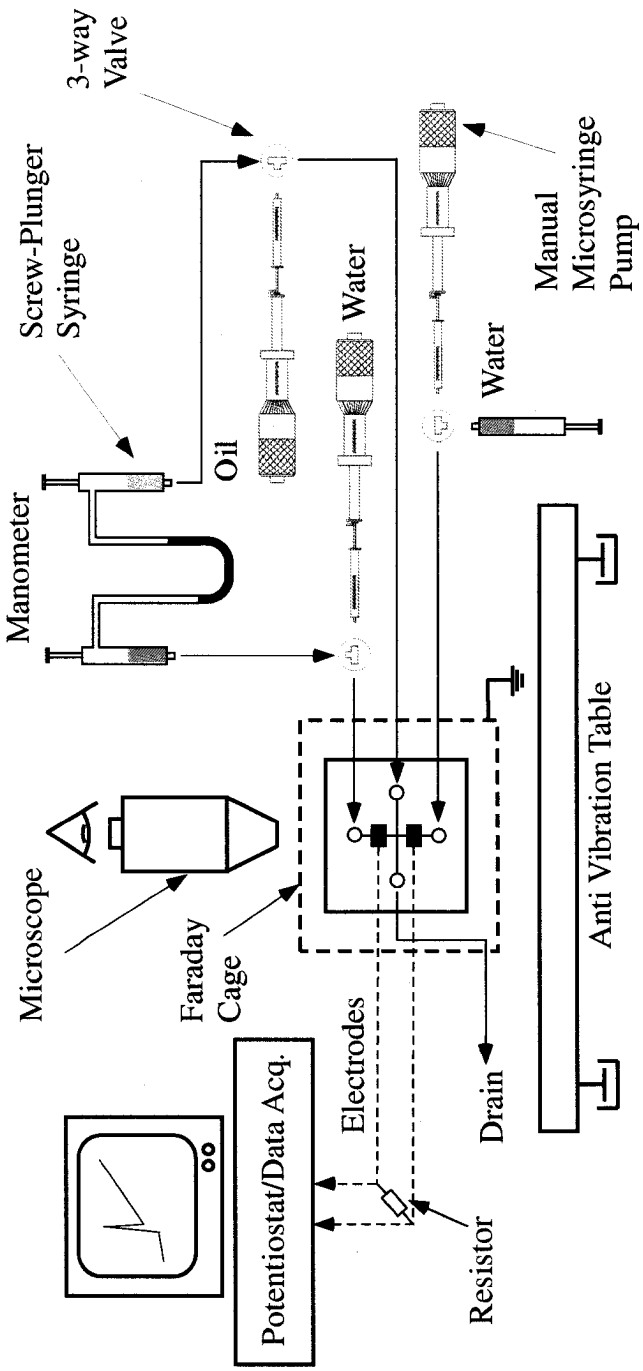

Figure 3.17: General layout of the experimental setup. Three sets of manual microsyringe pumps pump the fluids to the microchip. Electrodes are connected to the potentiostat/data acquisition.

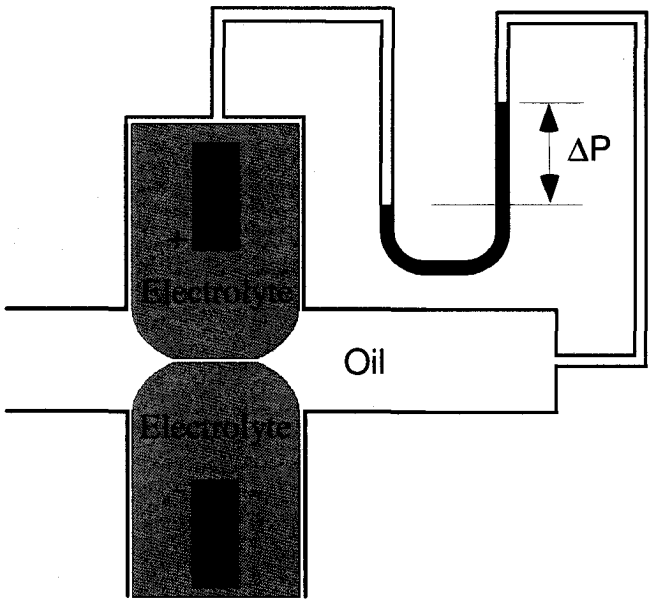

Figure 3.18: The pressure difference between the two channels is equivalent to the capillary pressure.

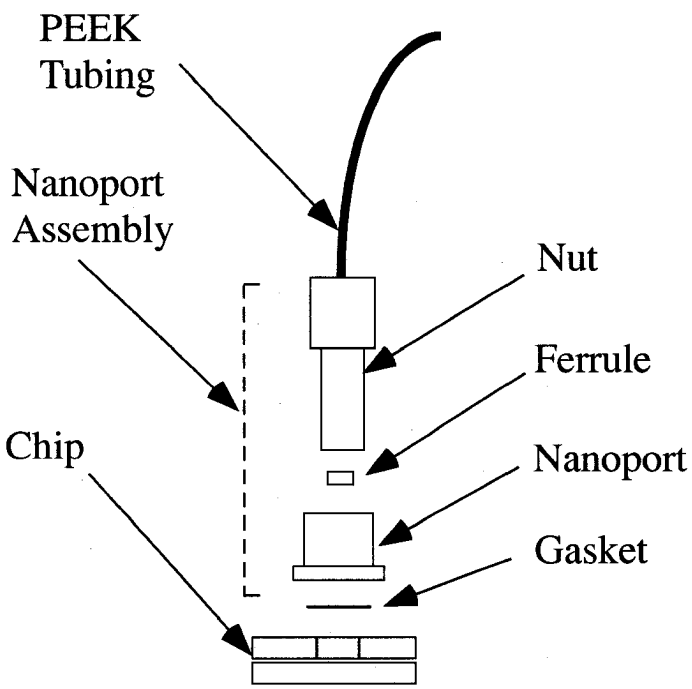

Figure 3.19: Schematic diagram of the Nanoport assembly.

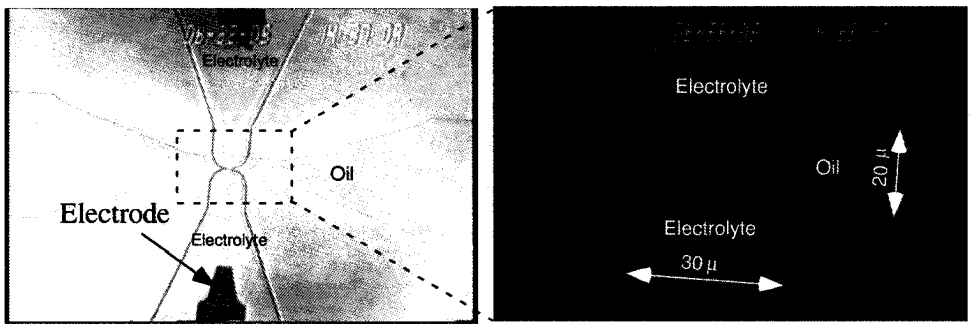

Figure 3.20: The left photograph shows a wide angle view of the intersection. The oil phase is Bitumen/Toluene (1:2) and the water phase is an aqueous solution of 1% Sodium Chloride. The right photograph is a zoomed-in-view of the intersection of the chip at 40× magnification under microscope. The size of the water and oil channels are $3\mu m$ and $20\mu m$, respectively and the depth is 8.5 μm.

Table 3.1: Summary of materials used in the experiments.

Surfactant	Water Phase	Electrolyte	Electrolyte Concen.	Solvent
Lecithin	HyPure	NaCl	1%	Toluene
Bitumen	Deionized	NaCl	1%	Toluene
Bitumen and De-emulsifier	Deionized	NaCl	1%	Toluene
TEGOPREN	HyPure	KCl	1 M	n-Decane

Chapter 4

DC Electric Breakdown

4.1 Introduction

In this chapter electric break down of thin oil films between two oil/water interfaces is studied. The films are formed in the microfluidic device described in the previous chapter and direct current (DC) polarization is used as the destabilizing force. The current passing through the system is measured during the application of potential to detect breakdown of the film. The sudden conductance change, which corresponds to changes in the current passing through the system, indicates breakup of the film. Four sets of experiments designed in this chapter explore the following issues:

1. Perform thin film experiments close to real emulsion droplet size.
2. Investigate as to whether critical potential can be utilized as a measure of stability of thin films.
3. Explore possibility of using the developed microfluidic system as a diagnostic and evaluation tool for emulsion stability in large scale industrial applications.
4. Improve our understanding of electric break down of thin liquid films.

One of the major limitations of conventional thin film experiments is the minimum film area and maximum pressure attained in these techniques. As

mentioned in Chapter 1, conventional thin film experiments are performed using different variations of porous plate cell (TLF apparatus) [Sheludko, 1967; Khristov *et al.*, 2000; Taylor, 2002; Anklam *et al.*, 1999*a*; Anklam *et al.*, 2001]. The hole drilled in the porous glass in this technique is limited to at least few hundred microns in diameter due to fabrication limitations. This limitation leads to film diameters much larger than those formed between micron sized droplets [Velev *et al.*, 1995; Pereira *et al.*, 2001]. Furthermore, the equilibrium capillary pressures attained using conventional techniques can be significantly lower than those occurring in micron size emulsion droplets. This is due to the decrease in critical pressure (pressure at which the film breaks) with increase in film area [Khristov *et al.*, 2002]. In other words, the larger the film area, the lower the critical pressure. Therefore, in conventional porous plate techniques, the experimental condition under which the films are formed can be dramatically different than those in micron size emulsion droplets. To form micron size emulsion droplets, microfabrication technology is incorporated in development of a microfluidic device to study thin films close to real emulsion droplet sizes.

To measure stability, thin liquid films are usually de-stabilized by fluid pressure whereas, the film is de-stabilized by application of electric field in this study. It is important to address the correlation between the two methods. In this study, the concept of critical potential of break down is extended to a qualitative measure of stability of thin emulsion films.

Finally, it is interesting to explore if the idea of lab-on-a-chip can be exploited for industrial applications in oil/oilsands industries. However, the applications can be extended to any water in oil emulsion systems.

In the first section of this chapter, the effect of electric field on a film is described theoretically. The first experiment, lecithin in toluene, is the most rigorous test in this chapter. Lecithin was chosen due to its simplicity, emulsification ability, and its wide applications in industry. Then another surfactant (TEGOPREN 7008) was used for similar experiments and breakup curves were compared against those of lecithin's.

Water in bitumen emulsion [Sjoblom *et al.*, 2003; Fordedal *et al.*, 1996; McLean and Kilpatrick, 1997*a*; McLean and Kilpatrick, 1997*b*; Langevin *et al.*, 2004; Yarranton, 1997] is a wide spread problem in most oil production plants particularly in oilsands extraction facilities where water is added to separate the bitumen from the sand grains. Two experiments are designed to study the stability of these films with and without commercial de-emulsification agents.

Electric break down of thin liquid films has been used in bilayer lipid membranes for biomedical applications such as electroporation [Zimmermann *et al.*, 1974; Weaver and Chizmadzhev, 1996; Zimmermann, 1982; Pethica and Hall, 1982; Benz and Zimmermann, 1981; Chernomordik *et al.*, 1983]. Despite development of pore nucleation theories, the mechanism of break down is not well understood. In the case of thin films (not bilayers) no theory seems to be available to explain the mechanism of electric field mediated film rupture.

4.2 Theoretical Background

In order to assess the stability of an oil film trapped between two phases, one can compress the film by applying pressure. Increase of pressure across the film leads to reduction in its thickness. To keep the film intact, disjoining pressure would balance the external pressure applied. Pressure can be increased until film rupture occurs. Pressure at which the film breaks is called "critical pressure" and is considered an important concept in thin film stability.

Analogous to critical pressure, one can define the concept of "critical potential". Application of an electric field across a film gives rise to a Maxwell stress at the film interface [Crowley, 1973; Masliyah and Bhattacharjee, 2006]. The stress is due to different dielectric constants from one medium to another. The exerted force is proportional to the square of the potential difference. Extremely small thickness of a film ($\sim 10nm$) leads to substantially high electrical fields in the intermediate phase. Therefore, a thin liquid film can be broken with a rather small potential difference.

A thin liquid film, as depicted in Fig. 4.1, can be modeled as a sandwich of two outer media with dielectric constant ε_1 and an intermediate medium with dielectric constant ε_2. As a first approximation, it is assumed that all phases (both inner and outer) are perfect dielectric. In other words, there are no free charges in the system. Therefore, the governing equation that describes the potential distribution in all three phases is Laplace equation [Masliyah and Bhattacharjee, 2006]. To calculate the net force exerted on the left interface (L), it is necessary to integrate the Maxwell stress on the closed surface *abcd*. The normal force per unit area at interface, L, is given by

$$F_{xL} = \frac{1}{2}(\varepsilon_2 E_2^2 - \varepsilon_1 E_1^2) \tag{4.1}$$

where E_1 and E_2 represent electric fields in medium 1 and 2, respectively. Following the above procedure, one can calculate the normal stress on the right interface, R,

$$F_{xR} = -\frac{1}{2}(\varepsilon_2 E_2^2 - \varepsilon_1 E_1^2) \tag{4.2}$$

which is equivalent to the stress on the left interface but in the opposite direction.

Since the forces on the two interfaces are in opposite directions, the film is either under compression or tensile tension. This depends on the dielectric constants of the two media. If $\varepsilon_1 > \varepsilon_2$, the stress is compressive, and if $\varepsilon_2 > \varepsilon_1$, then the force is tensile [Masliyah and Bhattacharjee, 2006]. In the case of a thin film of oil between two water droplets, the dielectric constant of water is substantially higher than that of oil. Therefore, application of electric field compresses the film.

When free charges do exist in the external phases such as aqueous solution of sodium chloride, the analysis of the complete system involves a solution of the Poisson-Boltzmann equation for the aqueous electrolyte phases, with a Laplace equation in the oil film phase [Bard and Faulkner, 2001; Slevin *et al.*, 2003]. Figure 4.2 schematically depicts a typical situation representing the intended experimental system, where an electric potential difference, ΔV, is

applied across a planar composite system consisting of two aqueous phases with a thin oil film of thickness, δ, trapped between them. In general, for an oil film formed between two aqueous electrolyte phases, both the permittivity and conductivity of the oil phase will be much smaller than those of the aqueous electrolyte phases.

The electric field in the oil film in this case is equal to $\Delta V/\delta$ [Crowley, 1973; Masliyah and Bhattacharjee, 2006; Anklam *et al.*, 1999*c*]. This electric field gives rise to oppositely directed Maxwell stresses at each of the oilwater interfaces. The Maxwell stress at the left (L) and right (R) interfaces are given by

$$F_{xL} = \frac{\varepsilon_1}{2}\left(\frac{\Delta V}{\delta}\right)^2 \tag{4.3}$$

and

$$F_{xR} = -\frac{\varepsilon_2}{2}\left(\frac{\Delta V}{\delta}\right)^2 \tag{4.4}$$

respectively, where ε_2 is the dielectric permittivity of the oil film. The stress increases when ΔV increases and δ decreases.

Equations 4.3 and 4.4 reveal the nature of the force exerted on the film. However, they depend on two variables namely, dielectric constant of the film and electric field inside the film, that may be difficult to estimate. The dielectric constant of a thin liquid film is often different than that of the bulk liquid [Hanai *et al.*, 1964]. The dielectric constant can be estimated through capacitance measurements at equilibrium, but electric breakdown of thin film is a rapid dynamic process that renders it difficult to measure capacitance just prior to breakup. Estimation of electric field inside the film is also another issue of concern. Having measured the thickness of the film (δ), one can roughly estimate the electric field inside the film as $E_2 = \Delta V/\delta$ where ΔV is the potential drop across the film. For a conducting fluid separated by a non-conducting film, one can assume that the electric potential drop across the film to be equal to the applied potential difference across the electrodes [Anklam *et al.*, 2001].

In addition to the Maxwell stress, existence of multipolar forces due to application of a high electric field may be considered as another source of stress on

a film. However, the experimental results presented in the next chapter indicate that the deformation of a film under the effect of electric field is proportional to the square of the applied potential. Therefore, one can conclude that the above model would suffice.

As a film is compressed by either mechanical pressure or Maxwell stress, the disjoining pressure is altered. Similar to the mechanical pressure, an increase in electric pressure on the film surface will be balanced by an increase in the disjoining pressure inside the film until the electric pressure outweighs the disjoining pressure and the film ruptures. In this work, the electric potential corresponding to the rupture is called the critical potential and can be considered as an alternative measure of stability of a film.

4.3 Critical Potential

4.3.1 Lecithin Stabilized Films

Figure 4.3 depicts the typical conductance behavior of films formed using three different concentrations of lecithin in toluene. Here, the x-axis represents time. The right hand side y-axis represents the electric potential. As the figure shows, the potential increases at a rate of $25mV/s$. When the film is intact (at low potentials), the current linearly increases with the potential, the slope (potential/current) being 5.6 $M\Omega$. Since the oil film is virtually non-conducting, the measured current predominantly passes through the parallel resistor ($5.6M\Omega$). During this phase, the two interfaces of the film, which act as the two conducting media of a capacitor, acquire a charge. The increase of charge due to increase of potential gives rise to concomitant increase in electric field across the film. As described in the previous section, the Maxwell stress is proportional to the square of electric field inside the film phase. Therefore, the Maxwell stress or the compressive force increases with the square of the applied potential. Once the potential reaches the critical value, the film ruptures. Breakup of the film releases the stored charges which rapidly migrate toward the electrodes. This

abrupt increase in charge flow gives rise to the spike in the current which is evident in the figure. The spike of the current can be perceived as discharge of an overloaded capacitor. A capacitor accumulates charges on its conductive plates. By increasing the potential across the conductive plates, a current is established in the circuit, which is proportional to the rate of potential variation:

$$i = \frac{dq}{dt} = C\frac{dV}{dt} \tag{4.5}$$

where i, q and C are the current, the accumulated charge, and the capacitance of the capacitor, respectively. Increasing the potential difference across the capacitor over a certain threshold potential (critical potential) results in overloading the capacitor, in which case, charge may be transferred through the dielectric separator. This charge transfer gives rise to a sudden increase in the current passing through the circuit which causes discharge of the capacitor.

It is evident from the Fig. 4.3 that the critical potential varies with the surfactant concentration. The film with the lowest amount of surfactant shows the least critical potential while the film with 2 wt % lecithin indicates a high critical potential. To show a correlation between film stability and critical potential, statistically significant number of data are required which is the subject of the next section. However, this figure demonstrates the possibility of application of electric breakdown as a measure of stability of water in oil emulsion films.

Figure 4.4 depicts conductance of a lecithin film in parallel with a resistor ($5.6M\Omega$) and that of the resistor alone. As expected, for a pure resistor, a line with a constant slope corresponding to the value of the resistor is measured. The slope of the line is $1.82 \times 10^{-7}A/V$ which is equivalent to $5.47M\Omega$. The second curve is that of a lecithin film in parallel with the resistor. The breakup of the film is manifested by the spike of the current at $320mV$. The slope of the curve before breakup is equivalent to that of the parallel resistor. In other words, the conductance of the system is equivalent to that of the resistor. This implies that the film of lecithin in toluene is a non-conducting film.

4.3.2 TEGOPREN Stabilized Films

Figures 4.5 depict the conductance behavior of TEGOPREN 7008 stabilized film in n-decane in parallel with the resistor similar to the experimental procedure in the previous section. The straight line represents only the parallel resistor ($5.6M\Omega$ nominal value) without the chip in the circuit. The film shows a much higher stability than lecithin stabilized films. The breakup occurs at $1100mV$. The interesting point about this graph is the conductance of the film. The graph reveals a clear deviation from the two previous measurements. The deviation shows a higher current being drawn from potentiostat for the same potentials. Since the parallel resistor is constant, the only possible pathway for the extra current to go through is the film itself. In other words, the film shows a substantial leakage compared to the lecithin film shown in Fig 4.4. The figure indicates that the TEGOPREN film leaks current from the early stages of polarization, whereas the lecithin film does not show any sign of leakage despite the very thin nature (close to bilayer) of the lecithin film. From Figs 4.4 and 4.5, one can conclude that the lecithin in toluene film is non-conducting whereas TEGOPREN in n-decane is more permeable to the current under electric polarization. It is evident from the figure that behavior of thin films under effect of electric polarization can be quite different.

Comparing the conductance measurements of the films formed with TEGOPREN and lecithin, suggests a substantial difference in the nature of the two films which can be associated with the surfactant molecules present in the oil phase. While lecithin is a mixture of few relatively small molecules with a molecular weight of about 800 Dalton (depending on the source of lecithin), TEGOPREN exhibits a substantial larger molecular weight close to 60,000 Dalton. The thickness of lecithin film is about 4-9 nm whereas in TEGOPREN, the thickness reaches 40 to 60 nm [Anklam *et al.*, 1999*a*; Anklam *et al.*, 1999*b*].

TEGOPREN is a heterodisperse polymeric surfactant which may result in conductivity due to heterogeneity and defect in the film. However, the conductivity of the film is mainly due to the conductivity of TEGOPREN molecules.

TEGOPREN is a copolymer with poly(dimethyl siloxane) backbone and grafted hydrophobic and hydrophilic chains. Although there is no direct measurement of conductance of this polymer, similar polymers with dimethyl siloxane backbone are well known for their conductive characteristics [Trapa *et al.*, 2005; Fonseca and Neves, 2002; Sun *et al.*, 1996]. From Fig. 4.5, the conductivity of the film can be calculated as 10^{-4}S/m. For similar polymers, conductivity values within $10^{-5} - 10^{-4}$S/m has been reported in literature [Fonseca and Neves, 2002; Sun *et al.*, 1996]. Other possible mechanisms of charge transfer across a film or a nonconducting media such as electroporation [Zimmermann *et al.*, 1974] or charge transfer through micelles [Morrison, 1993; Strubbe *et al.*, 2006; Dukhin and Goetz, 2006] are unlikely since the leaking in TEGOPREN films happens at the very start of potential ramp, while in cases of previously the mentioned mechanisms, the onset of leaking is expected to happen at a threshold potential.

4.4 Lecithin in Toluene Films

4.4.1 Interfacial Tension Measurement

Lecithin is an oil soluble surfactant which reduces interfacial tension of the oil/water system dramatically due to its high affinity to adsorb at the interface. In order to study adsorption kinetics of lecithin in oil/water interface, a K100 tensiometer (KRUSS, Germany) was used to measure interfacial tension of toluene/water in presence of lecithin. Figure 4.6 depicts the kinetics of interfacial tension of toluene/Water (water phase contains 1% NaCl) at different surfactant (lecithin) concentration. The interfacial tension of pure toluene/water was 34.47 ± 0.02 mJ/m^2 (the solid line).The dashed line at the bottom of the figure shows the lowest measurement range of the instrument which was 1.00 mJ/m^2. At 0.001 wt % bulk lecithin concentration, the interfacial tension started at 32.169 mJ/m^2 and reduced to 1.383 mJ/m^2 after 1 hr. At higher bulk concentrations of the surfactant, the adsorption happens much quicker and interfacial tension drops to a lower value. At 0.01 wt %, the

interfacial tension drops below 1.000 mJ/m^2 after less than 10 minutes. At high concentrations such as 1 and 2 wt % the interfacial tension drops to less than 1.000 mJ/m^2 within 2 minutes. Measurement of equilibrium interfacial tension for high concentrations of lecithin was not possible with this technique. Using spinning drop method, Shinoda *et al.* [1993] measured interfacial tension of hexadecane/water+propanol system in presence of lecithin. Their measurements determined the interfacial tension to be 0.0005 mJ/m^2. This extremely low interfacial tension was manifested in microchip experiments as well. The pressure difference between oil water channels after a long adsorption time was so low that detecting the pressure difference between two channels posed considerable difficulty.

4.4.2 Lecithin Film Breakdown

It is apparent from Fig. 4.3 that the critical potential is unique to each film formed using a different lecithin concentration. Figure 4.7 shows how this critical potential provides insight regarding the stability of a thin film. In these experiments, the lecithin molecules were allowed to adsorb for a fixed time at oil-water interfaces before bringing them together to form the film (adsorption time). The two interfaces were then brought together to form the film. Once formed, the film was left for period of 1 minute before application of the electric potential (drainage time). Figure 4.7 depicts the variation of the critical potential with lecithin bulk concentration in toluene. The data corresponding to each lecithin concentration represent averages and standard deviation calculated over at least 15 measurements. The adsorption time was fixed at 2 minutes in these experiments. The figure shows a direct correlation between concentration of the surfactant and the stability of the film. At low concentrations the film seems to be much less stable than those of high concentrations. The trend of the graph seemingly is that of a Langmuirian adsorption.

Figure 4.8 shows the variation of the critical potential with lecithin adsorption time for a system comprised of 2 wt % lecithin in toluene. As the adsorption

time increases, the stability again reaches a saturation value very quickly. After 2 minutes of adsorption, the stability reaches a maximum value beyond which the stability is constant.

The increase in critical potential with lecithin bulk concentration and time is representative of an enhanced film stability caused by adsorption of lecithin at the interface. Figure 4.9 depicts a schematic diagram of surface coverage by surfactant molecules. The top picture shows a highly concentrated surface covered with the surfactant molecules. Due to long adsorption time or high concentration of surfactant in the bulk, more molecules are adsorbed at the interface. Therefore, the film exhibits higher stability evidenced by high critical potential. The bottom figure shows a low surface coverage interface. The lack of surfactant molecules reduce the stability and makes the film more susceptible to spontaneous breakup.

Figures 4.7 and 4.8 indicate that the critical potential provides a robust platform for studying stability of water in oil emulsion films. The method can clearly distinguish between slight differences in surfactant concentration which leads to changes in film stability. The effects of both adsorption time and concentration of surfactant on film stability are manifested in a Langmuir adsorptiom form which is the subject of the next section.

4.4.3 Adsorption Kinetics and Isotherms

The stability of toluene films in water is sterically imparted by lecithin, which adsorbs to the toluene-water interfaces. Using the Langmuir adsorption model, the isotherms and kinetics of adsorption can be expressed as

$$\frac{\theta}{\theta_{max}} = \frac{KC_b}{(1 + KC_b)} \tag{4.6}$$

and

$$\frac{\theta}{\theta_{max}} = 1 - \exp(-kC_b t) \tag{4.7}$$

respectively, where θ is the fractional coverage of the oil-water interface by lecithin, θ_{max} is the maximum fractional interfacial coverage, K is the equilib-

rium constant, k is the adsorption rate constant, C_b is the bulk lecithin concentration, and t is the time. If the critical potential is linearly dependent on the film stability and if stability is directly proportional to the surface coverage, then the data in Figs. 4.7 and 4.8 can be fitted to the isotherm and the rate of surface coverage, using single adjustable parameters. The solid lines in Fig. 4.10 and 4.11 depict these best fits, scaled linearly with respect to the maximum critical voltage, V_{max}. In Fig. 4.10, the fitting parameter is K and in Fig. 4.11, the parameter is k. It is evident that the data are in good agreement with the trends of Langmuirian adsorption in both thermodynamic and kinetic aspects. An interesting observation in this respect is the rapid attainment of saturation observed in the present study. In adsorption experiments using larger surface areas of oil-water interfaces, several hours are often required to attain the plateaus in adsorption. Our results are acquired in a few minutes, indicating that the small area of the film allows a rapid diagnosis of the adsorption process. The advantage of this method over some of the conventional methods is that one can flush the water channels after each measurement and form a fresh oil/water interface. This removes the old adsorbed layers and reproducible experiments can be performed in rapid succession.

4.5 TEGOPREN in n-decane

Following Anklam and coworkers [1999, 2000], TEGOPREN 7008, which is an oil soluble surfactant with substantial application in food and cosmetic industries as an effective water in oil emulsifier, was used. The bulk concentration of the surfactant was kept at 0.52 wt % in n-decane. The average critical potential is $1136mV$ which was substantially higher than those of lecithin.

4.6 Bitumen in Toluene

4.6.1 Pure Bitumen in Toluene

In order to compare our technique with the standard thin liquid film apparatus, a set of experiments was designed similar to those of Taylor *et al.* [2002]. Taylor *et al.*, in their experiments found that stability of bitumen in toluene emulsion does not directly correlate with concentration of bitumen. In other words, higher concentrations of bitumen do not necessarily lead to higher film stability, but stability peaks at 33 wt % bitumen in toluene. Figure 4.12 shows the disjoining pressure isotherms of bitumen in toluene films [Taylor *et al.*, 2002]. The concentration was varied from 10 to 50 wt % (1:10 to 1:1 bitumen to toluene mass ratio). The figure shows that the maximum critical pressure of rupture occurs at 33 wt %, while at 50 wt % concentration, the critical pressure decreased. In these measurements, the critical disjoining pressure of the 1:2 solution was higher than that of 1:1. Furthermore, it was reported in the same communication that at dilutions higher than 1:3 the film becomes unstable.

Figure 4.13 shows the results of similar experiments conducted using the microchip. The critical potential measurement demonstrates a maximum stability at a concentration of 33 wt %, which is analogous to the measurements from Taylor *et al.*. At 50 wt % bitumen in toluene concentration, the stability of the film decreased by $50mV$ below that of 33 wt %. At higher dilution or lower concentration of bitumen, the film was unstable which is in accord with Taylor's findings.

4.6.2 Bitumen and De-emulsifier in Toluene

To evaluate the efficacy of the developed microfluidic setup in industrial applications, a set of experiments was designed using a regular emulsion breakers used in the oilsands industries. The de-emulsifier used in this study was a comb grafted block copolymer diluted in xylene provided by Champion Technologies (Houston, USA) [Xu *et al.*, 2004; Wang *et al.*, 2005]. Henceforth it will be called

surfactant "A".

The de-emulsifying agent (surfactant "A") was added to the diluted bitumen in toluene solution. The concentration of bitumen was chosen to be 33 wt %, since this concentration proved to demonstrate the highest stability of the emulsion film. The concentration of chemical "A" was varied from 0 ppm to 200 ppm (part per million in the oil phase). The results of critical potential versus concentration of the chemical "A" are depicted in Fig. 4.14. The average critical potential of breakup for 33% bitumen in toluene without any additive is $227mV$, in accord with previous tests. Adding the de-emulsifying agent, even at very low concentrations such as 10 ppm, show a measurable reduction in stability of the film. Gradual increase in the concentration of chemical "A" resulted in a decrease in the film's stability up to 50 ppm where a minimum stability is observed. The minimum critical potential was measured to be 166mV at 50 ppm. Above this concentration, the de-emulsifying agent counteracts its purpose. In other words, the best concentration of this particular de-emulsifier for the given bitumen concentration is 50 ppm and overdosing the system beyond this concentration increases the stability of the film.

An effective concentration window in the ppm range is a well documented observation in case of flocculants and de-emulsifiers used in a variety of applications including dewatering sludges, froth treatment, mineral processing, etc.[Suzuki *et al.*, 2006; Long *et al.*, 2005; Pena *et al.*, 2005]. Furthermore, some of these studies clearly document the sensitivity of the measured optimal surfactant dosages on the experimental conditions [Pena *et al.*, 2005] In this context, the reproducibility of the present microfluidic measurements is indicative of the stable and identical conditions achieved in the films repeatedly. It is of interest to note that the value of the optimum concentration for a typical de-emulsifier used in petroleum processing plants is reported to be between 50 to 300ppm [Pena *et al.*, 2005]. It is evident from these results that the microfluidic device provides highly sensitive measurements of the optimal dosage of a de-emulsifier.

4.7 Conclusion

In this chapter, using the developed microfluidic device, electric mediated breakdown of thin liquid films was studied. The developed system proved to be a successful tool to form thin liquid films at micron size scale. The novel design of the system provides a unique opportunity, for the first time, to carry out experiments on micron sized emulsion films close to real pressures and film areas observed in emulsions.

The experiments with lecithin films proved that the critical potential can indeed distinguish stability of films accurately. The stability of the films were changed both by varying lecithin concentration and adsorption time. It was evident from the results that the critical potential can resolve subtle differences of the adsorbed lecithin layer. The stability of the film successfully correlated with the adsorption models of Langmuir.

The comparison of conductance curves of TEGOPREN and lecithin films reveals an interesting feature of electric break down. TEGOPREN films show a marked leakage even under low polarization whereas lecithin films seem to be non-conducting. This comparison suggests that behavior of films is greatly influenced by the nature of surfactant and that of the solvent. The current leakage through TEGOPREN films can be explained by conductivity of TEGOPREN copolymer. It was shown that the measured conductance of the film is in accord with those reported in literature for similar polymers. Moreover, the leakiness of films started from the very beginning of the polarization which is a strong evidence of partial conductivity of TEGOPREN molecules. Lecithin films, on the other hand, exhibit a different behavior. Lecithin films seem to be extremely non-conducting and no leakage was observed. This is despite the extremely small thickness of lecithin stabilized films. Comparison of the breakdown of lecithin and TEGOPREN films reveals a marked difference between the two surfactants. Not only the critical potentials of the two systems are substantially different but also they demonstrate different conductances.

The bitumen film experiments shows the capability of the developed mi-

crofluidic system in performing diagnostic and classification experiments on industrial de-emulsification systems. The results of the bitumen tests with no de-emulsifier was in accord with the critical pressure measurements, proving that critical potential can be used as a measure of stability of films. The second experiment (with industrial de-emulsifier) also proved that the technique presented here provides a unique experimental procedure that can widely be used in large scale industrial applications.

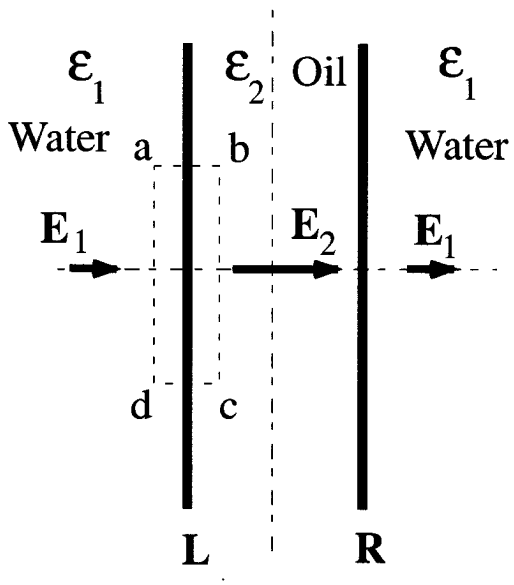

Figure 4.1: A simple model for thin films. A film of one liquid with dielectric constant ε_2 sandwiched between two liquids with dielectric constant ε_1.

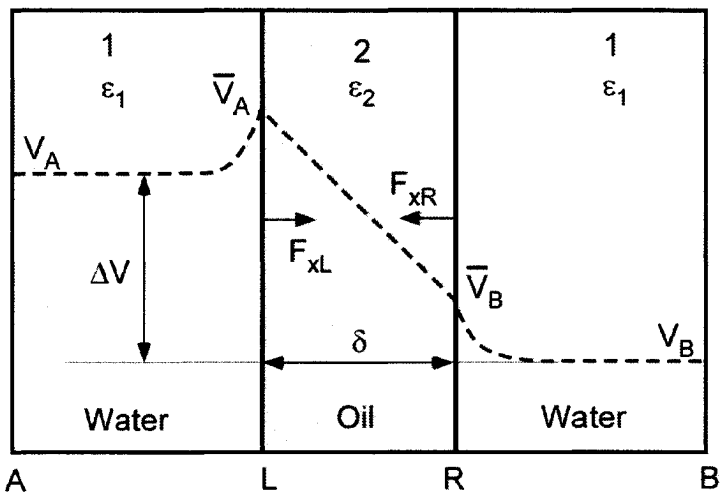

Figure 4.2: A simple model for electrical forces acting on a planar thin oil film formed between two aqueous electrolyte phases. The left hand side reservoir is raised to a potential V_A, and the right side reservoir to a voltage V_B. Assuming identical electric double layers are formed in the aqueous phases at the oil-water interfaces, the potential difference across the film is $\bar{V}_A - \bar{V}_B = V_A - V_B = \Delta V$. The electric field inside the oil film due to this potential difference will give rise to Maxwell stresses on the L and R interfaces, which are denoted by F_{xL} and F_{xR}, respectively. The interfacial electrical stresses on the water side will be zero.

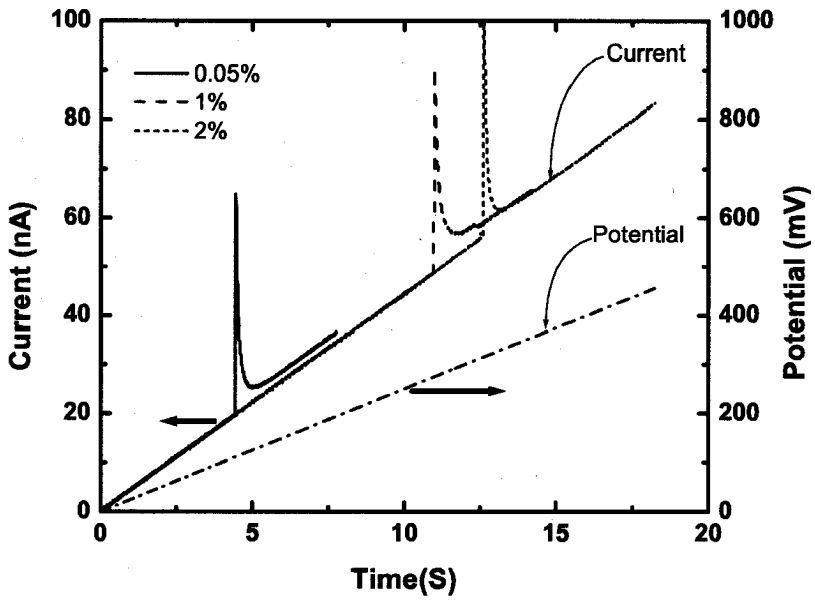

Figure 4.3: Current vs. time measurement for 0.05, 1 and 2 wt % concentration of lecithin in toluene. The dashed-dot line depicts the applied potential. The slope of the line is 25mV/s.

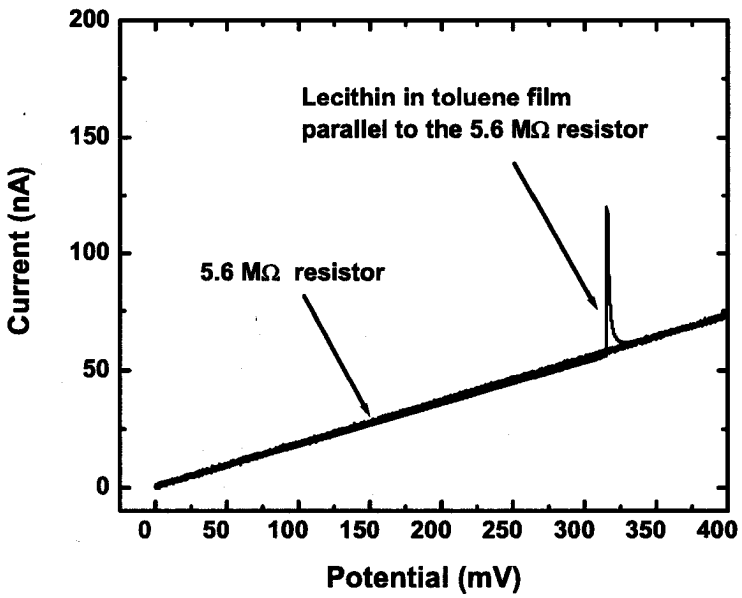

Figure 4.4: Current vs. time for a lecithin film in parallel to a $5.6M\Omega$ resistor compared to that of $5.6M\Omega$ resistor alone. Since the slope of the film with the parallel resistor does not deviate from the slope of the resistor, one can conclude that the film is non-conductive

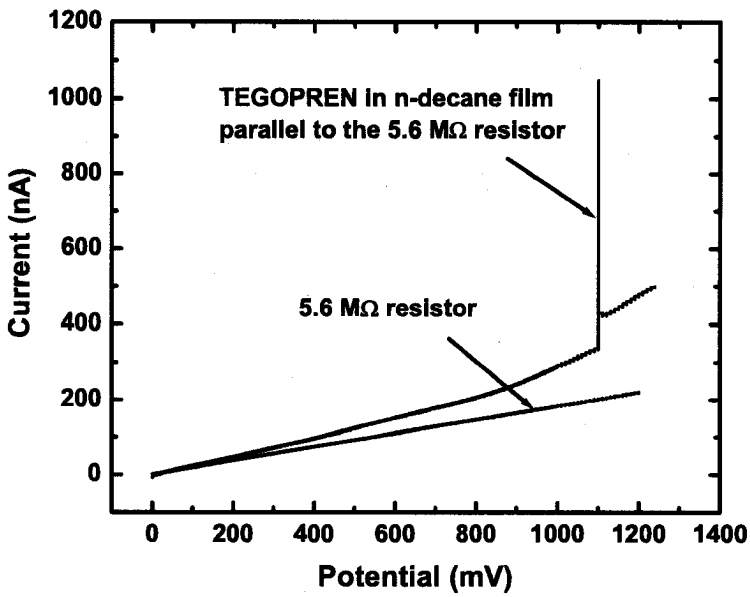

Figure 4.5: Current vs. time for a TEGOPREN film in parallel to a $5.6M\Omega$ resistor compared to that of the $5.6M\Omega$ resistor alone. The film shows deviation from the resistor which is due to the conductivity of the film.

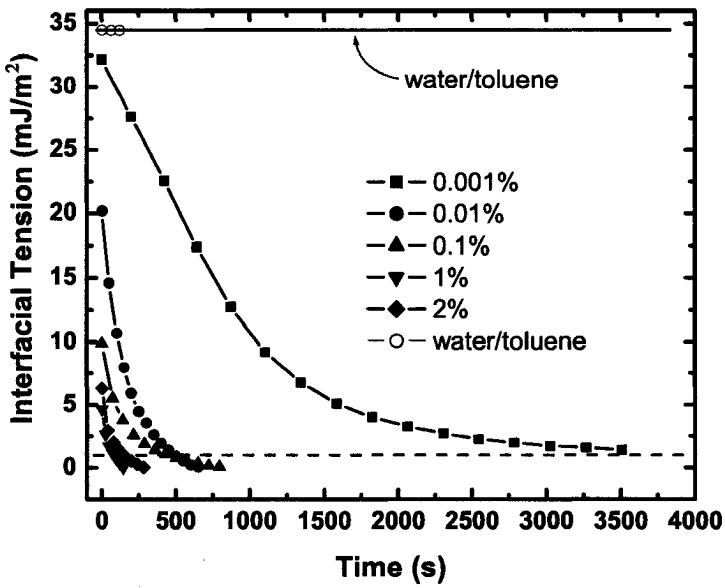

Figure 4.6: Interfacial tension measurements for 0.001, 0.01, 0.1, 1 and 2 wt % lecithin in toluene. The open circles represent interfacial tension of toluene/water without any lecithin. The water contains 1 wt % NaCl.

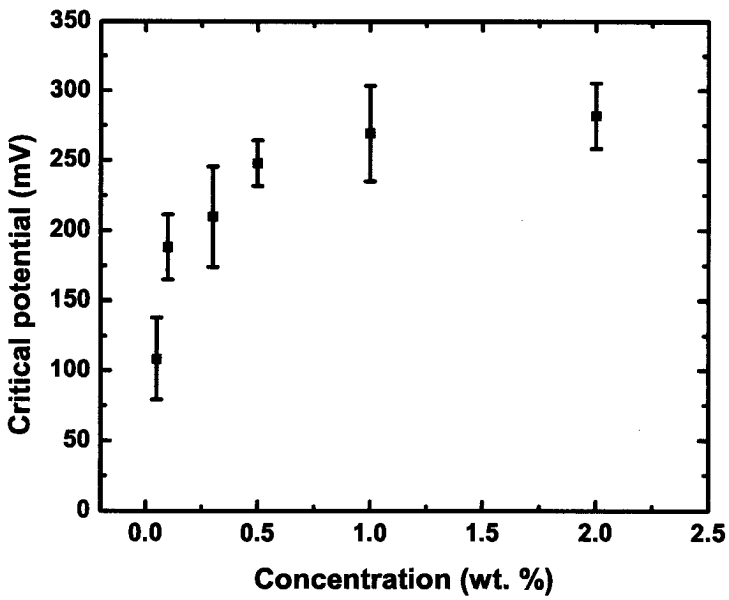

Figure 4.7: Average critical potential for different concentrations of lecithin in toluene (0.05, 0.1, 0.3, 0.5, 1 and 2 wt %). Adsorption and drainage times are kept at 2 and 1 min., respectively. Error bars represent standard deviation.

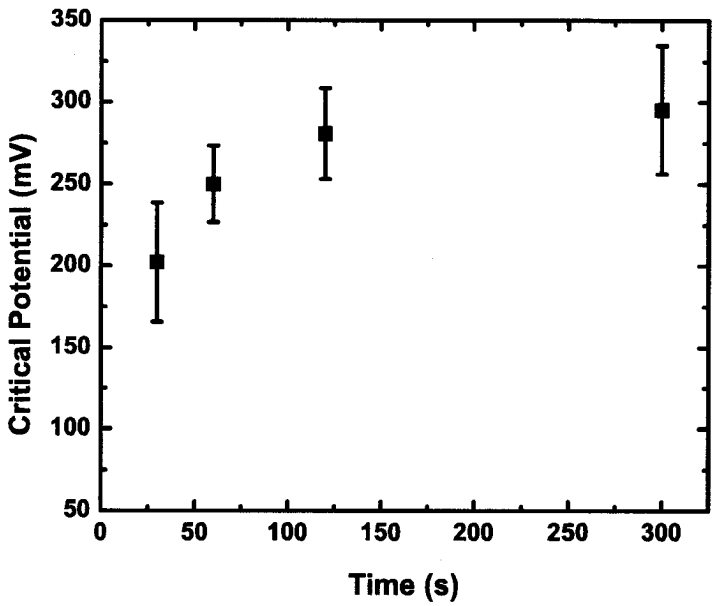

Figure 4.8: Average critical potential for a system of 2 wt % lecithin in toluene. The adsorption time has been changed from 30 s to 300 s.

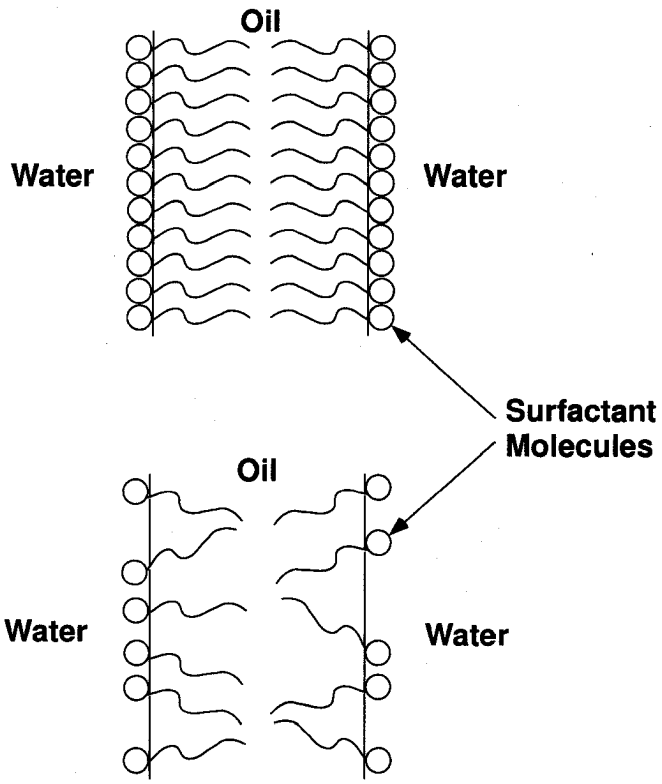

Figure 4.9: A schematic diagram of surface coverage by a surfactant. The top diagram shows a highly compacted interface due to long adsorption time or to high concentration of surfactant in the oil that results in higher film stability. The bottom diagram depicts a poor surface coverage which leads to lower film stability.

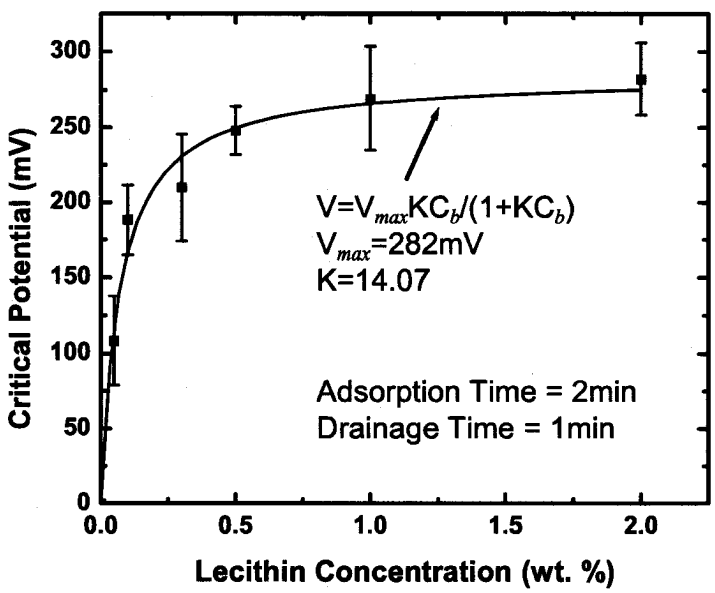

Figure 4.10: Average critical potential vs. concentration (wt %) of lecithin depicting the isotherm. Symbols depict experimental values. The line is obtained by fitting the isotherm equation to the data using Langmuir adsorption model.

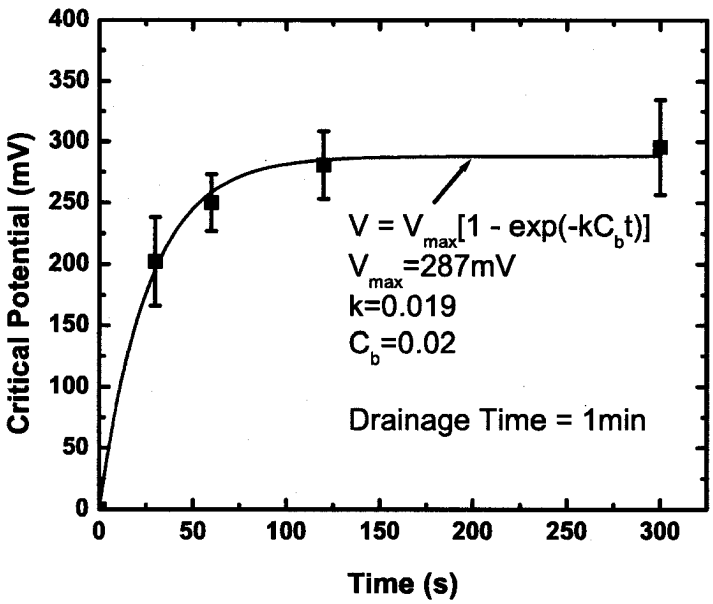

Figure 4.11: Effect of adsorption time on stability of a film showing adsorption kinetics. Symbols depict experimental values. The line is obtained by fitting the kinetic equation to the data using Langmuir adsorption model.

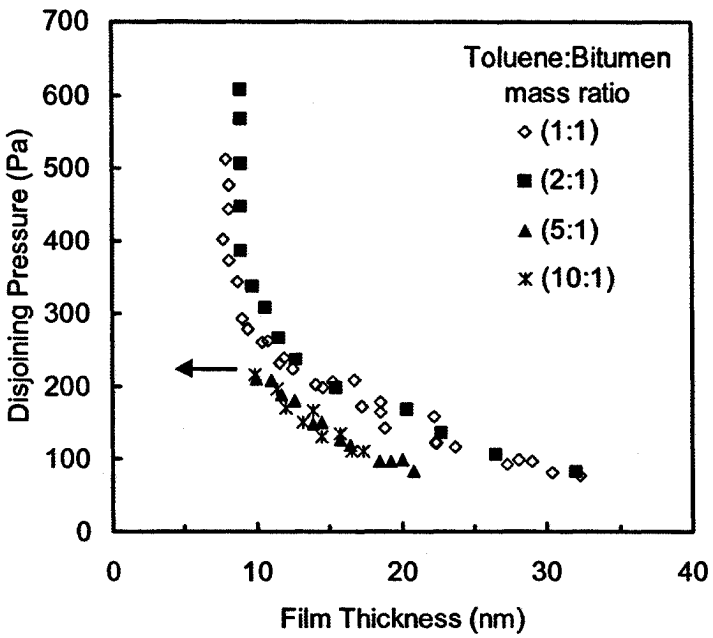

Figure 4.12: Disjoining pressure isotherms for films of diluted bitumen in toluene (from Taylor *et al.* [2002]).

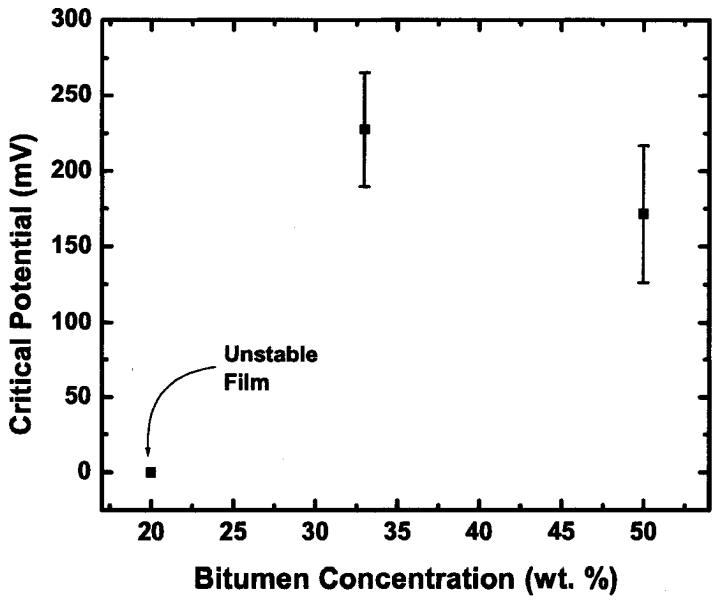

Figure 4.13: Stability of bitumen in toluene films.

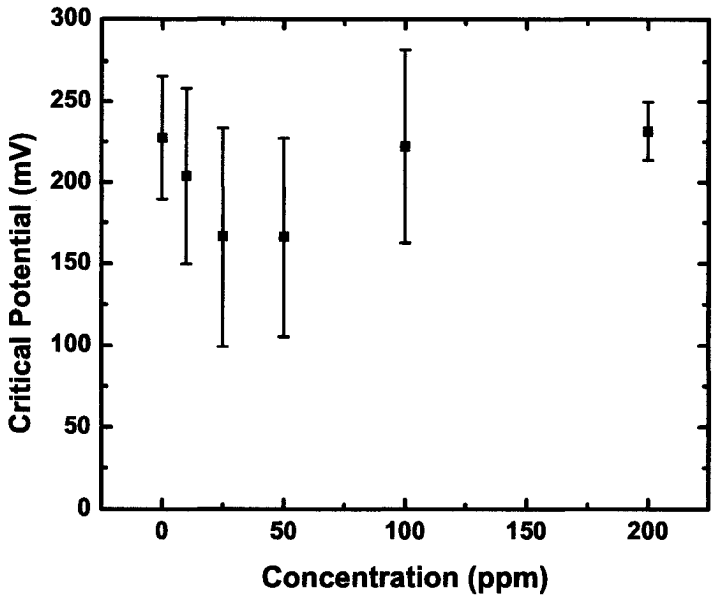

Figure 4.14: Effect of chemical "A" on stability of bitumen film. The film phase is 33 wt % bitumen in toluene.

Chapter 5

AC Impedance Spectroscopy

5.1 Introduction

In this chapter, application of Impedance Spectroscopy (IS) to measure capacitance and cross-sectional area of thin films, and to study the dynamics of film drainage is presented. In addition, effects of DC polarization on capacitance of the film are investigated by performing IS in presence of a DC bias voltage.

Impedance Spectroscopy is a powerful and widely used technique for characterizing the electrical properties of complex systems, particularly, those pertaining to the interfaces of solid/liquid and liquid/liquid systems. Normally, the technique is comprised of application of an AC potential across a system, with simultaneous measurement of the current flow through it. The ratio of the amplitude of the applied voltage to the measured current provides insight regarding the system's impedance. Depending on the electrical response of the system, which is a combination of capacitive, inductive, and resistive behaviors, the sinusoidal current also exhibits a phase shift relative to the applied voltage. Analysis of the amplitude ratio and phase shift provides a comprehensive quantitative estimate of the system's electrical response. Since this technique employs AC signals, usual DC polarization effects can be avoided in these measurements. Consequently, IS has become the technique of choice for probing the characteristics of electrochemical systems, including batteries, fuel cells, colloidal suspensions, and emulsion films [Barsoukov and Macdonald, 2005].

Impedance spectroscopy has been widely used in biological membrane characterization [Alcaraz *et al.*, 1998; Alcaraz *et al.*, 2001; Chilcott *et al.*, 2002; Asami, 2002; Cho *et al.*, 2006; Naumowicz *et al.*, 2006; Park *et al.*, 2006]. This technique provided the early estimates of the thickness of a cell membrane in 1925 [Fricke and Morse, 1925]. One of the pioneering works in capacitance measurement of thin films was conducted by Hanai and coworkers [1964, 1965]. They measured the capacitance of bilayer lipid membranes using impedance spectroscopy. They also studied the effect of DC potential on breakup of these films.

Conventional impedance measurements of thin films are limited to large diameter films. In these measurements, the film is usually formed in a large ($\sim$ 1 mm) hole drilled in a Teflon plate, across which electrodes are placed. Therefore, implications of this method to small emulsion films formed between micron sized droplets, as in the developed microfluidic device, are unknown. In micron-scale films, capillary pressures and rigidity of the interfaces are substantially higher than those of large films. This leads to the speculation that their thinning might differ from those observed using the macro-scale experiments or predicted by the standard models. In this respect, the IS technique, in conjunction with the microfluidic system developed in this study provides a means of assessing the electrical properties of small cross-section films formed between microscopic droplets.

It is impossible to view the film perpendicular to its plane in the microfluidic chip. Thus, the commonly adopted optical characterization techniques for visualization of the film cross-sectional area in traditional methods (TLF) cannot be applied to a microfluidic system. Moreover, in traditional techniques, one may incorporate interferometric methods to evaluate the equivalent thickness of the film. In the microchip developed in this study, however, the film is seen along its plane. Consequently, although one can obtain a reasonable estimate of the "length" or diameter of the film using an optical microscope, the total area of the film cannot be optically determined. Due to this limitation, opti-

cal interferometric measurement of thickness is also not feasible. Finally, it is quite counterintuitive to have a large optical characterization system associated with the microfluidic chip, which will hamper its portability and versatility. In this regard, IS provides a facile and an alternative means of characterization of these films in a microfluidic chip and constitutes an enhanced electrochemical detection mode that can potentially substitute optical detection methods used in thin film characterization using traditional instruments.

Although DC potential can be used for measurement of electric charge accumulation and capacitance, it has numerous disadvantages that affect the reliability of such measurements. For instance, application of DC polarization results in electroosmotic flow. This flow may affect ion distribution, cause pressure build up across the interfaces, and alter the electrical response of the system considerably from that corresponding to a stationary condition. AC potentials, on the other hand, do not affect the system to such an extent due to periodic change in polarization and very low amplitudes. In addition to the above, IS can be implemented at very low amplitudes ($\sim 10\ mV$) where alteration of the system by the measurement technique is negligible. In contrast, DC measurements generally incorporate higher potentials, which, in turn, may disturb the system being probed. Furthermore, application of a DC potential in an electrolyte may cause electrolysis, which not only can disturb the chemical composition of the system but can also result in polarization of the electrodes.

The major disadvantage of impedance spectroscopy is associated with the possible ambiguity in interpretation of results [Barsoukov and Macdonald, 2005]. The electrical components in an equivalent circuit are usually simple constant elements, whereas in real electrochemical systems, the elements are spatially distributed, which sometimes renders it difficult to model using simple lumped parameter electrical circuits. Another disadvantage of equivalent circuit technique pertains to the uncertainties in assigning a proper circuit model that represents the system behavior accurately. The procedure of finding an equivalent circuit is based on curve fitting of a speculated circuit to the data. Therefore,

for a given impedance measurement, there may be more than one equivalent circuit that can be fitted to the experimental data. This problem can be addressed, to some extent, by choosing the circuit that physically resembles the electrochemical system the best.

Thus, one of the primary goals of this chapter is to show the applicability of impedance spectroscopy in high impedance systems as presented in our experimental setting. In this chapter, the theory of impedance spectroscopy and its basic concepts are first described. Following this, the experimental setup and procedure are described. In the Results and Discussion, the preliminary impedance measurements of chips are first described. The equivalent circuits and calculation procedures are presented. Then, the area of the films for different lengths is evaluated. Drainage time of small emulsion films formed between micron sized droplets are measured in Section 5.4.2. The effect of adsorption time on the capacitance of the film is also investigated. Finally, the influence of DC polarization on capacitance is studied. The chapter is concluded with some key observations regarding applicability of impedance spectroscopy in the developed microfluidic device in Section 5.5.

5.2 Theoretical Background

5.2.1 Impedance

Impedance can be defined as the total complex opposition of an electrical system to alternating current and is expressed in ohms. The impedance of an RC circuit is calculated by both the resistance and capacitive reactance [Floyd, 1981; Driscoll, 1973]. Consider Fig. 5.1 as a simple RC circuit. A resistor R is placed in parallel with a capacitor C. An AC potential source V drives the total current I in the circuit. If the potential is in a form of $V = V_0\ sin(\omega t)$ the current will have a sinusoidal shape with the same frequency. However, the current will not necessarily be in phase with the potential, therefore, the current

will have the following form

$$I = I_0 \ sin(\omega t + \phi) \tag{5.1}$$

where ϕ is the phase shift between the current and potential. The current passing through the resistor, R, can be calculated as

$$i_R = \frac{V}{R} \tag{5.2}$$

or

$$i_R = \frac{V_0}{R} \ sin(\omega t) \tag{5.3}$$

Similarly, the current through the capacitor can be written as

$$i_C = C \ \frac{dV}{dt} \tag{5.4}$$

or

$$i_C = C \ V_0 \ \omega \ cos(\omega t) \tag{5.5}$$

Therefore, for the total current I, one can write

$$I = I_0 \ sin(\omega t + \phi) = \frac{V_0}{R} \ sin(\omega t) + C \ V_0 \ \omega \ cos(\omega t) \tag{5.6}$$

Now, if one considers a potential with $-\pi/2$ shift with respect to the original phase, one can write

$$I_0 \ sin(\omega t + \phi - \pi/2) = \frac{V_0}{R} \ sin(\omega t - \pi/2) + C \ V_0 \ \omega \ cos(\omega t - \pi/2) \tag{5.7}$$

Since a linear system is assumed, the current on the right hand side of the equation will also follow the same phase shift as the input potential. Therefore, the total current is

$$I_0 \ cos(\omega t + \phi) = \frac{V_0}{R} \ cos(\omega t) - C \ V_0 \ \omega \ sin(\omega t) \tag{5.8}$$

Considering Euler's formula

$$e^{jx} = cos(x) + j \ sin(x) \tag{5.9}$$

where j is $\sqrt{-1}$, one can multiply Eq. 5.6 by j and add to Eq. 5.8 resulting in

$$I_0\, e^{j(\omega t+\phi)} = \frac{V_0}{R}\, e^{j(\omega t)} + j\, C\, V_0\, \omega\, e^{j(\omega t)} \tag{5.10}$$

or

$$I_0\, e^{\phi} = \frac{V_0}{R} + j\, C\, V_0\, \omega \tag{5.11}$$

The above relation is the equivalent of Ohm's law ($V = I\ R$) in an AC circuit

$$V_0 = \frac{1}{(\frac{1}{R} + jC\omega)}\, I_0\, e^{\phi} \tag{5.12}$$

In Eq. 5.12, I_0 and ϕ are the amplitude and the phase shift of the current, respectively. The value in the bracket is the total impedance of the circuit, which is comprised of a real part (resistance) and an imaginary part (reactance). Therefore, for the parallel RC circuit depicted in Fig. 5.1 the total impedance is equivalent to

$$Z = \frac{1}{(\frac{1}{R} + jC\omega)} \tag{5.13}$$

Similarly, for an RC circuit in series, it can be shown that the impedance is equivalent to

$$Z = R + \frac{1}{jC\omega} \tag{5.14}$$

In a purely resistive system, the impedance is equal to the sum of all resistances, whereas in a purely capacitive system, it is equivalent to the capacitive reactance. A real dielectric material, however, always exhibits both resistance and reactance effects. Consequently, the impedance, Z, of a homogeneous material may be expressed in terms of a resistive element R in parallel with a capacitive element C as follows

$$Z(\omega) = \frac{1}{G + j\omega C} \tag{5.15}$$

Although the conductance and the capacitance are independent of frequency, it is evident from equation 5.15 that the total impedance is dependent on frequency.

5.2.2 Nyquist Plot

The expression of impedance $Z(\omega)$ is made up of a real (resistance) and an imaginary (reactance) part. it is common practice to express the variations of these quantities over a wide range of frequencies employing Nyquist or Bode plots. These plots form the essential basis of analyzing the frequency response of a dielectric system to an imposed alternating signal. A Nyquist plot is the plot of the impedance corresponding to different frequencies, with the real part plotted on the X axis and the imaginary part on the Y axis. Each point on a Nyquist plot represents the impedance vector (or phasor) of the system for a specific frequency. Therefore, in a Nyquist diagram, the impedance is expressed as a vector with length $|Z|$ and angle ϕ. Figure 5.2 depicts a typical impedance measurement of a simple electrical circuit. Figure 5.2a shows the equivalent circuit for a dielectric system (indicated by the resistor R_1 and the capacitor C_1 in parallel) connected to an external circuit through electrodes. The resistance R_2 represents the additional resistance of this electrical circuit. In Fig. 5.2b each point (filled circle) corresponds to an impedance vector at a certain frequency. Note that the vertical axis is the negative of the imaginary part. A complete sweep over the frequency range from $\omega \rightarrow 0$ to $\omega \rightarrow \infty$ yields a semicircular locus of the impedance vector. The figure also indicates how the amplitude and the phase angle of the impedance vector are determined from the Nyquist plot. If the equivalent circuit of the system is altered during a frequency sweep, there will be a deviation from the semicircular locus. A shortcoming of the Nyquist diagram is that the frequencies associated with the measurement data are not explicitly indicated in the figure.

As indicated in Fig. 5.2, the high frequency impedance data are on the left hand side of the curve and low frequency data on the right hand side. The impedance of the circuit in Fig. 5.2 can be written as

$$Z(\omega) = \frac{1}{G_1 + j\omega C_1} + \frac{1}{G_2} \tag{5.16}$$

In the above equation if ω is negligibly small or $\omega \rightarrow 0$, then the total impedance

is

$$Z(\omega) = \frac{1}{G_1} + \frac{1}{G_2} \tag{5.17}$$

which is equivalent to the sum of both resistors in series. If $\omega \rightarrow \infty$ then the impedance can be written as

$$Z(\omega) = \frac{1}{G_2} \tag{5.18}$$

which is equivalent to the resistance of resistor R_2. Therefore, one can conclude that G_1 and G_2 (or R_1 and R_2) can be estimated from the intersections of the curve in the Nyquist plot with the X axis.

Unlike Nyquist plot, in which frequency information are not expressed, the Bode plot includes the impedance values with respect to the frequency. However, Bode and Nyquist plots contain similar information, implicitly. Since Nyquist diagram is commonly used for the fitting of the equivalent circuit to the experimental data, therefore, it is used to represent the experimental and equivalent circuit data.

5.2.3 Equivalent Circuit

Figure 5.1 shows the equivalent electrical circuit for a simple homogeneous dielectric system. A heterogeneous system can be represented as a combination of several such simple elements joined in series, the total impedance of which is given by

$$Z_N(\omega) = \sum_{n=1}^{N} \frac{1}{G_n + j\omega C_n} \; ; \qquad G_n = \frac{1}{R_n} \tag{5.19}$$

where the subscript "n" identifies the conductances and capacitances of each of the simple elements. The term "equivalent" inherently suggests that the electrical representation of the dielectric system is an approximation to the possible electrical response of the system. This is indeed the case for complex systems, where the physical system may not be represented as a unique equivalent circuit model. It is important to note that for a given impedance measurement, there may be more than one equivalent circuit that can be fitted to the frequency response data. Thus, the choice of the best equivalent circuit is primarily based

on the predicted physics, followed by statistical elimination of the less accurate models.

5.3 Experimental Setup and Procedure

The experimental setup for impedance measurements was described earlier in Section 3.5. The frequency response analyzer used for measurements was a Solartron 1260 (Solartron, USA), connected to a PC for data acquisition through a GPIB interface (National Instruments, USA). To reduce the effect of electromagnetic noise, a custom made Faraday cage was used. The cage was grounded using a scientific ground available in the building. The microchips used in the reported experiments are all identical, featuring channel depth of $15\mu m$ and width of $65\mu m$ at the intersection.

To measure the length of the films, a stage micrometer with $10\mu m$ resolution was used for calibration. Then, ImageJ freeware (NIH, USA) was utilized to measure the length of the film. The area of the film, calculated from the capacitance, was correlated to the length. This correlation between length and area of film can be incorporated to the measurements of other liquid systems as an estimate of the film area.

The films were formed using 2 wt. % lecithin in toluene. The water phase contained 1 wt. % NaCl as described in Section 3.6.1. This system was chosen for impedance spectroscopy for two reasons. First, lecithin films are capable of forming bilayers, which have a constant thickness over a wide range of pressures. A bilayer is an extremely thin film formed by two layers of surfactant with virtually no solvent core. Therefore, the mechanism of stability in these films is strong short-range steric interactions. Using such a system ensures that the films formed using lecithin are "identical" in different experimental systems. In particular, since we incorporate the specific capacitance of lecithin films from the thin liquid film (TLF) apparatus to calibrate the measurements in the microfluidic chip, one has to ensure that the conditions under which the films are formed in both systems are identical.

The second advantage of lecithin in toluene film is its extremely low interfacial tension with water, which is typically in the order of $1\mu J/m^2$ [Shinoda *et al.*, 1993]. Once again, this allows for some sort of "platform independence" of the system when subjected to IS experiments in the microfluidic chip and the TLF apparatus. For a proper quantification of the experimental data, the capillary pressure or the disjoining pressure in both systems has to be virtually identical. Due to the substantial size difference of these two devices, achieving equal capillary pressures is very difficult with most combinations of liquids and surfactants. Unless these pressures are identical, the film thickness will be different in these systems, possibly leading to different measures of the dielectric constant of a film. Therefore, lecithin in toluene film is used, which reduces the interfacial tension to very low values, thereby ensuring that the pressure difference in both systems is minimal. To form the films, the experimental procedure described in Section 3.7 was followed. The sweeping frequency range and adsorption and drainage times are described for every experiment separately in the following.

5.3.1 Impedance Measurement in the Microfluidic Chip

Figure 5.3 depicts the Nyquist diagram derived from the impedance measurement of an empty chip (filled with air) over the frequency range from $100kHz$ to $1MHz$. Since there is no electrolyte in the chip (the channels are filled with air), a predominantly capacitive response is expected. The solid line shows the least-squares fitting of a simple RC circuit (Fig. 5.1) model to the experimental data (symbols). The capacitance of the chip (henceforth referred to as stray capacitance) is in the order of 10^{-11} F $(10pF)$.

Figure 5.4 depicts the results of impedance measurement of the chip over a wide range of frequencies from 100Hz to 1MHz when it is filled with electrolyte (aqueous solution of 1 wt. % or 0.17M NaCl). Unlike the empty chip, the electrolyte filled system exhibits a substantially resistive behavior. The solid line depicts the results of least-squares curve fitting of the equivalent circuit

shown in Fig. 5.5 to the experimental data (symbols). The circuit is comprised of two parallel sub-circuits. The upper part consists of the parallel resistor ($5.6M\Omega$) and the stray capacitance of the empty chip ($60pF$). The bottom sub-circuit represents the equivalent circuit of the fluid system, consisting of a purely resistive element representing the electrode/electrolyte interfaces (72.2 kΩ), and the RC components of the electrolyte (the bottom left part of the circuit with a resistance of 1.9 $M\Omega$ and a capacitance of 845.5 pF). The liquid resistance and capacitance were calculated from the least-squares analysis. It is evident that the impedance of the electrolyte is predominantly resistive.

The bottom-left portion of the circuit diagram represents the equivalent circuit of the electrolyte. An aqueous solution of sodium chloride with ionic strength of 0.17 M has a molar electric conductivity of $\sim 100 \times 10^{-4}\ Sm^2/mol^{-1}$. Considering the dimensions of the water channel at the narrowest section ($65 \times 15\ \mu m^2$) and the distance between electrodes ($100\ \mu m$), the resistance of the electrolyte can be calculated as $60k\Omega$, which is in good agreement with the calculated value of $72.2 \pm 5k\Omega$ from least-squares fitting of the equivalent circuit to the experimental data. However, the circuit shown in Fig. 5.5 was not used for analyzing the experimental data for the thin liquid film impedance.

Figure 5.6 compares the Nyquist diagrams of the empty chip, a chip filled with water and a lecithin stabilized toluene film formed in water. The Nyquist plot of the film shows an intermediate behavior between the capacitive behavior of the empty microchip and the predominantly resistive behavior of the aqueous electrolyte solution. The impedance measurements before breakup of the film reveal a predominantly capacitive behavior (which is evident from the negligible real component of the curve) whereas after breakup, the resistive characteristic dominates. This is due to charge accumulation on the film which gives rise to an increase in capacitance of the cell. The figure also shows that despite the extremely small size of the film, the impedance spectroscopy technique is capable of differentiating between film and continuous water phase.

5.3.2 Equivalent Circuit Analysis of Film Drainage and Rupture

The problem of selecting an equivalent electrical circuit becomes quite difficult in presence of a thin film, since it involves considering the electrical response of the external circuit, the electrode/electrolyte interfaces, and the impedance of the water columns in addition to the film impedance. In this context, if the other impedance elements are comparable to or larger than the impedance of the film, it becomes quite difficult to accurately estimate the resistive and capacitive components of the film impedance.

Figure 5.7 depicts the proposed equivalent circuit for the system which is used for the analysis of the experimental results described in the following section. The circuit is comprised of two sections. The first section including C_1 and R_1 represents the thin film. The second part corresponds to the electrode/electrolyte interfaces (the two electrode/electrolyte interfaces are lumped into one element) and the bulk electrolyte resistance. These two components form the rest of the electrochemical system. The right hand side of the circuit in Fig. 5.7 (indicated as Electrode/Electrolyte) represents the interface between electrode and electrolyte. The resistor R_2 is the charge transfer resistance across the electrode/electrolyte interface and the capacitor C_2 resembles the double layer capacitance. Resistance of the solution (electrolyte) is represented by R_3. Using equation 5.19, the total impedance can be calculated as

$$Z_{total}^{-1}(\omega) = \frac{1}{R_p} + \frac{1}{Z_l} \tag{5.20}$$

where R_p is the resistance of the parallel resistor ($5.6M\Omega$) and Z_l represents the impedance of the lower sub-circuit, which, in turn, can be expressed as

$$Z_l(\omega) = \frac{1}{G_1 + j\omega C_1} + \frac{1}{G_2 + j\omega C_2} + \frac{1}{G_3} \tag{5.21}$$

One can add other elements to the circuit to improve the resemblance of the equivalent circuit to the electrochemical system. Adding more elements to the circuit might result in lower least-squares residuals during regression anal-

ysis, albeit at the expense of more adjustable parameters in the model. Larger number of fitting parameters can lead to more ambiguity in the results such as multiple answers, and larger standard errors for the estimated impedances of the elements. In impedance spectroscopy, the equivalent circuit is generally kept as simple as possible retaining only the necessary (or leading order) elements.

Figure 5.8 shows a typical Nyquist plot of an intact film. A close look at the figure shows that the measured impedance is comprised of two semicircles, which leads to the notion that at least two capacitors are required in the equivalent circuit. The circuit depicted in Fig. 5.7 can be used as the simplest representation of the electrochemical system dealt with in this study.

Equations 5.20 and 5.21 involve 5 unknown variables (C_1, R_1, C_2, R_2, and R_3). These variables can be approximated by fitting equations to the experimental data. LEVM fitting program (LEVM, by Ross Macdonald) [Macdonald, 2005] was used to find the best values for the above variables. LEVM is a complex least square fitting freeware that is used for impedance spectroscopy. The circuit depicted in Fig. 5.7 and the experimental values (total impedance of the chip) including frequency, real and imaginary parts of the impedance were defined in the program. Then, the best values for the unknown elements were calculated using the non-linear least squares algorithm by minimizing the sum of the least square errors. Care must be taken to avoid the local minima in the minimization procedure by changing the initial conditions several times and checking the total error value.

Once all circuit elements are found, the capacitance of the film can be calculated. To calculate the capacitance of the film, the two oil/water interfaces are first formed while they are kept away from each other (Fig. 5.9a). In this case, the film is not formed. The impedance of the system corresponding to this situation includes the impedance of all elements and interfaces except that of film. This establishes the base impedance of the system. After measuring the base impedance, the film is formed and once again the impedance is measured (Fig. 5.9b). The stray capacitance of the chip measured in the previous section

is omitted in the final equivalent circuit. This is due to the method of capacitance calculation used here. The capacitance of a film is calculated using the difference in capacitance when a thin film is formed and when the two water/oil interfaces are far from each other. Therefore, the stray capacitance is canceled, simplifying the equivalent circuit.

To calculate the capacitance of C_1 after film formation, all circuit elements were fixed at the values prior to film formation except C_1 and R_1. The value of the capacitance of the film was calculated from the difference in the capacitance of C_1 in the two cases.

5.4 Results and Discussion

Measurement of film area is presented in the next section followed by measurement of drainage time in small emulsion films. Adsorption process is studied using impedance measurement in Section 5.4.3. Finally, effect of DC polarization on the capacitance of micron sized emulsion films is described followed by concluding remarks.

5.4.1 Measurement of the Film Area

Since the cross section of the channels is not circular, the film area is not known. Capacitance is proportional to area of the film. Therefore, one can use impedance spectroscopy to find the area of the film. To calculate area of film, a good estimate of the specific capacitance (F/m^2) is vital. Fortunately, lecithin films are well studied in literature due to their wide application in bioengineering. Hanai *et al.* [1964] measured the specific capacitance of lecithin stabilized film from 0.395 to 0.405 $\mu F/cm^2$, therefore, the specific capacitance used in this study is 0.400 $\mu F/cm^2$.

Figure 5.10 depicts the measured film area versus film's length. The length of the film was measured optically. The area of the film is estimated using the total capacitance, the specific capacitance, and the length of the film. The figure shows that the area of the film is linearly proportional to the length, from

20 μm to 40 μm. This correlation can be explained, taking into account the depth of the channel. At the outset of formation, the film grows both laterally and vertically. Once the length of the film becomes equal to the depth of the channel ($15\mu m$), it grows mostly laterally. Therefore, above $15\mu m$, the area of the film is proportional to its length. In films shorter than $15\mu m$, on the other hand, area is proportional to the square of the length as it is evident from the figure where the area of the $20\mu m$ film is four times that of the $10\mu m$ film.

It is important to note that one can assume that the specific capacitances of lecithin stabilized toluene film in the microchip and the TLF apparatus are equivalent if the film thickness and dielectric constant of the film in both these systems are equal. Under such incompatible conditions where capillary pressures can be quite different, equivalence of the thicknesses is hardly guaranteed. However, lecithin films benefit from two important characteristics which make such an assumption viable. First, lecithin forms a bilayer. A bilayer or Newton Black Film (NBF) is a thin liquid film formed by two layers of surfactant without any solvent core. Such films are stabilized by strong short-range steric interactions. Bilayers are fairly rigid films which maintain a constant thickness over a wide range of pressure. Furthermore, lecithin adsorbed interfaces exhibit a markedly reduced interfacial tension (order of $\mu J/m^2$ [Shinoda *et al.*, 1993]). The rigidity of the film and the extremely low interfacial tension achieved by this system provide reasonable grounds to assume that the specific capacitances in both systems are equal.

5.4.2 Drainage Time in Small Emulsion Films

Capacitance of a capacitor is inversely proportional to the separation of the two conducting media or directly proportional to the thickness of non-conducting medium:

$$C = \varepsilon \frac{A}{d} \tag{5.22}$$

in which ε, A, and d represent dielectric permittivity, area of capacitor plates, and separation between the two plates, respectively. Assuming a constant dielec-

tric permittivity during the course of an experiment, one can study the dynamics of the film thickness using capacitance measurement. Therefore, impedance spectroscopy is incorporated to investigate the change of film thickness after formation. Figure 5.11 shows the capacitance of the film during drainage time. Drainage time is the time span before application of potential during which the film is left to reach the equilibrium state (Section 3.7.2). Similar to the previous section, the experimental system under investigation was comprised of 2 wt. % lecithin in toluene as the oil phase and aqueous solution of 1 wt. % NaCl as the water phase.

It is evident from Fig. 5.11 that the capacitance of the film does not change markedly after formation, hence the film attains the final equilibrium thickness in less than 30 seconds. This observation corroborates our previous observation based on DC measurements that the drainage time of the microscopic films in the microfluidic device is much smaller than the drainage time of large films formed in conventional devices (*e.g.*, TLF apparatus).

Drainage of thin films is generally governed by several factors. The most important factor is the interfacial interaction between the two interfaces manifested as the disjoining pressure. While disjoining pressure can be considered as the sole constituent factor in film stability and drainage, there are other parameters that influence these processes. For instance, viscosity of the film forming medium (*e.g.* oil) plays an important role in dictating the speed of equilibration since higher viscosity slows down the drainage of the film. In the case of conventional experiments such as the TLF apparatus described in Section 2.1.2, since the area of the film is substantially larger than those formed between micron sized emulsion droplets, the drainage process can take minutes or even hours [Panchev *et al.*, 2006]. Furthermore, in small droplet sizes, high capillary pressure of the droplet gives rise to substantial rigidness of the interface which may not be achievable in large scale films where phenomena such as lens (or dimple) formation [Ivanov, 1988; Kralchevsky and Nagayama, 2001] is very common. This would give rise to the question as to whether such phenomena occur in

small emulsion films as well. Figure 5.11 indicates that micron sized droplets drain much quicker than larger drops, even though the interfacial tension of lecithin stabilized films is extremely low.

5.4.3 Adsorption Time in Small Emulsion Films

Figure 5.12 shows the capacitance measurement of the film versus adsorption time (Section 3.7.2). The film formation follows the procedure described, but the adsorption time of surfactant is changed from 30 sec. up to 10 min.

The figure depicts decay of the capacitance with time. The value of capacitance is 0.55 pF at 30 s. Unfortunately, due to limitations of impedance spectroscopy, measurement of impedance before 30 seconds is not possible. The interface reaches the minimum capacitance value after 5 minutes. The figure shows a 40% decrease in capacitance of the film.

The decrease in capacitance can be associated with two possible phenomena. First, longer adsorption time causes higher surface coverage. Increase of surfactant molecules per unit area of interface corresponds to concomitant decrease in dielectric constant of the film, which, in turn, leads to reduction in capacitance. Secondly, it is reported that the thickness of lecithin film varies from 40 to 70$\mathring{A}$ which could change capacitance of the film. This variation of thickness could readily be accounted for by the change in capacitance. However, the reported thickness variation is due mainly to change in bulk concentration of surfactant, and not adsorption time. The experiments with TLF apparatus performed in parallel with this work also did not suggest any marked change in final film thickness with adsorption time [Panchev *et al.*, 2006]. Therefore, it is concluded that the reduction in capacitance is predominantly governed by reduction in dielectric permittivity of the film due to adsorption of surfactant molecules. This also can be tested by fitting the Langmuir adsorption model to the experimental data, which is depicted as the dashed line. Recalling Langmuir kinetic adsorption equation 4.6, one can write

$$\exp(-kC_b t) = 1 - \frac{\theta}{\theta_{max}} \tag{5.23}$$

where θ is the fractional coverage of the oil-water interface by lecithin, θ_{max} is the maximum fractional interfacial coverage, k is the adsorption rate constant, C_b is the bulk lecithin concentration, and t is the time. The left hand side of the above equation is fitted to the data in Fig. 5.12.

The above observation is in accord with the DC breakdown of the film described in the previous chapter. The value of critical potential of the film expressed a similar trend with adsorption time. Both measurements, despite the substantial difference in nature, follow the Langmuir kinetics.

To compare both DC and AC measurements, one can non-dimensionalize both axes (Figs. 5.12 and 4.8) with respect to the saturation values as full surface coverage. Comparison of these impedance measurements with DC breakdown measurements in Fig. 4.8 are shown in Fig. 5.13. In the figure, both measurements are non-dimensionalized. It is evident that both measurement techniques are in good agreement. Note that the non-dimensionalization is performed on the raw data using the average value of the final equilibrium point, therefore the standard deviation of lower values (such as 30 and 120 seconds) are smaller than those of larger values.

The figure suggests that the DC breakup method is a considerably accurate and reliable technique. It features a robust assessment technique as well as better standard deviation. Particularly, in such small systems where impedance spectroscopy is more prone to measurement errors due to limitations in sensitivity and resolution, DC breakup technique can be considered the method of choice.

5.4.4 Impedance measurement in presence of DC polarization:

Figure 5.14 depicts the change in capacitance of film due to an electric field. In the figure, the horizontal and vertical axes depict the DC potential and capacitance of the film, respectively. The capacitance is non-dimensionalized with respect to the first point where applied potential is zero. The DC potential

is ramped at the rate of 50mV/step. At each step, an impedance measurement is performed over the range of frequency from $10kHz$ to $1MHz$. The capacitance at each step is calculated using the circuit of Fig 5.2.

The increase in capacitance is associated with reduction in film thickness. As discussed in the previous chapter, the applied potential difference across the electrodes directly translates into equal potential drop across the thin film, owing to the substantial conductivity of the aqueous phase. The applied potential over the extremely small thickness of the film gives rise to an enormous electric field ($\sim 10^8\ V/m$). This large electric field, in turn, causes a compressive normal force which results in thinning the film. Therefore, the capacitance of the film would increase following the applied potential.

Figure 5.14 provides interesting insight regarding the intermolecular interactions of the film. Once the potential is applied, the compressive force is proportional to the square of the applied potential (Eq 4.1), while the disjoining pressure of the film balances the applied force. The solid line in the figure is a least-squares fit of a quadratic function in the form of αV^2. Note that the capacitance is proportional to the inverse of film thickness. Therefore, the figure suggests that the disjoining pressure (or intermolecular interactions between surfactant molecules adsorbed at the interface) changes linearly within the range of applied potential and/or thickness. This observation is in accord with Crowley's electromechanical model [Crowley, 1973] where the intermolecular interactions of the two oil water interfaces are modeled using a simple Hooke's law. In other words, one can assume that these interactions are linear within the range of applied potential. Therefore, a constant modulus of elasticity provides an adequate platform for modeling these films. The dashed line in the figure represents the measurements performed by Babakov *et al.* [1966], which is in good agreement with our measurements.

Furthermore, one can conclude that Maxwell stress can be considered as the leading order factor in disintegration of the film. While application of such high electric fields across the film gives rise to multipolar forces, Fig. 5.14 shows that

the film deformation can simply be explained by Maxwell stress.

5.5 Conclusion

In this chapter, impedance spectroscopy was used to study thin liquid films formed between micron sized emulsion droplets. The first goal of the study was to investigate applicability of this method for extremely small scale films. The method was useful in distinguishing between formation and breakup of the film. Furthermore, impedance measurements of the aqueous phase resulted in good agreement between measured conductance and those reported in literature.

Area of the film was one of the unknown characteristics of films formed in the developed microfluidic device. Employing IS technique, the particular chip used in this study was calibrated successfully. The calibration curve (Fig. 5.10) can be used for estimation of the film area of other liquids as well.

Drainage of small films formed between micron sized emulsion droplets was studied using the impedance measurement technique. The measurements showed that the equilibration time in small films is substantially quick. In conventional techniques, where large films are formed, due to deformability of the interfaces, the volume of the trapped liquid between the two interfaces can be substantial. The large volume of the liquid has to drain through the small gap between the two interfaces which leads to a considerable amount of time to reach equilibrium. In small scale films, on the other hand, as it is discussed in Section 5.4.2, the equilibration time is much quicker, which can be associated with the high capillary pressure and rigidity of the interface.

Effect of adsorption time on capacitance of film was investigated. The results showed that the capacitance reaches a minimum value after a few minutes. This is due to saturation of the interface by surfactant molecules. Interestingly, the saturation time is in good agreement with DC measurements in the previous chapter, although the two methods are completely different in nature.

Finally, the influence of DC polarization on the capacitance of the film was studied. The measurements showed that the applied potential establishes a

normal force on the film proportional to the square of the polarization.

Table 5.1: Summary of calculation of film area. The specific capacitance used to calculate area is $0.4\mu F/cm^2$.

Film Length (μm)	Capacitance (F)	Standard Deviation	Calculated Area (μm^2)	Standard Deviation
10	1.53E-13	1.13E-13	38.3	28.32
20	6.60E-13	3.05E-13	165	76.23
30	1.06E-12	3.07E-13	266	76.67
40	1.28E-12	4.1E-13	320	102.40

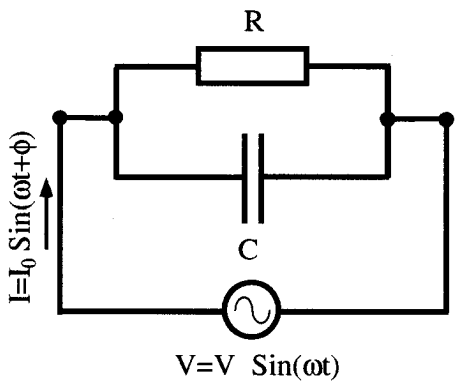

Figure 5.1: A simple parallel RC circuit. This circuit also represents the electric model for a homogeneous dielectric material.

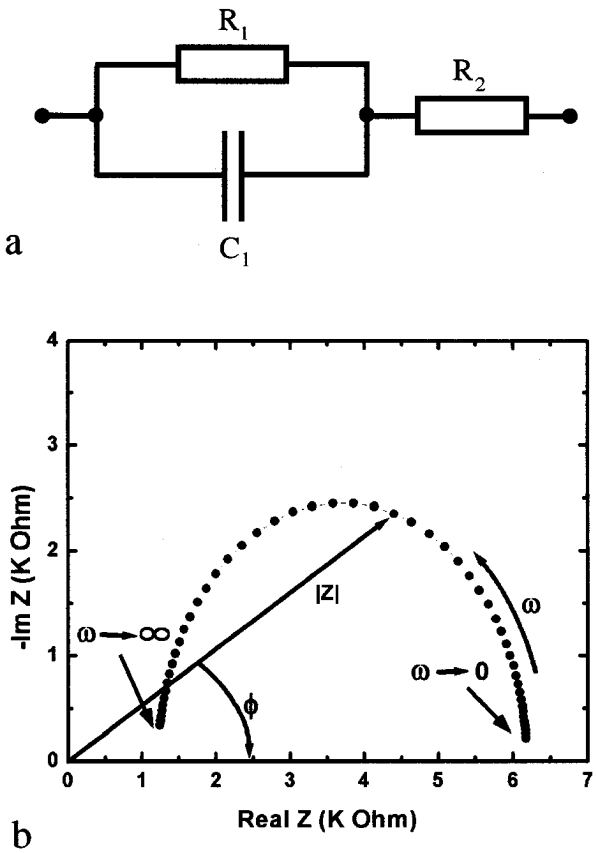

Figure 5.2: a) Equivalent circuit for a pure electrolyte. R_1 and C_1 represent the resistance and capacitance of electrode/electrolyte interface and R_2 is the resistance of the electrolyte b) Typical Nyquist plot for the circuit shown above.

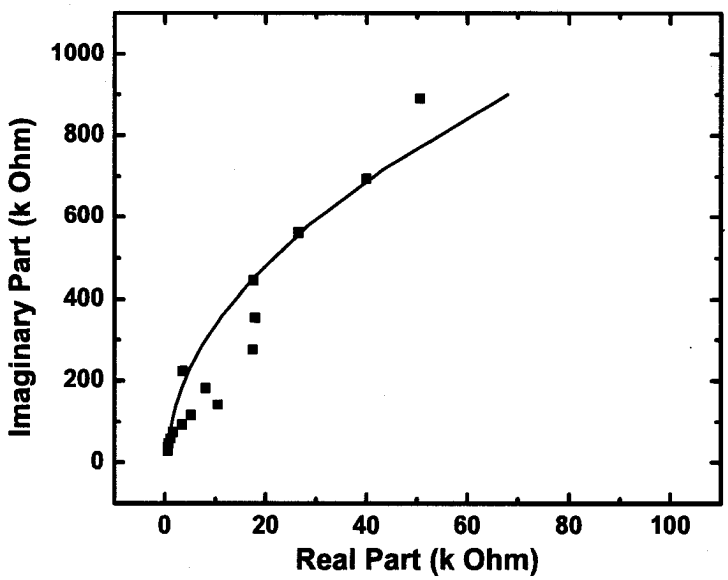

Figure 5.3: Nyquist diagram of an empty chip (filled with air).

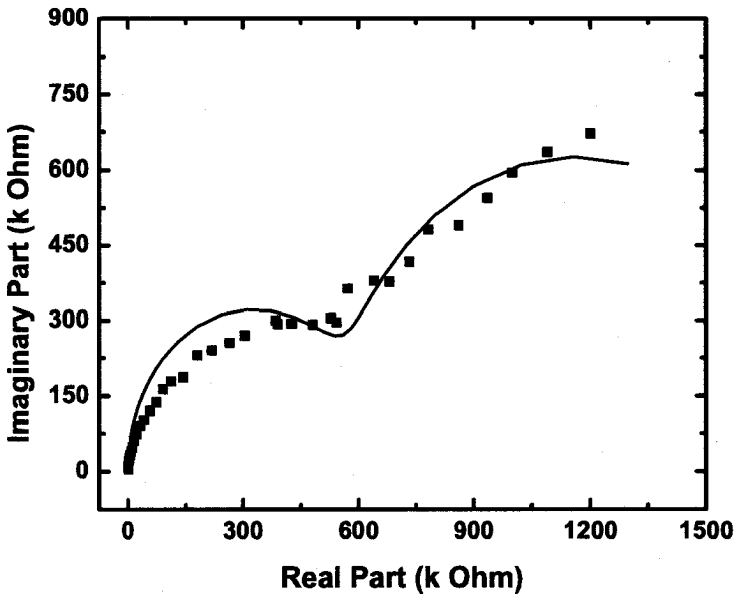

Figure 5.4: Nyquist diagram of the chip filled with electrolyte. The solid line demonstrates the results of the model circuit in Figure 5.5.

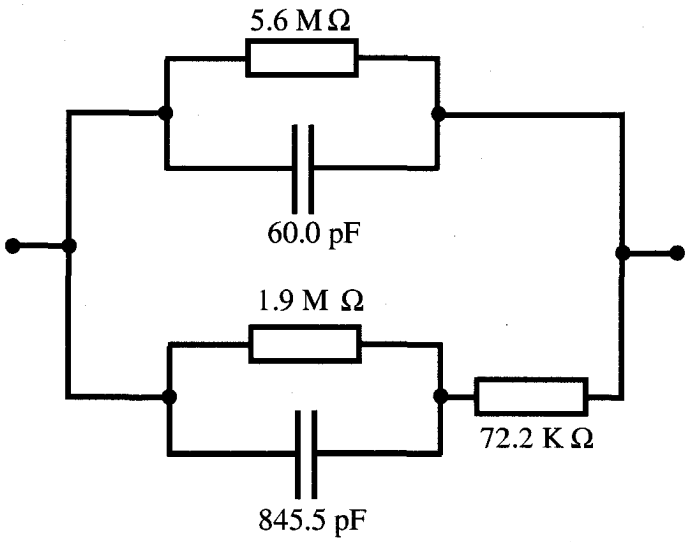

Figure 5.5: Equivalent circuit calculated for the chip with electrolyte.

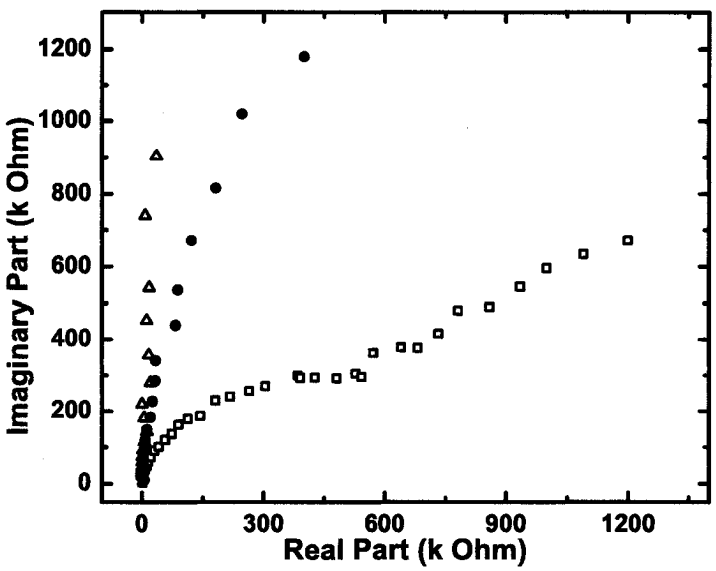

Figure 5.6: Nyquist diagram of a the empty chip (△), chip filled with water (□), and a film (•).

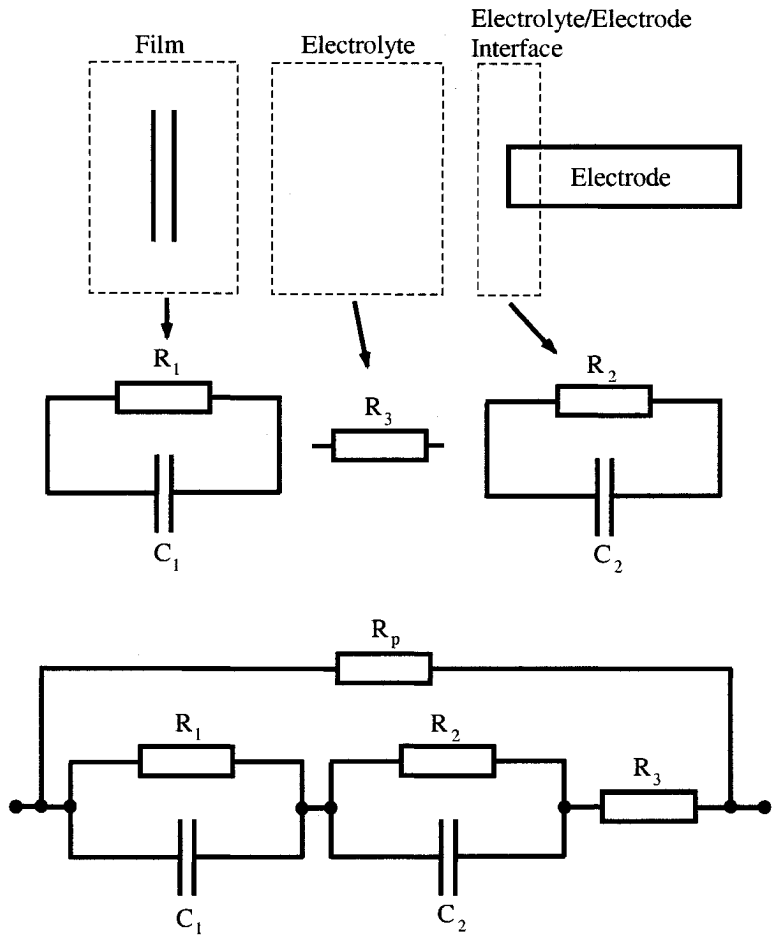

Figure 5.7: Equivalent circuit of the chip while the film is formed. R_1 and C_1 represent the film while R_2 and C_2 are equivalent elements for the double layer at the electrodes. The resistance of the electrolyte is accounted for by R_3 and the parallel resistor is shown by R_p .

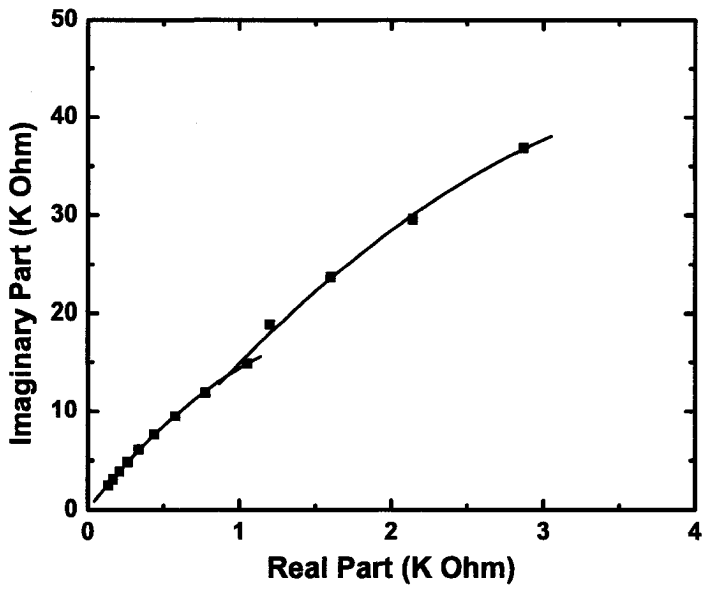

Figure 5.8: The Nyquist plot of a film. The figure shows the presence of two semi-circle.

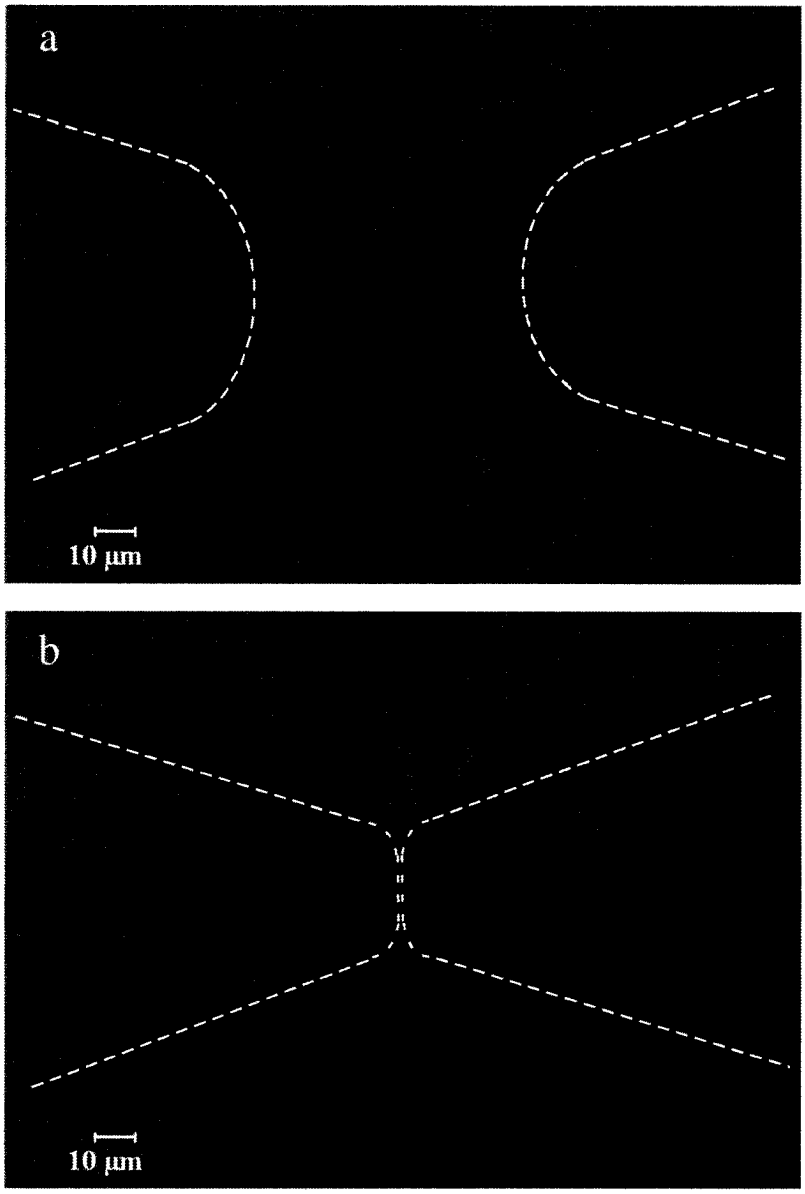

Figure 5.9: Optical microscope image of the chip. The dashed line depicts the oil/water interface. For capacitance calculation, first, the two interfaces are formed as depicted in (a) and the impedance measurement can be performed. Then the film is formed as shown in (b) and another IS is conducted. The difference between the two capacitance is capacitance of the film.

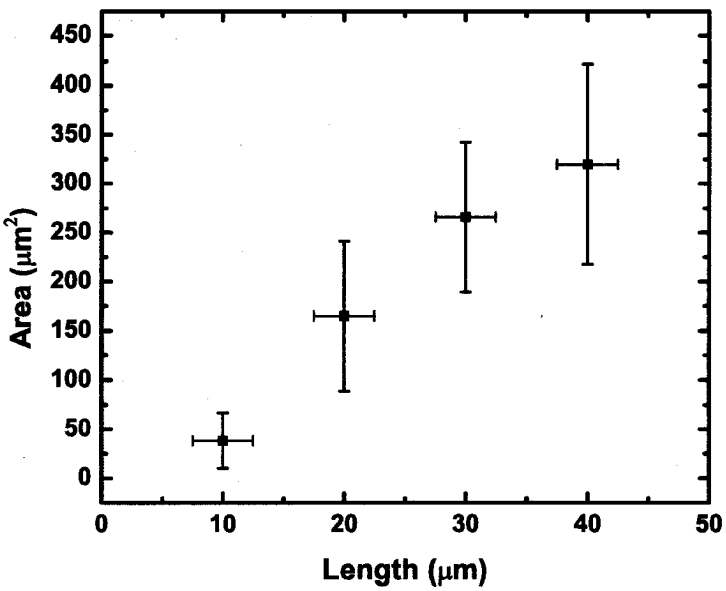

Figure 5.10: Calculated are of a film vs. length of the film. The length is measured optically.

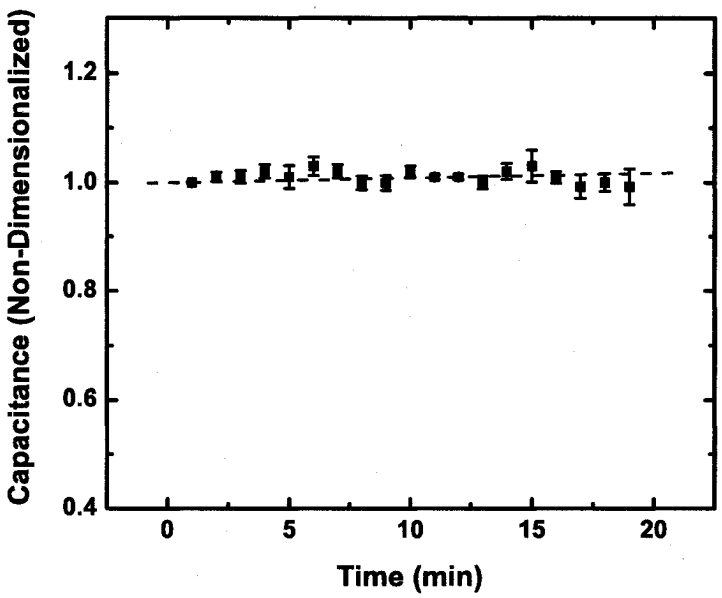

Figure 5.11: Capacitance changes vs. drainage time of the film. The figure shows no marked difference in drainage time of the film which suggest a quick attainment of equilibrium condition in small films.

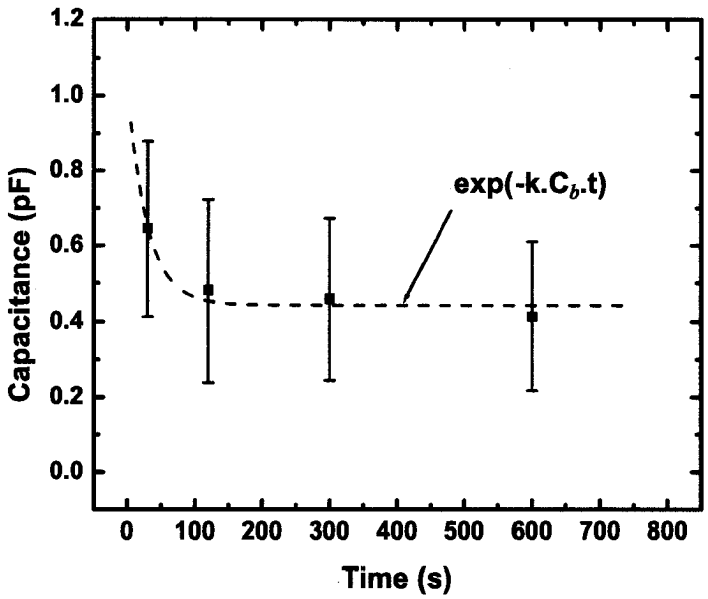

Figure 5.12: Capacitance of lecithin films vs. adsorption time.

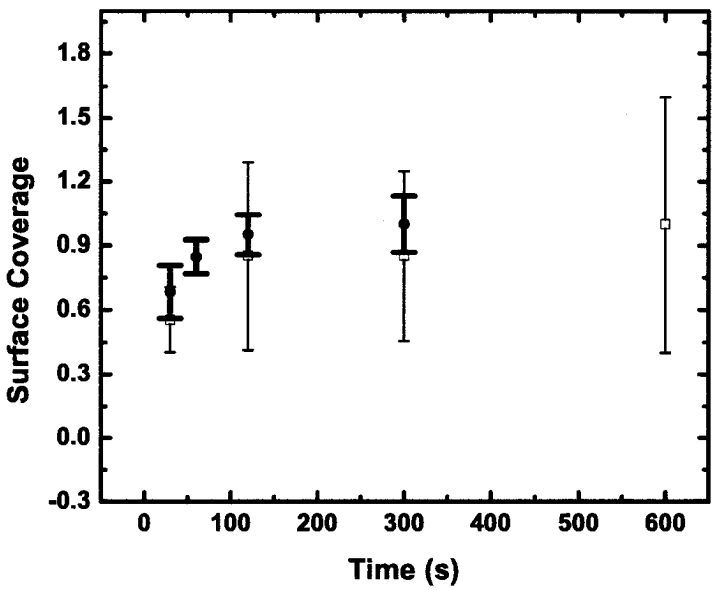

Figure 5.13: Non-dimensionalized surface coverage of surfactant versus adsorption time. Squares (□) represent the AC measurements whereas solid circles (•) represent DC measurements reported in previous chapter.

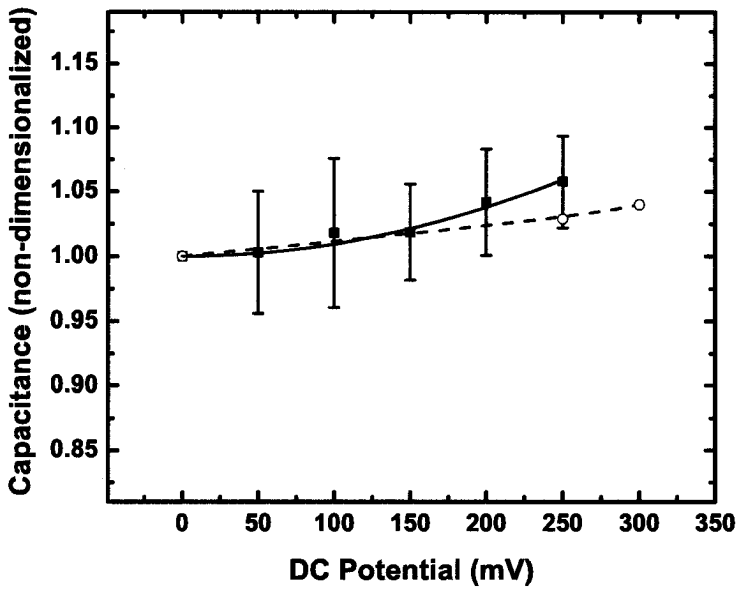

Figure 5.14: Effect of DC polarization on capacitance. Data are non-dimensionalized with respect to the first point where the applied potential is zero.

Chapter 6

Conclusions and Recommendations

This chapter provides a brief overview of conclusions related to each objective of the thesis. Following the concluding remarks, recommendations for future work are presented. The objectives of the thesis were:

1. Develop an experimental setup to study thin liquid films at micron scale.
2. Incorporate microfluidic techniques to create stable hydrostatic conditions to form thin liquid films.
3. Employ electrochemical destabilization/detection of the liquid film and study applicability of electric breakdown as a stability criterion.
4. Study drainage behavior of micron size emulsion films and the effect of DC field on the capacitance of the films.
5. Explore applicability of the developed technique for an industrial emulsion system.

In the following, the conclusions pertaining to the studies pursuing the above objectives are presented.

6.1 Develop an experimental setup to study thin liquid films at micron scale

Most practical emulsions in industry or nature are comprised of micron size droplets. In the case of de-emulsification applications, micron size emulsion droplets pose serious separation challenges. Therefore, behavior of thin liquid films formed between such small droplets is of interest. Available experimental techniques are not suited for micron size thin liquid films, leaving doubts about the applicability of the conventional models developed based on large area films to those of micron size films. For instance, the equilibrium capillary pressure (or disjoining pressure) depends on the curvature or the size of the droplets; the smaller the droplets, the higher the equilibrium disjoining pressure. Furthermore, stability of a film corresponds to its area. Large area films break much easier than small ones.

In this study, an experimental setup was successfully developed for studying micron size emulsion films. The method provided a robust platform for assessing the stability of thin liquid films formed between micron size emulsion droplets. Since the electrochemical destabilization is incorporated, the study was limited to water in oil emulsions, however, the method has no limitation in forming other type of films such as oil in water emulsion or foam films if pressure destabilization is employed.

6.2 Incorporate microfluidic techniques to create stable hydrostatic conditions to form thin liquid films

Microfluidics, as an emerging new technique for small scale systems, was successfully employed in the development of the experimental system. The concept of lab-on-a-chip was explored to develop an experimental tool both for scientific and industrial applications. The developed microfluidic system was capable of forming micron size thin liquid films between two water droplets. Due to the

small size of the microchannels, oil/water interfaces with small radius of curvature ($\sim 6.5\mu m$) were formed. Such curvatures replicate high capillary pressures that exist in small droplet sizes.

The most important challenge in the development of the microfluidic chip was to maintain a hydrostatic or stationary condition within the chip. The hydrostatic condition had to be maintained despite the high capillary pressure, thermal fluctuations, pressure fluctuations, and constant interfacial tension changes due to adsorption. Stable hydrostatic condition was achieved by implementing few modifications to the chip design and the experimental setup. Chip modifications included selective hydrophobization of the substrate, tapering the channels, oil/water channels aspect ratio, evaporation control, and substrate material. Electric and hydraulic modifications in the setup included an air cushion, a parallel resistor, and a Faraday cage. By implementing all of the above modifications a robust and reliable design was developed in which small thin liquid films were formed. Furthermore, the requirement for stationary condition using the experiment was successfully met.

Employing microfabrication techniques, rapid and cost effective production of the device is possible. Using the microfabrication procedure developed in this study the device can easily be replicated and mass produced as a disposable chip. Furthermore, numerous experiments can be conducted in one chip very quickly.

6.3 Employ electrochemical destabilization and detection of the film and study applicability of electric breakdown as a stability criterion

Emulsion systems comprised of lecithin in toluene and water were used. Electric breakdown of thin liquid films was studied by applying a ramp electric potential across the film. The rupture of the film was detected by the abrupt change in the conductance of the film.

In order to test sensitivity of critical potential to the stability of a film, concentration of lecithin was varied from 0.05 to 2 wt %. Consequently, the average critical potential of breakup showed marked changes corresponding to the variation of the surfactant concentration. The critical potential of lecithin films reached a saturation value at 1% lecithin concentration. The saturation of critical potential can be explained using Langmuir adsorption model. Langmuir adsorption model predicts that adsorption (or surface coverage) of a surfactant to an interface increases with the bulk concentration of the surfactant. Langmuir model also predicts that adsorption reaches a saturation point, beyond which, surface coverage does not increase with concentration. As the surface coverage increases, stability of the film increases as well. The comparison between the critical potential of lecithin films and Langmuir adsorption model shows that critical potential distinguishes changes in stability of the film due to variation in surfactant concentration.

Similarly, variation of adsorption time was in accord with Langmuir adsorption kinetics. Increase in adsorption time was followed by concomitant increase in the film's stability and critical potential. Critical potential measurements of lecithin films showed that after two minutes of adsorption, stability of the film did not increase. This is due to saturation of the interface by lecithin. Furthermore, standard deviation of critical potential was improved due to the small size of the film compared to those reported in literature.

TEGOPREN, as a copolymer surfactant, was used to stabilize n-decane films. The film showed much higher stability than those of lecithin in toluene. This is due to the high emulsification potential of TEGOPREN and greater thickness of the film. Furthermore, the conductance curve of the film deviated from that of lecithin showing a substantial current leakage through the film. The current leakage can be explained considering the conductivity of TEGOPREN molecules. Once the two monolayers of TEGOPREN molecules adsorbed on the two oil/water interfaces are close enough, limited electric charge can be transferred from one side to the other. The conductivity of the film formed by

TEGOPREN is in accord with those reported for similar copolymers.

6.4 Study drainage behavior of micron size emulsion films and the effect of DC field on the capacitance of the film

Since the area of the film is not well defined in the developed microfluidic device, AC impedance spectroscopy was implemented. Therefore, using impedance spectroscopy and the specific capacitance of lecithin films, the area of the films were estimated. This estimation can be used for calibration of the chips.

Impedance measurement of aqueous solution of electrolyte was measured using this technique in the chip and the results were in accord with those reported in literature.

Impedance measurement of films up to 20 minutes after formation showed that their capacitance remains constant. This led to the fact that in the case of small emulsion droplets, due to high capillary pressure and rigidity of the water oil interface, the film drained much quicker than those of larger area films. In conventional thin liquid film measurements, lens formation is one of the phenomena that hinders attainment of equilibrium state. Once the lens is formed, a large amount of liquid is trapped inside the lens. Attractive van der Waals interactions between the two interface squeezes the trapped liquid out. Impedance measurement of micron size films formed in the developed microfluidic device showed no sign of impedance changes due to lens formation. In the microfluidic device developed in this study, there is no visual reference that could confirm the results of impedance measurement, however, visual observations of films with a diameter of $100\mu m$ confirms that in small and high pressure films, equilibrium is reached very quickly.

The effect of adsorption time on capacitance of the film was investigated using impedance spectroscopy. The measurements showed that capacitance of the film reaches a saturation value quickly, which is due to saturation of surface coverage of the surfactant. Once the surface overage is at its maximum value,

the capacitance of the film reaches the saturation point. The measurement for 30 second adsorption shows a capacitance slightly higher than those of long adsorption time which is due to less surface coverage of the film. This is in accord with critical potential measurements on similar films that showed the same behavior.

Capacitance of the film was measured under the effect of a DC field. Application of the electric field results in a compressive force on the film. This compressive force reduces the thickness of the film, which can be detected by the increase in capacitance. The electric force is proportional to the square of the electric field. The results of the tests indeed show that the capacitance of the film increases with the square of the electric field.

6.5 Explore applicability of the developed technique for an industrial emulsion system

The developed experimental setup was used on water in diluted bitumen as an industrial emulsion system. The objective of the tests was to explore the applicability of such an experimental setup on an industrial emulsion. To change the stability of the emulsion, a de-emulsifier was added to the oil phase. Variation of concentration of the de-emulsifier was detected by concomitant changes in the critical potential. The bitumen film had the maximum stability without the de-emulsifier. Increase of the de-emulsifier concentration reduced the stability of the film to a minimum corresponding to a 50ppm de-emulsifier dosage. Further increase of the de-emulsifier concentration resulted in increased stability. This observation is in accord with those reported in literature. The result of this experiment proves that the microfluidic device developed in this study is suited for such industrial applications. The developed experimental device not only provides an robust method for thin film stability measurement but also can easily be used for industrial applications as mentioned above.

6.6 Recommendations

6.6.1 AC breakdown and frequency dependence of electric breakdown

In this study, the applied potential for film breakdown studies was DC. However, one can break a liquid film using AC electric potential as well. In the case of AC potential, the critical potential depends on two parameters; amplitude and frequency. Amplitude of the AC electric potential acts similar to a DC potential by imposing a compressive Maxwell stress on the film which is proportional to the square of the applied electric field. As well, frequency of the applied potential plays an important role in breakdown. If the frequency of the applied potential is close to the resonance frequency of the film, the film may break at lower amplitudes.

The natural frequency of the film can be estimated using conventional long wave theory approach. Comparison of the calculated natural frequency and that of the measured resonance would be a test for validity of the long wave theory for electric breakdown of thin liquid films. Furthermore, the results of this research can be used for developing more efficient electro-coalescers used in petroleum industries. Usually, electro-coalescers use a constant frequency AC potential for separation of water from oil. If the frequency of the applied potential is close to the natural frequency of the system, an efficient coalescer with low energy consumption can be developed.

6.6.2 Light intensity measurement

The disadvantage of the microfluidic device developed in this study is the lack of direct film thickness measurement. In conventional thin liquid film experiments, since the cross section of the film is directly visible, interferometric thickness measurement is possible. In the microfluidic device developed in this study, however, the view direction is along the film surface. Therefore, no optical measurement is possible. In the developed device, thickness measurement

is possible by means of impedance spectroscopy, but such estimation requires accurate dielectric constant information of the film, which has to be measured using conventional thin film experiments.

One solution to this problem is embedding two optical fibers in the water channels. One fiber can be considered as the light source while the other one, placed on the other side of the film, receives the light. When the film goes through the thinning process, variation of light intensity would provide the required thickness information similar to conventional techniques. Such an experiment would provide a wealth of knowledge about the behavior of micron size films.

6.6.3 Automation of the developed microfluidic setup

The developed experimental tool in this study is capable of rapid and sequential stability measurements on films. In the developed device, due to the small area of the interfaces, adsorption of surfactant happens quickly, resulting in reduced turn-around time for each test. Moreover, by flushing the channels after each experiment, fresh interfaces can be formed quickly. However, the manual operation of the experiment is labor intensive. Furthermore, the results of the tests can vary depending on the proficiency of the operator. By automation of the tests, repeatable and reproducible data can be generated quite readily.

Automation of the system is possible by adding an image processing system to the microscope that can analyze the image of the interfaces and form the film. Such an automated system can add significant value to a production line such as those of oil sands extraction where control of the amount of emulsifier/de-emulsifier plays a crucial role in the quality of the end bitumen product.

Bibliography

Ahn, K., J. Agresti, H. Chong, M. Marquez and D. A. Weitz (2006). *Appl. Phys. Lett.* **88**, 264105.

Alcaraz, A., H. Holdik, T. Ruffing, P. Ramirez and S. Mafe (1998). *J. Membr. Sci.* **150**, 43.

Alcaraz, A., P. Ramirez, J. A. Manzanares and S. Mafe (2001). *Journal of Physical Chemistry B* **105**, 11669.

Anklam, M. R., D. A. Saville and R. K. Prud'homme (1999*a*). *Langmuir* **15**, 7299.

Anklam, M. R., D. A. Saville and R. K. Prud'homme (1999*b*). *Colloid Polym. Sci.* **277**, 957.

Anklam, M. R., D. A. Saville and R. K. Prud'homme (1999*c*). *Abstracts of Papers of the American Chemical Society* **218**, U669.

Anklam, M. R., D. A. Saville and R. K. Prud'homme (2001). *Polym. Adv. Technol.* **12**, 70.

Asami, K. (2002). *Progress in Polymer Science* **27**, 1617.

Babakov, A. V., Ermishki.Ln and E. A. Liberman (1966). *Nature* **210**, 953.

Bailes, P. J. and S. K. L. Larkai (1981). *Transactions of the Institution of Chemical Engineers* **59**, 229.

Bailes, P. J. and S. K. L. Larkai (1987). *Chemical Engineering Research and Design* **65**, 445.

Bard, A.J. and L.R. Faulkner (2001). *Electrochemical Methods*. 2nd ed.. Wiley. New York.

Barsoukov, E and J. R. Macdonald (2005). *Impedance spectroscopy: theory, experiment, and applications.* 2nd ed.. Wiley-Interscience. Hoboken, N.J.

Benz, R. and U. Zimmermann (1981). *Biochim. Biophys. Acta* **640**, 169.

Benz, R., F. Beckers and U. Zimmermann (1979). *J. Membr. Biol.* **48**, 181.

Bruin, G. J. M. (2000). *Electrophoresis* **21**, 3931.

Chabert, M., K. D. Dorfman and J. L. Viovy (2005). *Electrophoresis* **26**, 3706.

Cheng, J and Kricka, L. J., Eds.) (2001). *Biochip Technology.* Harwood Academics Publishers. Philadelphia.

Chernomordik, L. V., S. I. Sukharev, I. G. Abidor and Y. A. Chizmadzhev (1983). *Biochim. Biophys. Acta* **736**, 203.

Chilcott, T. C., M. Chan, L. Gaedt, T. Nantawisarakul, A. G. Fane and H. G. L. Coster (2002). *J. Membr. Sci.* **195**, 153.

Cho, Y. H., T. Yamamoto, Y. Sakai, T. Fujii and B. Kim (2006). *Journal of Microelectromechanical Systems* **15**, 287.

Cole, K. S. and R. H. Cole (1941). *J. Chem. Phys.* **9**, 341.

Coster, H. G. L., E. Steudle and U. Zimmermann (1976). *Plant Physiol.* **58**, 636.

Coster, H. G. L., T. C. Chilcott and A. C. F. Coster (1996). *Bioelectrochem. Bioenerg.* **40**, 79.

Cottrell, F. G. and J. B. Speed (1911).

Crowley, J. M. (1973). *Biophys. J.* **13**, 711.

Derjaguin, B. V., A. S. Titijevskaia, II Abricossova and A. D. Malkina (1954). *Disc. Faraday Soc.* p. 24.

Dimitrov, D. S. and R. K. Jain (1984). *Biochim. Biophys. Acta* **779**, 437.

Driscoll, F. (1973). *Analysis of electric circuits.* Prentice-Hall, INC. Englewood Cliffs, NJ.

Dukhin, A. S. and P. J. Goetz (2006). *Journal of Electroanalytical Chemistry* **588**, 44.

Eow, J. S., M. Ghadiri, A. O. Sharif and T. J. Williams (2001). *Chemical Engineering Journal* **84**, 173.

Evans, E. A. and S. Simon (1975*a*). *Biophys. J.* **15**, 850.

Evans, E. and S. Simon (1975*b*). *J. Colloid Interface Sci.* **51**, 266.

Everitt, C. T. and D. A. Haydon (1968). *J. Theor. Biol.* **18**, 371.

Exerowa, D and A. Scheludko (1971*a*). *Comp. Rend. Acad. Bulg. Sci.* **24**, 47.

Exerowa, D. and A. Scheludko (1971*b*). *Comp. Rend. Acad. Bulg. Sci.* **24**, 47.

Exerowa, D and P. M. Kruglyakov (1998). *Foam and Foam Films.* Elsevier. New York.

Floyd, T (1981). *Principles of electric circuits.* Charels E. Merrill publishing. Columbus, OH.

Fonseca, C. P. and S. Neves (2002). *J. Power Sources* **104**, 85.

Fordedal, H., Y. Schildberg, J. Sjoblom and J. L. Volle (1996). *Colloids Surf., A* **106**, 33.

Fricke, H. and S. Morse (1925). *Journal of General Physiology* **9**, 153.

Gad-el Hak, M., Ed.) (2002). *The MEMS Handbook.* CRC Press. Boca Raton.

Goldszal, A. and M. Bourrel (2000). *Ind. Eng. Chem.* **39**, 2746.

Hanai, T., D. A. Haydon and J. Taylor (1965*a*). *J. Theor. Biol.* **9**, 422.

Hanai, T., D. A. Haydon and J. Taylor (1965*b*). *J. Theor. Biol.* **9**, 433.

Hanai, T., J. Taylor and D. A. Haydon (1964). *Proc. R. Soc. London, A* **281**, 377.

Harrison, D. J., K. Fluri, K. Seiler, Z. H. Fan, C. S. Effenhauser and A. Manz (1993). *Science* **261**, 895.

Hool, K. O., R. C. Saunders and H. J. Ploehn (1998). *Rev. Sci. Instrum.* **69**, 3232.

IUPAC (1979). *Manual of symbols and terminology for physicochemical quantities and units.* 2nd ed.. Pergamon Press, 1979.. Oxford ; New York.

Ivanov, I. B. (1988). *Thin liquid films.* Marcel Dekker. New york.

Khristov, K., D. Exerowa and G. Minkov (2002). *Colloids Surf., A* **210**, 159.

Khristov, K., S. D. Taylor, J. Czarnecki and J. Masliyah (2000). *Colloids Surf., A* **174**, 183.

Kralchevsky, P. A. and K. Nagayama (2001). *Particles at fluids interfaces and membranes.* Elsevier Science B. V.. Amsterdam.

Krugliakov, P. M. (1993). Thin hydrocarbon films in aqueous medium as a model of w/o emulsions.. In: *First World Congress on Emulsions.* Vol. 2. Paris. p. 31.

Krugliakov, P. M. and I. G. Rovin (1978). *Physical Chemistry of Black Hydrocarbon Films (in Russian).* Nauka. Moscow.

Langevin, D., S. Poteau, I. Henaut and J. F. Argillier (2004). *Oil and Gas Science and Technology-Revue De L Institut Francais Du Petrole* **59**, 511.

Long, J., Z. Xu and J. H. Masliyah (2005). *Energy Fuels* **19**, 1440.

Macdonald, J. R. (2005). *LEVM/LEVMW manual.* Macdonald, J. R. and Solartron Group Limited.

Manz, A. and Becker, H., Eds.) (1998). *Microsystem technology in chemistry and life science.* Springer Verlag. Berlin.

Masliyah, J. H. and S. Bhattacharjee (2006). *Electrokinetic and Colloid Transport Phenomena.* John Wiley and Sons. Hoboken.

McLean, J. D. and P. K. Kilpatrick (1997*a*). *J. Colloid Interface Sci.* **196**, 23.

McLean, J. D. and P. K. Kilpatrick (1997*b*). *J. Colloid Interface Sci.* **189**, 242.

Midttun, O., H. Kallevik, J. Sjoblom and O. M. Kvalheim (2000). *J. Colloid Interface Sci.* **227**, 262.

Morrison, I. D. (1993). *Colloids Surf., A* **71**, 1.

Naumowicz, M., A. D. Petelska and Z. A. Figaszewski (2006). *Electrochim. Acta* **51**, 5024.

Panchev, N., K. Khristov, J. Czarnecki, D. Exerowa and J. H. Masliyah (2006). New method for water-in-oil emulsion film studies.. In: *EUFOAM 2006. 6th European Conference on Foams, Emulsions and Applications.* Potsdam, Germany.

Park, J. S., J. H. Choi, J. J. Woo and S. H. Moon (2006). *J. Colloid Interface Sci.* **300**, 655.

Pena, A. A., G. J. Hirasaki and C. A. Miller (2005). *Ind. Eng. Chem.* **44**, 1139.

Pereira, L. G. C., C. Johansson, H. W. Blanch and C. J. Radke (2001). *Colloids Surf., A* **186**, 103.

Pethica, B. A. and D. G. Hall (1982). *J. Colloid Interface Sci.* **85**, 41.

Priest, C., S. Herminghaus and R. Seemann (2006). *Appl. Phys. Lett.* **89**, 134101.

Randles, J. E. B. (1952). *Transactions of the Faraday Society* **48**, 828.

Randles, J. E. B. and K. W. Somerton (1952). *Transactions of the Faraday Society* **48**, 937.

Requena, J. and D. A. Haydon (1975). *Proc. R. Soc. London, A* **347**, 161.

Requena, J., D. F. Billett and D. A. Haydon (1975). *Proc. R. Soc. London, A* **347**, 141.

Rosen, D. and A. M. Sutton (1968). *Biochim. Biophys. Acta* **163**, 226.

Sheludko, A (1967). *Adv. Colloid Interface Sci.* **1**, 335.

Shinoda, K., Y. Shibata and B. Lindman (1993). *Langmuir* **9**, 1254.

Sjoblom, J., Ed.) (1996). *Emulsions and Emulsion Stability.* 1st ed.. Taylor and Francis Group. Boca Raton, FL.

Sjoblom, J., N. Aske, I. H. Auflem, O. Brandal, T. E. Havre, O. Saether, A. Westvik, E. E. Johnsen and H. Kallevik (2003). *Adv. Colloid Interface Sci.* **100**, 399.

Slevin, C. J., A. Malkia, P. Liljeroth, M. Toiminen and K. Kontturi (2003). *Langmuir* **19**, 1287.

Sluyters, J. H. (1960). *Recueil Des Travaux Chimiques Des Pays-Bas-Journal of the Royal Netherlands Chemical Society* **79**, 1092.

Sluyters, J. H. and J. J. C. Oomen (1960). *Recueil Des Travaux Chimiques Des Pays-Bas-Journal of the Royal Netherlands Chemical Society* **79**, 1101.

Strubbe, F., A. R. M. Verschueren, L. J. M. Schlangen, F. Beunis and K. Neyts (2006). *J. Colloid Interface Sci.* **300**, 396.

Stubenrauch, C. and R. von Klitzing (2003). *J. Phys.: Condens. Matter* **15**, R1197.

Sun, J. Z., D. R. MacFarlane and M. Forsyth (1996). *Journal of Polymer Science Part a-Polymer Chemistry* **34**, 3465.

Suzuki, A., H. Maruyama, H. Seki, I. Kashiki and N. Inoue (2006). *Ind. Eng. Chem.* **45**, 1123.

Swayne, E. N., J. Newman and C. J. Radke (1998). *J. Colloid Interface Sci.* **203**, 69.

Taylor, S. D. (2002). Ph.d thesis. University of Alberta.

Taylor, S. D., J. Czarnecki and J. Masliyah (2002). *J. Colloid Interface Sci.* **252**, 149.

Trapa, P. E., M. H. Acar, D. R. Sadoway and A. M. Mayes (2005). *J. Electrochem. Soc.* **152**, A2281.

Velev, O. D., G. N. Constantinides, D. G. Avraam, A. C. Payatakes and R. P. Borwankar (1995). *J. Colloid Interface Sci.* **175**, 68.

Wang, S. Y., E. Axcell, R. Bosch and V. Little (2005). *Energy Fuels* **19**, 1425.

Weaver, J. C. and Y. A. Chizmadzhev (1996). *Bioelectrochemistry and Bioenergetics* **41**, 135.

White, S. H. (1970). *Biophys. J.* **10**, 1127.

White, S. H. (1972). *Biophys. J.* **12**, 432.

White, S. H. and W. Chang (1981). *Biophys. J.* **36**, 449.

Xu, Y. M., J. Y. Wu, T. Dabros, H. Hamza, S. Y. Wang, M. Bidal, J. Venter and T. Tran (2004). *Can. J. Chem. Eng.* **82**, 829.

Yaros, H. D., J. Newman and C. J. Radke (2003). *J. Colloid Interface Sci.* **262**, 442.

Yarranton, H. Y. (1997). Ph. d. thesis. University of Alberta.

Zimmermann, U. (1982). *Biochim. Biophys. Acta* **694**, 227.

Zimmermann, U., G. Pilwat, A. Pequeux and R. Gilles (1980). *J. Membr. Biol.* **54**, 103.

Zimmermann, U, G. Pilwat and F. Riemann (1974). *Biophys. J.* **14**, 881.

Appendix A

Detailed Fabrication Procedure

A.1 Standard Procedure of Microfluidic Chip Fabrication

Every standard microchip (electronics or microfluidics) goes through three major steps. These three steps are as follows:

- Sputtering: covering the substrate with a thin layer of a metal
- Patterning: transferring the desired pattern to the substrate
- Etching: removing some areas of the substrate or metallic covering layer.

Figure 1 depicts the above steps. These steps form a closed cycle, which can be repeated as many times as the design requires. The microfluidic chip developed in this study consists of one cycle for glass etching and one cycle for electrodes. Although these steps provide the basics of microfabrication, there are numerous intermediate steps that are necessary for completion of a fabrication procedure. Some of these intermediate steps are standard and some of them are custom designed to fulfill special specifications of the chip. These intermediate steps are explained in detail in the following section.

A.2 Microfabrication of the Developed Microfluidic Device

Figure 2 shows the fabrication procedure developed for the microfluidic device used in this study. The left column in the figure, depicts the procedure developed

for fabrication of the microchannels on the bottom substrate. Once the channels are formed, the second fabrication cycle takes place. The second cycle, shown on the right column of Fig. 2, was designed for fabrication of the electrodes. In this section, fabrication steps depicted in Fig. 2 are briefly described.

A.2.1 Substrate material

The substrate material used in this study was borofloat glass from Schott (Schott AG, Germany). Another type of glass is 0211 glass that was used in this study but due to the shallow angle of channels provided by this glass, it was discontinued. Borofloat substrates are supplied as $4in \times 4in$ pieces and their thickness was $1.1mm$.

A.2.2 Design

Design of the substrate is the first step after determining the manufacturing process. A popular software to design the mask is L-Edit program which is a free software available at the Nanofab. Unfortunately, L-edit is not a user friendly software. Compared with other design software such as Autocad, L-edit is cumbersome to use. Autocad can be used for this purpose but based on the Nanofab's staff experience, it can produce some errors and confusions for the mask generator at small sizes. So, it was recommended to use L-edit software. Therefore L-Edit was used to design the masks. Since these chips have two masks (one for the channels and one for the electrodes), two separate layers were created in L-edit. These two layers were created in one file but the masks were written separately.

A.2.3 Mask generating

Once the design is finished, the outcome of the L-edit program is a file with two layers for the two masks. These masks can be written using an instrument called mask generator. Mask generator is a very delicate and accurate laser device that writes the mask information on a glass substrate covered with chrome and photoresist very accurately. Then the mask is developed using a standard developer. The masks developed for these chips contain nine chips. Figures 3 and 4 show an electrode's and a channel's mask.

A.2.4 Cleaning

Cleaning of a substrate is an important task before sputtering. Any contamination of the substrate surface would affect bonding of the sputtered material to the surface. This is done by mixing 25% volume of hydrogen peroxide and 75% sulfuric acid. The mixing procedure produces significant amount of heat which would heat up the solution up to 110 $^{\circ}C$. Substrates should be immersed in this solution for at least 15 minutes. This guarantees that all organic contaminations are removed. After washing and drying, the substrates are ready for sputtering.

A.2.5 Sputtering

Sputtering of the metalic layers are performed in a Lesker sputtering machine (Lesker, Germany). Two layers of metal are deposited on glass substrates; chromium and gold. Since gold does not stick to glass directly, a layer of chrome has to be deposited first. this layer can be as thin as 300$\mathring{A}$. The covering gold layer is usually between 1500 – 1800$\mathring{A}$.

A.2.6 Spinning the photoresist

The patterning process starts with spinning the photoresist. Photoresist is a polymer sensitive to UV light. It changes its chemical composition once exposed to light. The photoresist used for development of the microfluidic device was HPR 504. It is a thin or low viscosity resist, which can be spread over the substrate with a thickness of 1 micron. The spreading speed was 500 rpm for 10 seconds followed by 40 seconds of fast spinning up to 4000 rpm. This process would spread the resist over the substrate with a thickness of 1 micron.

A.2.7 Baking

After spinning, the photoresist is wet. Therefore, the photoresist layer is dried by baking in a furnace. For glass substrates covered by 1μm thick HPR 504 resist, 30 minutes baking in 115 degrees is recommended. The duration of baking depends on the type of resist. For HPR 504, baking times down to 20 minutes were tested and the results were acceptable.

A.2.8 Exposing

Once the resist is baked, it is ready for exposure. The exposure process started with setting the mask generated on a mask aligner tool. It can either be the channel or the electrode's mask. It is important to ensure that the mask is cleaned before mounting on the machine. Once the mask is mounted, the substrate can be placed on the substrate holder by turning the vacuum on. Alignment of the first layer mask is quite easy but if the second mask is mounted, then the alignment has to be performed precisely. There are three degrees of freedom in X-direction, Y-direction, and rotation around the Z-axis. The best and easiest way to align the mask is to use eye ball alignment followed by microscope alignment. After alignment, the substrate can be brought into contact with the mask. It is crucial to ensure that the substrate does not move or change its position once it contacts the mask, otherwise the alignment has to be performed again. It is also important to ensure that the mask and the substrate are in good contact. Any trapped particle could create a gap between the mask and the substrate. This could let the diffused light penetrate under the mask, thereby, causing a reduced size of the features or partial exposure of some parts. The exposure time was generally between 4 to 4.5 seconds.

A.2.9 Developing photoresist

Developing the photoresist is a chemical process, in which the exposed substrate is immersed in a developer. The developer dissolves the exposed parts of the photoresist, leaving the substrate covered with unexposed photoresist. The standard developer for HPR 504 and 506 is developer 354. For slower and more accurate processes, water can be added to dilute the developer (up to 50% volume). The standard development time for the resists mentioned above is 20 to 25 seconds in 100% of developer 354. However, the developing time may vary; depending on the resist parameters, temperature, and humidity. It is important to check the quality of the whole patterning process under a microscope after developing the resist.

A.2.10 Gold and chromium etching

Once the photoresist is exposed to UV light, the exposed parts are dissolved in the developer and one has direct access to the covering metallic layer (gold and

chromium). These bare metallic areas can be stripped by immersing the substrate in gold etchant first, and then chromium etchant. The standard chromium etchant is a mixture of nitric acid, ceric ammonium nitrate and water. The etching rate is about $800\mathring{A}/min$ when the solution is fresh. The proper gold etchant is a solution consisting of $400g$ of KI, $200g$ of I2 and $1000mL$ of water. The etching rate with this solution is $3000\mathring{A}/min$.

Since the etching process is an isotropic process, the substrate is etched in the horizontal direction (under-cutting) as much as in the vertical direction. Therefore, it is important to ensure that under-cutting is controlled. Under-cutting can be controlled by accurate timing. For substrates in this study, the gold etching time was 30 to 35 seconds and chromium etching was 20 seconds. It is important to note that this etching rate varies with thickness, age of the etchant, and temperature.

A.2.11 Glass etching

The patterning process is to create channels on glass substrates. Once the gold and the chromium layers are etched, the glass etching process starts. The common etchant solution for glass etching is hydrofluoric acid (HF) which attacks Si-O bonds aggressively. Because of the presence of other metals in the glass, another acid such as HCL or HNO3 should be added to the solution to convert insoluble metal fluorides to soluble salts in order to reduce surface roughness. Hydrofluoric acid is an extremely hazardous material and safety precautions are important. An example of a typical glass etchant consists of 20% (volumetric) of 40% HF, 14% of 70% HNO3 and 66% of water. This etchant gives an etching speed of about 1.5 microns/minute for 0211 and 0.4 microns/minute for Borofloat glass. This is a low etching speed for Borofloat, but guarantees a good channel profile.

The first step in etching glass substrates is to measure the thickness of the Cr+Au+resist layer using a profilometer. This makes the zero point of measurement, against which every measurement is compared. The measurements should be taken from different parts of the substrate and averaged out so that one has a better approximation of the thickness. Then, substrates are immersed in etchant solution for exactly five minutes. The thickness measurement after five minutes gives an approximation of the speed of etching. Following this approximation, the etching time can be estimated.

Following glass etching, the photoresist layer (using acetone), gold and chromium (using proper etchant as explained in previous sections) layers can be removed. It is important to ensure that there is no area covered with the photoresist leftover. Figure 5 illustrates an etched glass(Borofloat with 5μ deep channel) under a microscope.

A.2.12 Silanization

To make the oil channels hydrophobic, trichlorosilane (Aldrich, ISA) was used. First, the water channels were covered with covering tape. Then, the chips and a small beaker of trichlorosilane were placed in a desiccator under vacuum. Trichlorosilane evaporates under vacuum and forms a thin layer of hydrophobic coating on the oil channels. The same process was also implemented for the top substrate as well. The silanization time was 90 minutes.

A.2.13 Dicing

Once all etching processes are completed, the four-inch substrate should be diced into pieces. The special machine for this job is the dicing saw, which cuts the glass very accurately. Both top and bottom substrates can be diced with this machine.

A.2.14 Drilling

The top substrate is a plain piece of glass that makes the top wall of the channels. It also provides the connecting wells to access the channels. These wells should be drilled through the glass. Abrasive drilling is difficult due to the brittle nature of glass. The best tool for drilling in glass is an ultrasonic drill. It provides round and smooth circles with minimum chipping. Since no ultrasonic machine was available, a conventional drilling method was used. Abrasive drilling can be conducted using diamond coated drill bits (UKAM, USA). Few glass substrates were drilled on top of each other. However, one needs to ensure that there is no gap between the substrates. Diamond drill bits with 1mm diameter were used. A support for holding the substrates was fabricated locally in the workshop. The drill was a small variable speed drill which could provide a constant load on substrates by an adjustable weight mechanism. The recommended drilling speed by the manufacturer of the drill bits was 60,000rpm, which was not supported by

the drill available in the department. Drilling speed was about 500 to 1000rpm. The quality of the holes was not good, but acceptable to supply the fluid into the channel.

A.2.15 Glass bonding

Two clean flat glass substrates can be bonded together fairly strongly without any special treatment. The key is the cleanliness of the substrates. Any particle would keep the two substrates apart which causes leakage of the fluid from the channels. The first step is to make the glass surface clean and hydrophilic using water-soap solution. This would help the two surfaces stick to each other when brought to contact. Then, the substrates should be cleaned using a high pressure washing system. The washing procedure followed by high speed drying prepare the surface for bonding. When two substrates are ready, they can be brought into contact. Using a microscope for alignment of the substrates can be very difficult, therefore, features on the top substrate are usually avoided.

Bonding of two glass substrate using this method in not permanent. To make the bonding permanent, the chip should be heat treated in a furnace up to $500°C$ for a few hours. This technique can be used for substrates without any electrodes, since thin electrodes will be oxidized at such temperatures. However, high temperature heat treatment of substrates with glass is possible in furnaces with inert gas. Since such a furnace was not available, the substrates in this study were not heat treated.

Figures 6 to 8 show the 1st, 7th, and 8th generations of the microfluidic device. Figure 9 depicts a schematic assembly of the final chip using SolidWorks (SolidWorks, USA) software.

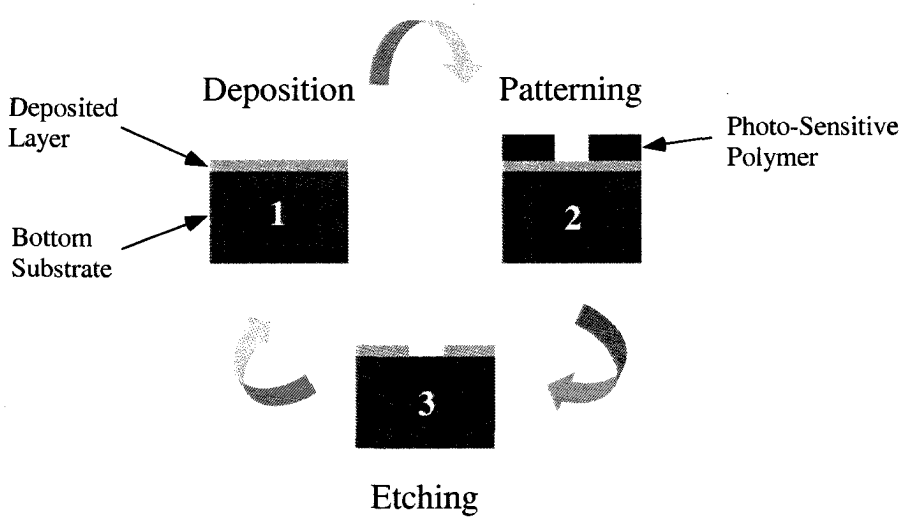

Figure 1: The three major steps in conventional photolithography microfabrication. These steps can be repeated as many times as required.

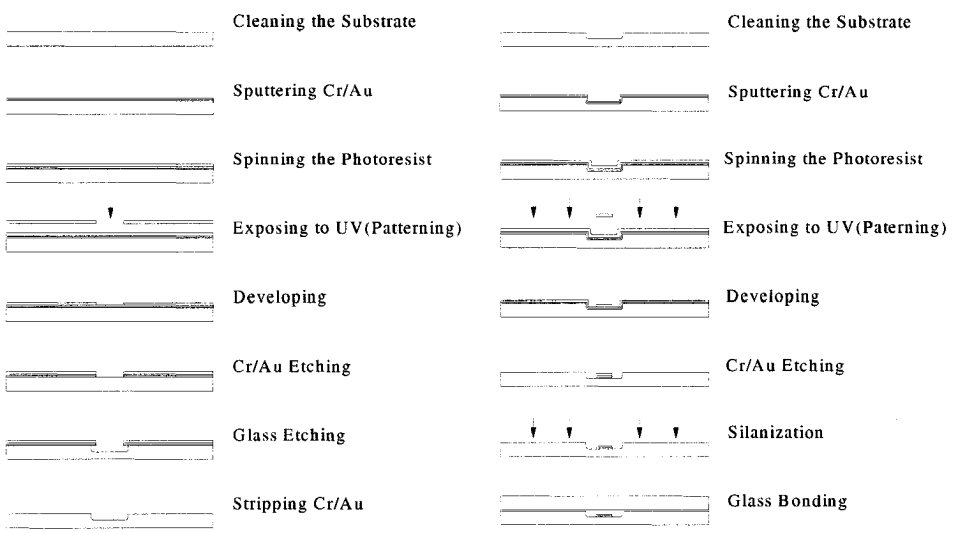

Figure 2: A complete fabrication process. The left column demonstrates the first process (channels) and the right column shows the second process (electrodes)

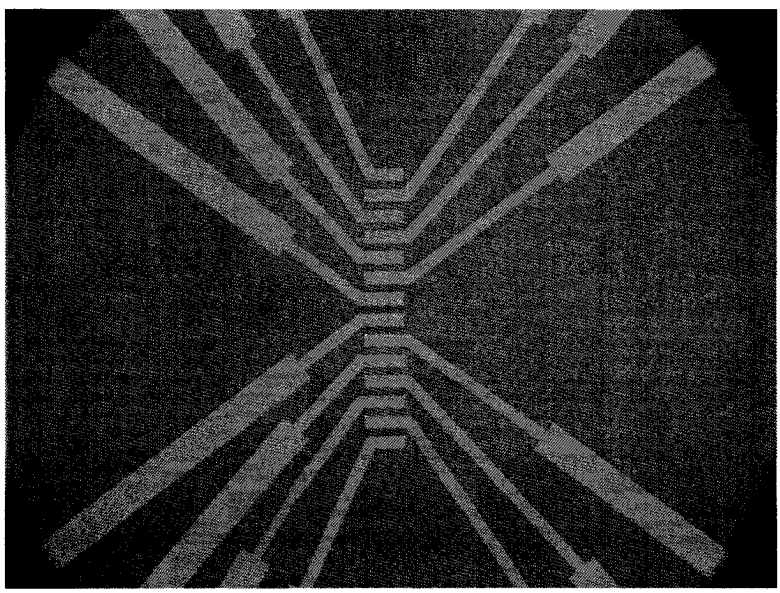

Figure 3: A mask for electrode layer developed for the first generation of chips

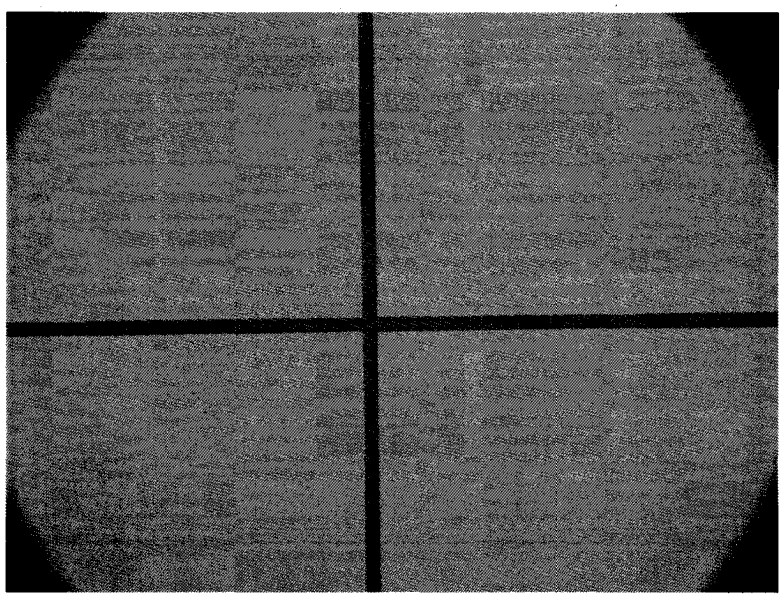

Figure 4: A mask for channels developed for the first generation of chips

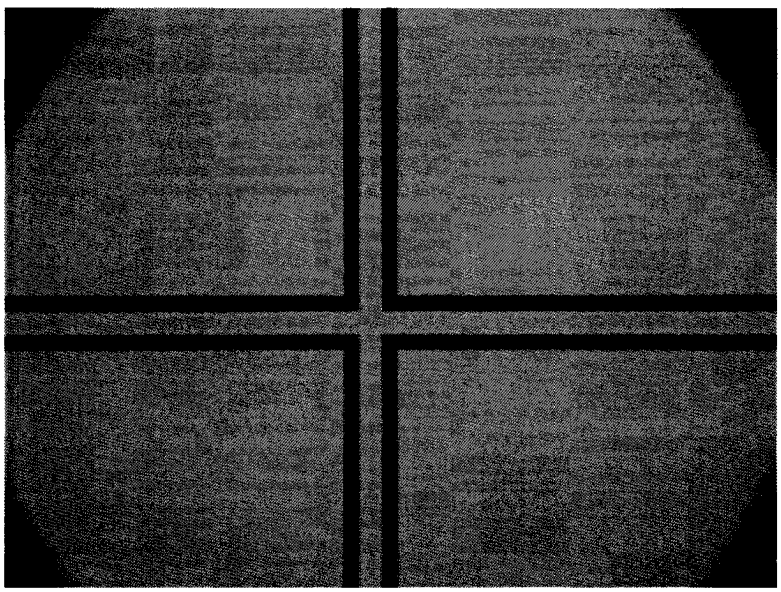

Figure 5: An optical micrograph of a bottom substrate after etching fabricated as the first generation of chips

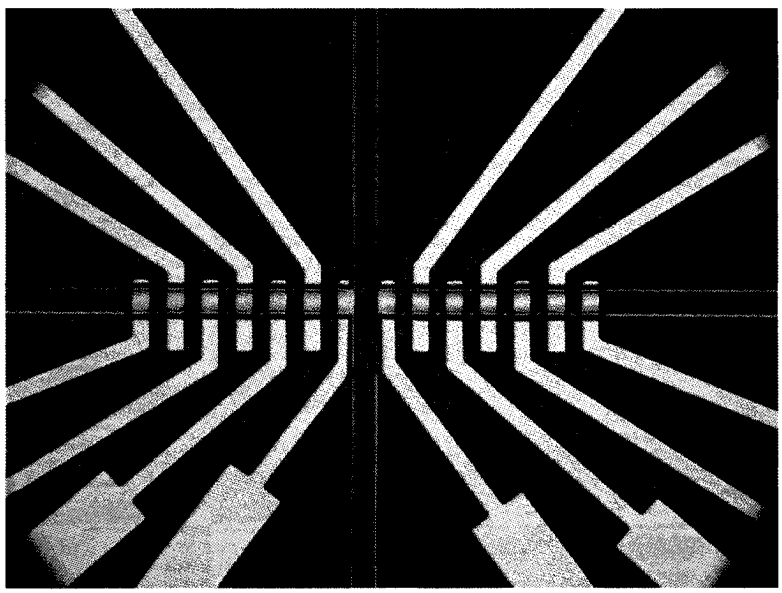

Figure 6: Optical micrograph of a complete bottom substrate developed as the first generations.

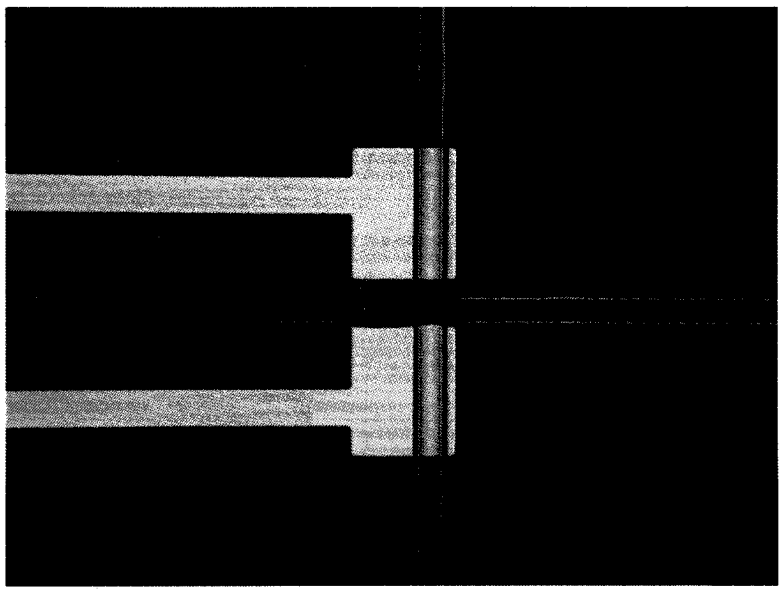

Figure 7: Optical micrograph of a complete bottom substrate developed as the first generations (a design different than the previous figure).

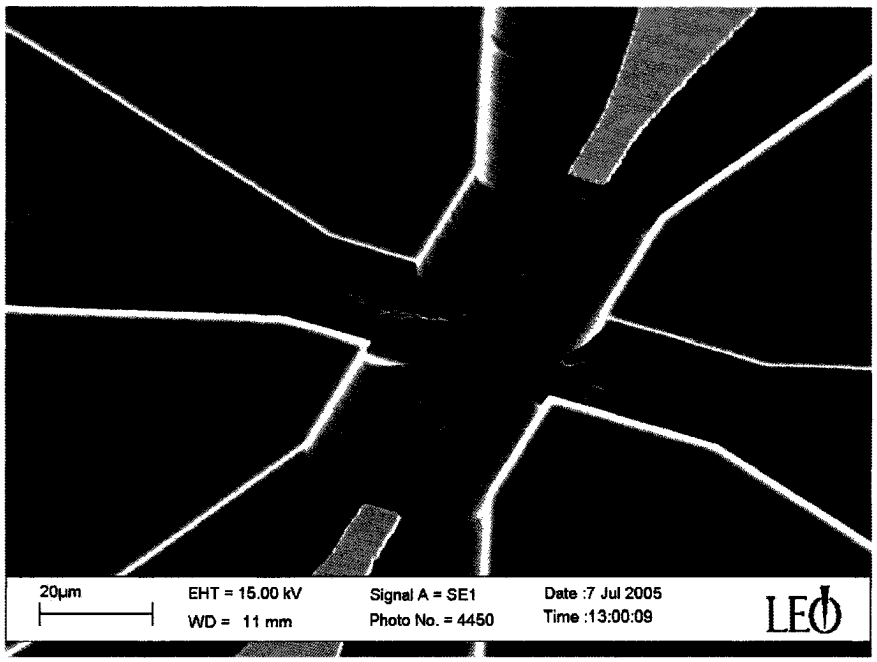

Figure 8: SEM micrograph of the bottom substrate developed as generation seven.

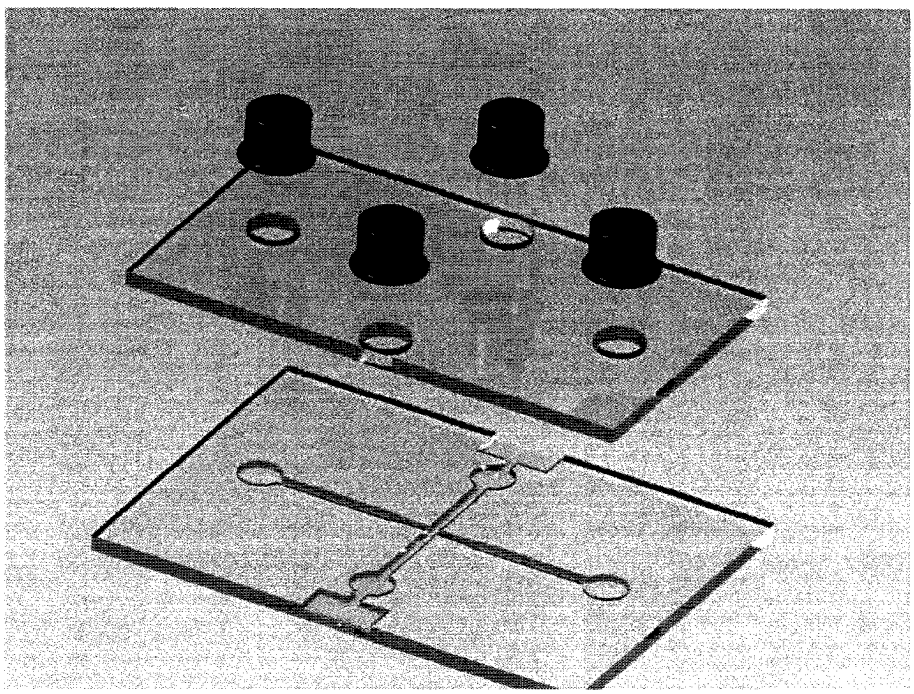

Figure 9: A schematic image of the final microfluidic device (generation eight) designed using SolidWorks (SolidWorks, USA).